

THÈSE DE DOCTORAT
DE L'UNIVERSITÉ PIERRE ET MARIE CURIE

École doctorale Sciences Mécaniques, Acoustique, Électronique et Robotique de Paris

Spécialité
Mécanique - Robotique

Présentée par

Anis Meguenani

**Contrôle de Robots collaboratifs : Une Approche
Énergétique aux problématiques de Sûreté**

Soutenance prévue le 30 Juin 2016

Devant le jury composé de :

M. Olivier STASSE	Directeur de recherche au LAAS-CNRS, Toulouse	Examinateur
M. Guillaume MOREL	Professeur à l'Université Pierre et Marie Curie	Examinateur
M. Philippe BIDAUD	Professeur à l'Université Pierre et Marie Curie	Directeur de thèse
M. Vincent PADOIS	Maître de Conférences à l'Université Pierre et Marie Curie	Encadrant

Contents

List of Figures	vii
1 Constraints incompatibility	1
1.1 Introduction	1
1.1.1 The problem	1
1.1.2 Contributions	7
1.1.3 Corresponding literature	8
1.2 The QP form and constraints incompatibility cases	10
1.2.1 Task formulation	10
1.2.2 Controller formulation	10
1.2.3 Articular constraints: classic formulation	11
1.2.4 Test case scenario for the experimental results	14
1.3 Articular constraints: new formulations	15
1.3.1 Joint velocity constraint incompatibility with jerk limits	17
1.3.2 Joint position constraint incompatibility with deceleration and/or jerk limits	22
1.4 Final bounds on the acceleration control variable	56
1.5 Conclusion	59
2 Energy based safe control	61
2.1 Introduction	64
2.2 Interaction forces and safety indicators	66
2.2.1 Kinetic energy	67

2.2.2	Potential energy	68
2.2.3	Relation between kinetic and potential energies	70
2.3	Safety limit values	72
2.3.1	Safety limit value for the pre-collision safety indicator	72
2.3.2	Safety limit value for the physical contact safety indicator	76
2.3.3	Energies constraints activation/deactivation	77
2.3.4	Task energy profile	78
2.4	Safe dynamic controller	80
2.4.1	Task formulation	80
2.4.2	Constraints formulation	81
2.4.3	Controller formulation	86
2.5	Experimental results: Simulation	86
2.5.1	Test case scenario	87
2.5.2	Obstacle intersecting with the robot trajectory and no constraints on energy	91
2.5.3	Nearby obstacle, not intersecting the robot trajectory and constraint on kinetic energy	93
2.5.4	Obstacle intersecting the robot trajectory and constraint on the kinetic energy	97
2.5.5	Obstacle intersecting the robot trajectory and constraint on the kinetic then potential energy	100
2.5.6	Obstacle intersecting the robot trajectory and constraint on the task energy profile	104
2.6	Conclusion	105
3	Safe human-robot interaction: experimental results	109
3.1	Introduction	111
3.2	Experimental setup	112
3.3	Test case scenario	112
3.3.1	Human-operator intersecting with the robot trajectory and no constraints on energy	113

3.3.2	Human-operator intersecting with the robot trajectory and constraint on kinetic energy	115
3.3.3	Human-operator intersecting with the robot trajectory and constraint on potential energy	116
3.3.4	Human-operator intersecting with the robot trajectory and constraints on kinetic then potential energies	119
3.4	Conclusion	120
A	Appendix	125
	Bibliography	129

List of Figures

1.1	Braking phase for the car in scenario 2 as it stops before hitting the wall.	3
1.2	Braking phase for the car in scenario 1 as it collides with the wall. Transparent frames show the continuation of the braking phase if the wall is removed.	5
1.3	State $S_{ k}$ of an articular joint one time-step before reaching its velocity limit \dot{q}_m . The producible jerk is limiting the range from which the control variable $\ddot{q}_{ k}^c$ can be picked. $\ddot{q}_{ k}^c$ cannot be zero. Therefore, the articular acceleration cannot be forced to zero when $\dot{q}_{ k}$ is equal to \dot{q}_m at the next time-step. The joint will continue to accelerate and the velocity limit will be violated. Because of the incompatibility with the producible jerk, it is impossible in this case to cope with the joint rate constraint.	13
1.4	State $S_{ k}$ of an articular joint one time-step before reaching its lower position limit q_m . The range of producible deceleration $\ddot{q}_{ k}^c$ is not sufficient to allow forcing the articular velocity to zero at the next time-step when ($q_{ k}$ becomes equal to q_m). Because of the incompatibility with the deceleration capability, it is impossible in this case to satisfy the joint position constraint.	14
1.5	State $S_{ k}$ of an articular joint one time-step before reaching the minimum position limit q_m . The range of producible deceleration $\ddot{q}_{ k}^c$ is limited by the available jerk capability. It is not possible to force the articular velocity to zero for the next time-step (when $q_{ k}$ will be equal to q_m). Because of the incompatibility with jerk capabilities, it is impossible in this case to cope with the joint position constraint.	14

1.6 Screenshots of the test case scenario simulation with the KUKA LWR4 robot.	15
1.7 State S of joint 0 during the test case scenario; The movement of the joint is not constrained. Top to bottom: position, velocity, acceleration and jerk.	16
1.8 State S of joint 0 during the braking phase to cope with a maximum velocity limit. The classic articular velocity constraint formulation (1.11b) is used. Top to bottom: velocity, acceleration and jerk.	19
1.9 State S of joint 0 during the braking phase to cope with a maximum velocity limit. In this test, the new constraint formulation (1.14) that takes into account the jerk capability $\ddot{q}_{M_0} = 25 \text{ rad.s}^{-3}$ is used. Top to bottom: velocity, acceleration, jerk and n_1	21
1.10 Zooms corresponding to Fig. 1.9.	21
1.11 State S of joint 0 during the braking phase to cope with a maximum position limit M_0 ; The new constraint formulation (1.27) that takes into account the deceleration capability $\ddot{q}_{m_0} = -100 \text{ rad.s}^{-2}$ is used. Top to bottom: position, velocity, acceleration, jerk and n_3	27
1.12 Zooms corresponding to Fig. 1.11.	27
1.13 State S of joint 0 during the braking phase to cope with a maximum position limit; The new constraint formulation (1.27) that takes into account the deceleration capability $\ddot{q}_{m_0} = -3 \text{ rad.s}^{-2}$ is used. Top to bottom: position, velocity, acceleration, jerk and n_3	28
1.14 Zooms corresponding to Fig. 1.13.	28
1.15 State S of joint 0 during the braking phase to cope with a maximum position limit q_{M_0} ; The new constraint formulation (1.33) that takes into account the jerk capability $\ddot{q}_{m_0} = -25 \text{ rad.s}^{-3}$ is used. Top to bottom: position, velocity, acceleration, jerk and n_5	33
1.16 Zooms corresponding to Fig. 1.15.	33
1.17 State S of joint 0 during the braking phase to cope with a maximum position limit; The new constraint formulation (1.33) that takes into account the jerk capability $\ddot{q}_{m_0} = -2500 \text{ rad.s}^{-3}$. Top to bottom: position, velocity, acceleration, jerk and n_5	34

1.18	Zooms corresponding to Fig. 1.17.	34
1.19	State S of joint 0 during the braking phase to cope with a maximum position limit q_{M_0} ; The new constraint formulation (1.41) that takes into account both positive and negative jerk capabilities $[\ddot{q}_{m_0}, \ddot{q}_{M_0}] = [-25, 25] \text{ rad.s}^{-3}$ is used. Top to bottom: position, velocity, acceleration, jerk and (n_7, n_9)	40
1.20	Zooms corresponding to Fig. 1.19.	40
1.21	State S of joint 0 during the braking phase to cope with a maximum position limit q_{M_0} ; The new constraint formulation (1.46) that takes into account both deceleration and jerk capabilities $\ddot{q}_{m_0} = -25 \text{ rad.s}^{-3}, \ddot{q}_{M_0} = -3 \text{ rad.s}^{-2}$ is used. Top to bottom: position, velocity, acceleration, jerk and (n_{11}, n_{13})	47
1.22	Zooms corresponding to Fig. 1.21.	47
1.23	State S of joint 0 during the braking phase to cope with a maximum position limit q_{M_0} ; The new constraint formulation (1.53) that takes into account the deceleration capability $\ddot{q}_{m_0} = -3 \text{ rad.s}^{-2}$ in addition to the positive and negative jerk limits $[\ddot{q}_{m_0}, \ddot{q}_{M_0}] = [-25, 25] \text{ rad.s}^{-3}$ is used. Top to bottom: position, velocity, acceleration, jerk and (n_{15}, n_{17}, n_{19})	55
1.24	Zooms corresponding to Fig. ??	55
1.25	State S of joint 0 during the braking phase to cope with a maximum position limit q_{M_0} ; The new constraint formulation (1.53) that takes into account the deceleration capability $\ddot{q}_{m_0} = -100 \text{ rad.s}^{-2}$ in addition to the positive and negative jerk limits $[\ddot{q}_{m_0}, \ddot{q}_{M_0}] = [-25, 25] \text{ rad.s}^{-3}$ is used. Top to bottom: position, velocity, acceleration, jerk and (n_{15}, n_{17}, n_{19})	56
1.26	State S of joint 0 when coping with both maximum position and velocity limits; Using the final articular constraint formulation (1.55) that takes into account all the limitations of the joint. Top to bottom: position, velocity, acceleration, jerk and $(n_1, n_{15}, n_{17}, n_{19})$	58
1.27	Zooms corresponding to Fig. 1.26.	58

2.1	View of a user sharing its workspace with the KUKA LWR manipulator. The kinetic energy of the system is modulated as a function of the distance between the human operator and the end-effector of the robot in order to best perform the task of the robot while ensuring safety.	65
2.2	Evolution of the kinetic energy constraint depending on the distance d between the end-effector and the obstacle.	73
2.3	Energy zones for the dynamic behaviour of the robot.	73
2.4	Evolution of the constraint on kinetic and potential energy depending on the distance d between the end-effector of the robot and the considered obstacle.	77
2.5	KUKA LWR4 serial robot within the XDE simulator near its considered obstacle. Case O_1 is when the obstacle intersects with the trajectory of the robot. Case O_2 is when the obstacle is nearby the robot but does not intersect with its trajectory	87
2.6	(a) Position tracking error for the end-effector along the x , y and z axis in cartesian space. (b), (c) and (d) are the real and desired position for the end-effector along the same axis.	88
2.7	(a) Braking capability of the robot expressed at the end-effector in the opposite direction to the considered obstacle (case O_2 in Fig. ??). (b), (c) and (d) are the instantaneous real and desired velocity for the end-effector in cartesian space.	89
2.8	Articular position, velocity and acceleration corresponding to the pick and place movement as the energy of the robot is not constrained.	90
2.9	Articular torque and jerk corresponding to the pick and place movement as the energy of the robot is not constrained.	91
2.10	(a) Kinetic energy of the robot in the direction of the considered obstacle (case O_2 in Fig. 2.5), computed using (2.54) and (2.55) during the pick and place movement. (b), (c) and (d) are the energy profiles corresponding to the pick and place task along the x , y and z axis in cartesian space.	92

2.11 Dissipated kinetic energy of the KUKA LWR4 expressed at the end-effector in the direction of the considered obstacle during collision.	93
2.12 (a) Potential energy generated within the robot-obstacle system during physical contact along the x axis in cartesian space. (b) Contact forces between the robot and the wall after establishment of physical contact along the x , y and z axis in cartesian space. (c) Actuation torques during physical contact with the considered obstacle.	94
2.13 Screen-shot of the KUKA LWR4 robot within the XDE simulator with the wall not intersecting its trajectory.	95
2.14 Screen-shot of the KUKA LWR4 robot within the XDE simulator during collision with the wall intersecting its trajectory.	95
2.15 Constrained kinetic energy of the robot expressed at the end-effector in the direction of a nearby considered obstacle (case O_2 in Fig. 2.5).	96
2.16 (a), (b) and (c) depict the real and desired position for the end-effector in cartesian space as the kinetic energy of the robot is constrained. (d), (e) and (f) are the real and desired velocity for the end-effector as the robot is submitted to the same constraint (case O_2 in Fig. 2.5).	96
2.17 Generated articular torque and jerk as the constraint on the kinetic energy of the robot is activated (case O_2 in Fig. 2.5).	98
2.18 Constrained kinetic energy of the robot expressed at the end-effector in the direction of the collided obstacle (case O_1 in Fig. 2.5).	99
2.19 (a) Potential energy generated within the robot-obstacle system during physical contact along the x axis in cartesian space. (b) Corresponding contact forces along the x , y and z axis in cartesian space. (c) Actuation torques during physical contact with the considered obstacle (case O_1 in Fig. 2.5).	100
2.20 (a), (b) and (c) depict the real and desired position for the end-effector in cartesian space as the kinetic energy of the robot is constrained. (d), (e) and (f) are the real and desired velocity for the end-effector as the robot is submitted to the same constraint (case O_1 in Fig. 2.5).	101

2.21	Constrained kinetic energy of the robot expressed at the end-effector in the direction of the collided obstacle (case O_1 in Fig. 2.5).	102
2.22	(a) Constrained potential energy within the robot-obstacle system during physical contact along the x axis in cartesian space. (b) Corresponding contact forces along the x , y and z axis in cartesian space. (c) Actuation torques during the physical contact with the considered obstacle (case O_1 in Fig. 2.5).	103
2.23	(a), (b) and (c) depict the real and desired position for the end-effector in cartesian space as the task energy profile of the robot is constrained. (d), (e) and (f) are the real and desired velocity for the end-effector as the robot is submitted to the same constraint (case O_1 in Fig. 2.5).	105
2.24	Constrained energy profile for the pick and place task along the x , y and z axis in cartesian space.	106
2.25	(a) The kinetic energy of the robot expressed at the end-effector as it physically interacts with the nearby obstacle (case O_1 in Fig. 2.5). (b) Corresponding contact forces along the x , y and z axis in cartesian space. (c) Actuation torques during the physical contact.	107
3.1	View of a user sharing its workspace with a KUKA LWR4 manipulator; with the experimental setup used to detect the human operator and control the robotic system.	113
3.2	(a) Kinetic energy of the robot in the direction of the human operator; (b) Potential energy within the human-robot system during physical contact. (c) Top: position tracking error; Middle: constraint of the articular acceleration of the first joint; Bottom: articular velocity of the first joint. d) Articular torques.	114
3.3	Constrained kinetic energy of the robot expressed at the end-effector in the direction of the approaching operator.	116
3.4	(a) Potential energy within the human-robot system during physical contact. (b) Articular torques.	117
3.5	Kinetic energy of the robot in the direction of the human operator.	118

3.6	(a) Potential energy within the human-robot system during physical contact along the x , y and z axis in cartesian space. (b) Articular torques. . . .	122
3.7	Constrained kinetic energy of the robot expressed at its end-effector in the direction of the approaching operator.	123
3.8	(a) Potential energy within the human-robot system during physical contact along the x , y and z axis in cartesian space. (b) Articular torques. . . .	124
A.1	Instantaneous producible maximum and minimum articular accelerations for joint 0 during the movement of the KUKA LWR4 as shown in Fig. 1.6.	126

Chapter 1

Constraints incompatibility

For reactive control laws, input data for the operational task are usually discovered at every time-step. In this case, articular constraints such as joint limits are usually handled through inequalities. Depending on the expression of these constraints, compatibility issues can appear which leads to constraints violation. Indeed coping for example with an articular position or velocity limit within a small amount of time (e.g. 1 ms) may be impossible considering the limited reaction capabilities (i.e. producible torque/deceleration and jerk) of the system. In this chapter, we reformulate the articular position constraint to take into account the maximum deceleration and jerk that can be generated by the actuators of the robot. Joint rate constraint expression is also modified to include jerk capabilities. The new formulations are implemented into a QP (quadratic programming) scheme to resolve the control problem of a redundant robot (KUKA LWR4) at the dynamic level. The resulting algorithms allow an automatic activation of these constraints at the right time to comply with the considered limits. A solution for the optimization control problem is guaranteed at every time-step, smoother control torques are produced and the viability of the state of the robot is guaranteed.

1.1 Introduction

1.1.1 The problem

In practical applications, a control approach for a robotic system is usually formulated depending on the nature of the operational task to be performed. Two cases are distinguished: proactive controllers when the objective of the operational task is already known (e.g. moving the end-effector from point A to point B) and reactive controllers in case the input data for the operational task are not known a priori but discovered at every time-step (e.g. tele-operation, co-manipulation applications, sensor-based control...etc.).

In both control cases, compliance to constraints and more importantly to the physical limitations of actuators is a must for any robotic system. This is particularly true in cases where constraints violation is highly critical (e.g. surgery, de-mining, nuclear plants decommissioning...etc.).

To ensure strict compliance, for proactive controllers, constraints and tasks can be handled offline. For example, to move the end-effector of a robot from point A to point B in cartesian space, trajectories can be generated directly at joint level. In this context, Katzschmann et. al in [Katzschmann 13] present a trajectory generating algorithm that takes into account the Max/min position, velocity, torque and even jerk capabilities of the robot actuators. On the other hand, when tasks or constraints are not known in advance (reactive control cases), *trajectories cannot be generated* and it becomes impossible to use the same approach to cope with constraints; That are therefore included *the hard way* in the controller.

In case of redundant manipulators, the control problem can either be formulated at the kinematic-level as the inversion of the following relation:

$$\dot{\mathbf{X}} = J(\mathbf{q})\dot{\mathbf{q}} \quad (1.1)$$

or at the torque-level when dynamic capabilities like contact forces control are needed:

$$\ddot{\mathbf{X}} = J(\mathbf{q})\ddot{\mathbf{q}} + J\ddot{\mathbf{q}} \quad (1.2)$$

$J(\mathbf{q})$, $\dot{\mathbf{X}}$, $\ddot{\mathbf{X}}$, $\dot{\mathbf{q}}$, $\ddot{\mathbf{q}}$ are respectively the operational task Jacobian matrix, the operational velocity and acceleration vectors and the joint velocity and acceleration vectors. If it stills possible to implement constraints using an analytical scheme [Ngo 05],[Ngo 06], the most general approach consists in formulating the control problem as a convex optimization one. Constraints are then expressed through both equalities and inequalities [Chen 94]-[Ma 02]. Independently from the type of controller, one problem remains open: for the current and every future time-step, is it always possible to find a solution to the optimization control problem ? Considering the naive classic expression of constraints, the answer is clearly: "No"; And this, because of the constraints incompatibility problem. To

better illustrate this issue, let's consider the following examples. Example 1: On a straight line, a car is cruising towards a wall. Its current velocity $v = 10 \text{ m/s}$, its distance to the wall $d = 10 \text{ m}$ and its deceleration capability $a_m = -1 \text{ m/s}^2$. In its current state, none of the constraints¹ of the car are violated; However, even if the vehicle starts *braking* from time-step² k using its full deceleration capability $a_m = -1 \text{ m/s}$ (control input), collision with the wall is inevitable. Indeed, as shown in Fig. 1.2, during its braking phase, the car hits the wall between time-steps $k + 1$ and $k + 2$ and thus, before bringing its velocity to 0. In this case, it is said that the constraint on the deceleration capability and the one on the position of the vehicle are incompatible. At time-step $k + 2$, there is no solution for the optimization control problem that does not violate the car's constraints at the next time-step. Example 2: On a straight line, a second car is also cruising towards the wall.

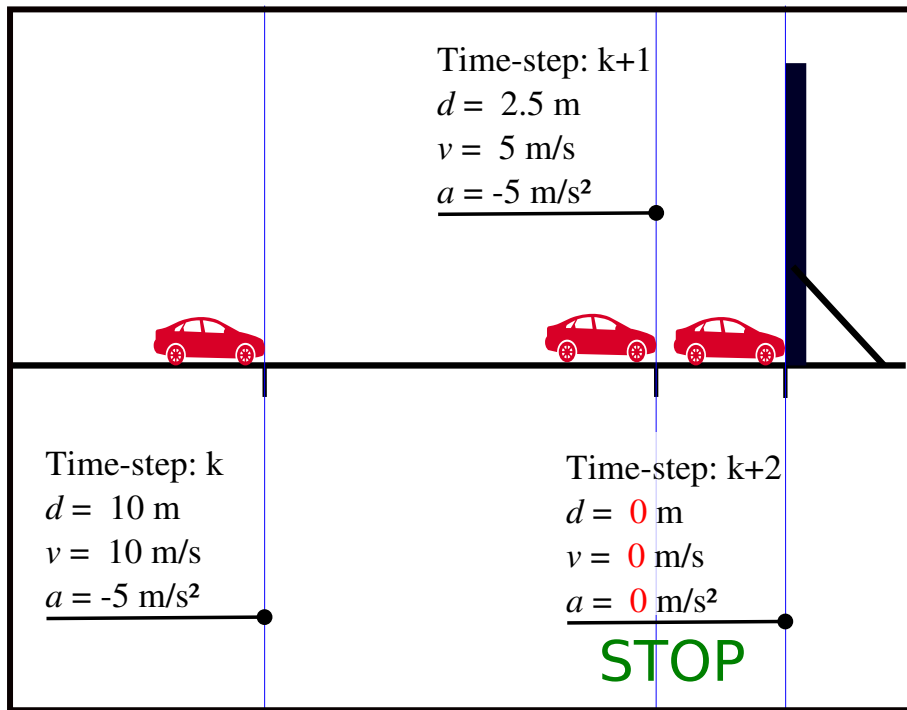


Figure 1.1: Braking phase for the car in scenario 2 as it stops before hitting the wall.

Its current velocity $v = 10 \text{ m/s}$, its distance to the wall $d = 10 \text{ m}$ and its deceleration capability is $a_m = -5 \text{ m/s}^2$. As shown in Fig. 1.1, the velocity of the car is brought to 0

¹The constraint on position and the constraint on the deceleration capability of the car.

²For this example, the time-step duration is 1 s.

within two time-steps and the car is stopped exactly at its position limit without hitting the wall. In this case, it is said that both constraints on deceleration and position are compatible and a solution is always available for the optimization control problem.

It is clear how the two constraints are compatible for the vehicle in the second scenario as the amount of deceleration it can produce is bigger than for the car in scenario 1, -5 m/s^2 compared to -1 m/s^2 . A **solution** to ensure constraints compatibility in the first scenario can be as following: considering its low deceleration capability (-1 m/s^2), the black car should start *braking* several time-steps in advance. Precisely, as shown in Fig. 1.1, 10 time-steps before reaching the wall and 50 m from it. These are the needed time and distance to completely stop the vehicle³. The only way to implement this solution is to reformulate the naive expression of the constraint on position. The new formulation must imperatively take into account the available deceleration capability in addition to the instantaneous state of the car plus the considered position limit: $f(d, v, a_m) \geq 0$. With such a formulation, every time the vehicle reaches an *extreme* state⁴, the constraint on the control variable is automatically activated, a *braking phase* is engaged and a *viable* [Aubin 91] solution is available for the optimization control problem as the car copes with its position limit.

We recall the concept of viability that is often used when dealing with the balance issue for humanoid robots. It can naturally be extended to the constraints incompatibility problem: *A state is viable if starting from this state there exists over an infinite horizon of time a sequence of control inputs that satisfies all constraints in the future*. Therefore, considering the notion of viability, unlike the state of the black car at time-step k in the first scenario, the state of the red one in the second scenario at the same time-step and for all the following time-steps is *viable*.

³Considering an initial velocity of $v = 10 \text{ m/s}$.

⁴An extreme state for the car is a state from which, considering its deceleration capability, if it starts decelerating using this maximum deceleration, it will stop just before hitting the wall.

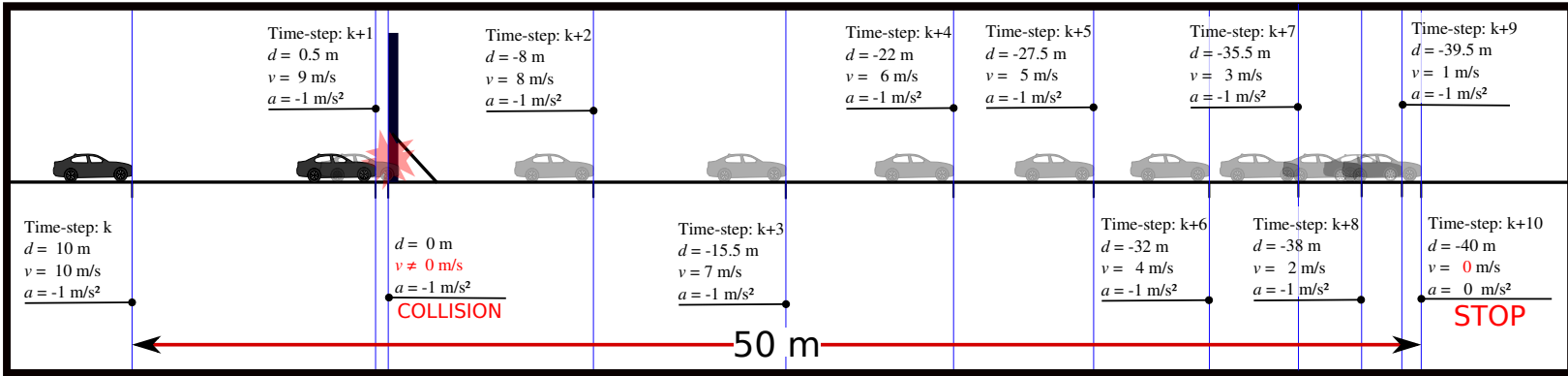


Figure 1.2: Braking phase for the car in scenario 1 as it collides with the wall. Transparent frames show the continuation of the braking phase if the wall is removed.

51

Articular space constraints			Operational space constraints		
Type 1: static constraints $S \leq S_M$	Dynamic constraints $S \leq \tilde{S}_M$		Type 4: Static constraints $w(S) \leq w_M$	Dynamic constraints $w(S) \leq \tilde{w}_M$	
	Type 2: Predictable limit \tilde{S}_M	Type 3: Non predictable limit \tilde{S}_M		Type 5: Predictable limit \tilde{w}_M	Type 6: Non predictable limit \tilde{w}_M

Table 1.1: Types of constraints that can be encountered when a reactive controller is used. $S = \{q, \dot{q}, \ddot{q}, \ddot{\ddot{q}}\}$ is the state of the robot in articular space. $w(S) = \{X, \dot{X}, \ddot{X}, \ddot{\ddot{X}}\}$ is the mapping of this state in operational space.

For reactive control schemes, possible encountered constraints are summarized in table 1.1. We distinguish two groups of constraints: articular space constraints that concern directly the state $S = \{\mathbf{q}, \dot{\mathbf{q}}, \ddot{\mathbf{q}}\}$ of the robot (e.g. constraints corresponding to the actuators position and joint rate limits) and operational space constraints that are expressed as non-linear functions of S and that are related to the movements of the robot in cartesian space. For example, a constraint of non-collision between the robot and an object within its workspace. Such a constraint can be written:

$$J_c(\mathbf{q}_{|k})\dot{\mathbf{q}}_{|k}\delta t + d_{|k} \geq 0 \quad (1.3)$$

where J_c is the Jacobian matrix associated to the closest part of the robot and projected along the unit vector associated to the shortest distance between the object and the robot, $\dot{\mathbf{q}}_{|k}$ is the generalised articular velocity of the robot, δt is the control sample time and $d_{|k}$ is the current closest distance between the robot and the object.

As shown in tab 1, each constraint from the two groups is either static or dynamic. A static constraint is a constraint which limit is constant and does not variate over time (e.g. physical position limit for an actuator). On the other hand, dynamic constraints are formulated with limits that can change in time (e.g. depending on sensory acquired data). Variations of these limits can be either predictable⁵ or non-predictable⁶.

To prevent a robotic system from getting into a non-viable state, all its constraints must be reformulated to include the reaction⁷ capabilities of its actuators, namely: producible articular deceleration/torque and jerk⁸. Naive expressions of constraints in tab 1 can be modified as following:

For type 1 constraints, just as the proposed **solution** for the car in example 1, considering constant deceleration and jerk⁹ capabilities and a static limit S_M , a formal solution that preserves viability can be computed for the control problem. For this, the formula-

⁵For example, a position related constraint for the end-effector regarding an object approaching the robot at a *constant* velocity.

⁶For example. The movement of a human operator nearby the robot.

⁷Coping with a constraint usually implies a braking phase that is induced by the actuators of the robot (analogue to the car examples).

⁸Each constraint in tab 1 with its naive formulation is compatible with the reaction capabilities of the robot in case of actuators that can produce infinite torque/deceleration and jerk.

⁹Which is not exactly the case for multi-body robots.

tion of this type of constraints should be changed to take into account the articular reaction capabilities of the robot; Namely, producible articular deceleration $[\ddot{q}_m, \ddot{q}_M]$ and jerk $[\ddot{\ddot{q}}_m, \ddot{\ddot{q}}_M]$. The same can also be done in case of constraints with dynamic predictable¹⁰ limits \tilde{S}_M (type 2). For type 3¹¹ constraints, a straight forward solution is to widely bound the variations of the dynamic limit \tilde{S}_M , which alters consequently the optimality of the control solution regarding the task to perform. The problem with constraints of type 4¹² is, even if the articular reaction capabilities can be considered constant in joint space, the non-linear and configuration dependent mapping¹³ of these performances in operational space makes the estimation of the braking profile impossible without any prediction on the future movements of the robot. Coping exactly with a static limit in cartesian space becomes a difficult task. Which is even more complex for dynamic constraints (type 5 and type 6¹⁴).

1.1.2 Contributions

In the presented work, the problem of constraints incompatibility is solved for constraints of type 1 and precisely for robots controlled at the dynamic-level. The constraints on articular positions, velocities, accelerations and jerk are expressed as inequalities within a QP formulation of a reactive control problem. The main contribution concerns the mathematical reformulation of the following constraints:

- No violation of joint position bounds.
- No violation of joint velocity bounds.

¹⁰Considering an exact prediction, these bounds can be handled as static limits.

¹¹A type 3 constraint can be for example the constraint on the kinetic energy of the robot expressed in articular space. Such a constraint can be expressed: $\frac{1}{2}M(\mathbf{q})\dot{\mathbf{q}}^2 \leq E_c^{art}$; With E_c^{art} the maximum allowed kinetic energy in articular space. When reflected on $\dot{\mathbf{q}}$, this constraint is written: $\dot{\mathbf{q}} \leq \sqrt{2M(\mathbf{q})^{-1}E_c^{art}}$.

¹²A type 4 constraint can be for example a constraint on the operational velocity of the robot end-effector. Such a constraint can be expressed: $\dot{\mathbf{X}} = J(\mathbf{q})\dot{\mathbf{q}} \leq \dot{\mathbf{X}}_M$; With $\dot{\mathbf{X}}_M$ the maximum allowed velocity for the end-effector in cartesian space.

¹³ $[\ddot{q}_m, \ddot{q}_M], [\ddot{\ddot{q}}_m, \ddot{\ddot{q}}_M] \rightarrow [\ddot{\mathbf{X}}_m, \ddot{\mathbf{X}}_M], [\ddot{\ddot{\mathbf{X}}}_m, \ddot{\ddot{\mathbf{X}}}_M]$

¹⁴A type 6 constraint can be for example the constraint on the operational velocity of the end-effector of the robot with a limit depending to the instantaneous distance to a considered moving obstacle.

To avoid incompatibilities, these new formulations take into account the reaction capabilities, i.e. articular deceleration and jerk producible by the actuators of the robot. One kind of incompatibility can occur for example when a braking phase¹⁵ is induced to stop the movement of an actuator at a static position limit within a short period of time, for e.g. one control sample time. This requires high deceleration and jerk capabilities that the robot may not be able to produce. Indeed, to be optimal, a robotic system must take the highest advantage of its dynamic capabilities within its limiting ranges. For example, to be as close as possible to a maximum allowed position with high articular acceleration and velocity and still be able to stop at time and not violate the considered limit. This can be achieved through a braking phase triggered n time-steps before reaching the limit and that takes into account the available deceleration capabilities of the system, namely: producible articular torque and jerk. Every time the considered actuator reaches an *extreme* state, the braking phase is automatically engaged and viability for the state of the robot is guaranteed.

1.1.3 Corresponding literature

The issue of constraints incompatibility exists since a long time and remains an open one. In [Park 98] the problem of high peak of torques and chattering phenomena is highlighted when the joint angle limit of a serial robot is reached. This results from decelerating the limiting joint in order to stop the motion in one sampling time. the following problems appear:

1. Collision with the joint angle limit when no sufficient control torque and/or jerk capabilities are available.
2. Vibrations by exciting hidden resonant modes of the manipulator which can lead to instability.

¹⁵The considered braking phase here is the result of the activation of the position related constraint. It is not caused by the objective task of the controller.

Park et al. in [Park 98] use a method called *P-Step-Ahead Predictor (PSAP)*. Articular position and velocity limits are detected far earlier and the braking phase is activated p time-steps in advance to reduce the required amount of torque. In addition, the modulation of a weighting matrix related to the manipulability measure [Yoshikawa 85] can be used for the same purpose. The problem with the proposed approach is the inevitable heuristic trial and error method to fix the acting parameters (e.g. p). Decré et al. in [Decré 09] were the first to formulate a mathematical solution to directly integrate the deceleration capabilities into the expression of a Cartesian position constraint; This resulted into a smoother articular velocity control input. Rubrecht et al. in [Rubrecht 10] extended the idea to articular constraints. The deceleration capabilities are integrated in the formulation of articular position constraints that are automatically activated n time-steps before the joint position boundaries. However, only kinematic-level control is considered. Lange in [Lange 14] and Suppa in [Lange 15] use a scaling method to generate an immediate Path-Accurate and Jerk-Limited stopping motion for industrial robots. This method can be transposed and used when coping with articular limits. The correct time for triggering the stopping motion needs however to be computed.

The organization of this chapter is as following: In section 2 we present the reactive controller that will be used to compare different formulations of articular constraints. We present the classic way used to formulate these constraints then, by studying the relationship between the joint parameters: q , \dot{q} , \ddot{q} , \dddot{q} and their corresponding limitations: $[q_m, q_M]$, $[\dot{q}_m, \dot{q}_M]$, $[\ddot{q}_m, \ddot{q}_M]$, $[\ddot{q}_m, \ddot{q}_M]$, we expose the different incompatibility cases that may occur. In section 3, the incompatibility cases are resolved and new formulations of velocity and position constraints that take into account the reaction capabilities of the robot are presented. In section 4 we formulate the final bounds reflected on the dynamic control variable to cope with all the articular limits of the system at the same time. In section 5 we conclude and give more insights on the generalisation of the presented formulations for constraints expressed in the cartesian space.

1.2 The QP form and constraints incompatibility cases

This section aims at establishing the general formulation of the constrained, redundant dynamic reactive control scheme. The objective is to compute the control torque $\tau_{|k}^c$ in order to perform a trajectory tracking task in joint space while coping at every time-step with articular position, velocity, acceleration and jerk constraints. We highlight the fact that in this particular case, desired trajectories for the joints of the robot are not known in advance but *discovered at every time-step* (tele-operation analogue situation). Incompatibility cases related to the classic way of expressing articular constraints are discussed.

1.2.1 Task formulation

The objective function of the controller is defined as an error to be minimized. A joint-space acceleration task is considered and the error is between the desired articular acceleration \ddot{q}^{des} and the expected acceleration \ddot{q}^c . \ddot{q}^{des} is computed as:

$$\ddot{q}_{|k}^{des} = K_p(\dot{q}_{|k}^* - \dot{q}_{|k}) - K_d\ddot{q}_{|k}^* \quad (1.4)$$

where $K_p, K_d \in \mathbb{R}^+$ are the proportional and derivative gains. The acceleration task function to be minimized is written:

$$g(\ddot{q}_{|k}^c) = \ddot{q}_{|k}^{des} - \ddot{q}_{|k}^c \quad (1.5)$$

1.2.2 Controller formulation

The proposed control strategy computes the control torque by minimizing the norm of the articular acceleration task function expressed in the following quadratic form:

$$\arg \min_{\tau_{|k}^c} \left\| g(\ddot{q}_{|k}^c) \right\|_{Q_t}^2 + \epsilon \|\tau_{|k}^c\|_{Q_r}^2, \quad (1.6)$$

subject to:

$$M(\dot{q}_{|k})\ddot{q}_{|k}^c + b(\dot{q}_{|k}, \ddot{q}_{|k}) = \tau_{|k}^c \quad (1.7)$$

With: $\ddot{q}_{|k}^c$ and $\tau_{|k}^c$ the optimization control variables. $b(q_{|k}, \dot{q}_{|k})$ are the non linear terms, namely gravity, Coriolis and centrifugal induced generalized forces. $M(q_{|k})$ is the joint space inertia matrix of the robot. Q_t and Q_r are positive semi-definite weighting matrices and $\|a\|_Q$ is the Q -weighted euclidean norm of a . $\epsilon \|\tau_{|k}^c\|_{Q_r}^2$ with $\epsilon \ll 1$ serves as a regularization task in order to ensure the uniqueness of the control solution and to minimize the norm of the computed control torque. In this case, Q_t and Q_r are identity matrices. It can be shown that the quadratic forms composing the tasks can be written as functions of positive semi-definite matrices. This LQP optimization problem is therefore convex and admits a unique global solution.

In addition to the equality constraints corresponding to the dynamic equation (1.7), the problem is also subject to inequality constraints described in the upcoming sections.

1.2.3 Articular constraints: classic formulation

First, we introduce some notations that will be used throughout the manuscript:

- $t \in \mathbb{R}^+$ denotes time.
- $k \in \mathbb{N}$ denotes the current discrete time-step.
- δt is the time-step duration of the discrete-time controller.
- $S_{|k} = \{q_{|k}, \dot{q}_{|k}, \ddot{q}_{|k}, \dddot{q}_{|k}\} \in \mathbb{R}$ is the state of the system at the current time-step describing its joint position, velocity, acceleration and jerk.
- $[q_M, q_m]$ are the Max/min joint position boundaries.
- $[\dot{q}_m, \dot{q}_M], [\ddot{q}_m, \ddot{q}_M], [\dddot{q}_m, \dddot{q}_M]$ are the joint velocity, acceleration and jerk boundaries.

The computed control input $\tau_{|k}^c$ at instant k must be such that the articular limits are not violated at the next time-step $k + 1$. These constraints can naturally be expressed in form

of inequalities:

$$\begin{cases} \mathbf{q}_m \leq \mathbf{q}_{|k+1} \leq \mathbf{q}_M, \end{cases} \quad (1.8a)$$

$$\begin{cases} \dot{\mathbf{q}}_m \leq \dot{\mathbf{q}}_{|k+1} \leq \dot{\mathbf{q}}_M, \end{cases} \quad (1.8b)$$

$$\begin{cases} \ddot{\mathbf{q}}_m \leq \ddot{\mathbf{q}}_{|k}^c \leq \ddot{\mathbf{q}}_M, \end{cases} \quad (1.8c)$$

$$\begin{cases} \boldsymbol{\tau}_m \leq \boldsymbol{\tau}_{|k}^c \leq \boldsymbol{\tau}_M, \end{cases} \quad (1.8d)$$

$$\begin{cases} \ddot{\mathbf{q}}_m \leq \ddot{\mathbf{q}}_{|k+1} \leq \ddot{\mathbf{q}}_M \end{cases} \quad (1.8e)$$

$\ddot{\mathbf{q}}_m, \ddot{\mathbf{q}}_M$ can be computed as explained in Annexe A.

To be easily accounted for, these constraints are expressed in function of the control variable $\ddot{\mathbf{q}}_{|k}^c$. Considering the literature [Rubrecht 10], [Decré 09], the classic approach to do that is based on the state of the system at instant k and a local discrete linear approximation of its behaviour within a δt time-step duration:

$$\begin{cases} \mathbf{q}_{|k+1} = \mathbf{q}_{|k} + \delta t \dot{\mathbf{q}}_{|k} + \frac{\delta t^2}{2} \ddot{\mathbf{q}}_{|k}, \end{cases} \quad (1.9a)$$

$$\begin{cases} \dot{\mathbf{q}}_{|k+1} = \dot{\mathbf{q}}_{|k} + \delta t \ddot{\mathbf{q}}_{|k}, \end{cases} \quad (1.9b)$$

$$\begin{cases} \ddot{\mathbf{q}}_{|k+1} = \frac{1}{\delta t} (\ddot{\mathbf{q}}_{|k}^c - \ddot{\mathbf{q}}_{|k}) \end{cases} \quad (1.9c)$$

Note: For a torque control input $\boldsymbol{\tau}_{|k}^c$ computed for the current time-step k and equivalent to an acceleration command $\ddot{\mathbf{q}}_{|k}^c$ (1.7), the expected articular acceleration at the next time-step $k + 1$ can be written:

$$\ddot{\mathbf{q}}_{|k}^c = \ddot{\mathbf{q}}_{|k+1} \quad (1.10)$$

Using (1.9), in case of a dynamic-level control (our case), constraints in (2.32) can be reflected on the acceleration control variable $\ddot{\mathbf{q}}_{|k}^c$ as following:

$$\begin{cases} \frac{2}{\delta t^2} (\mathbf{q}_m - \mathbf{q}_{|k} - \delta t \dot{\mathbf{q}}_{|k}) \leq \ddot{\mathbf{q}}_{|k}^c \leq \frac{2}{\delta t^2} (\mathbf{q}_M - \mathbf{q}_{|k} - \delta t \dot{\mathbf{q}}_{|k}), \end{cases} \quad (1.11a)$$

$$\begin{cases} \frac{1}{\delta t} (\dot{\mathbf{q}}_m - \dot{\mathbf{q}}_{|k}) \leq \ddot{\mathbf{q}}_{|k}^c \leq \frac{1}{\delta t} (\dot{\mathbf{q}}_M - \dot{\mathbf{q}}_{|k}), \end{cases} \quad (1.11b)$$

$$\begin{cases} \ddot{\mathbf{q}}_m \leq \ddot{\mathbf{q}}_{|k}^c \leq \ddot{\mathbf{q}}_M, \end{cases} \quad (1.11c)$$

$$\begin{cases} \ddot{\mathbf{q}}_m \delta t + \ddot{\mathbf{q}}_{|k} \leq \ddot{\mathbf{q}}_{|k}^c \leq \ddot{\mathbf{q}}_M \delta t + \ddot{\mathbf{q}}_{|k} \end{cases} \quad (1.11d)$$

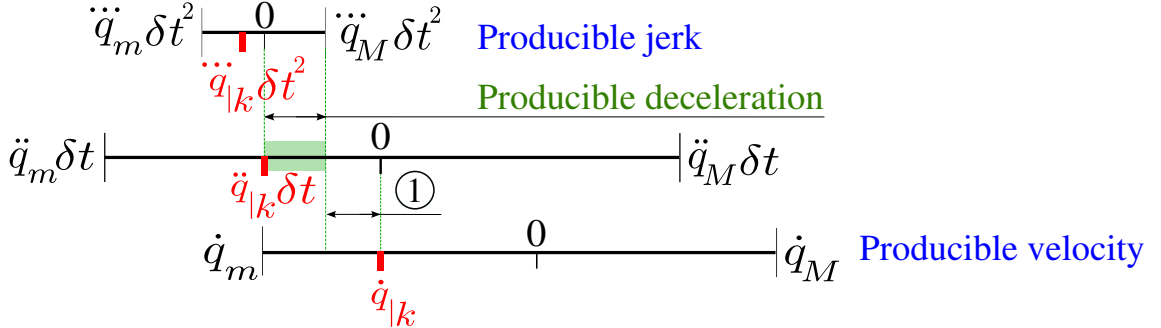


Figure 1.3: State $S_{|k}$ of an articular joint one time-step before reaching its velocity limit \dot{q}_m . The producible jerk is limiting the range from which the control variable $\ddot{q}_{|k}^c$ can be picked. $\ddot{q}_{|k}^c$ cannot be zero. Therefore, the articular acceleration cannot be forced to zero when $\dot{q}_{|k}$ is equal to \dot{q}_m at the next time-step. The joint will continue to accelerate and the velocity limit will be violated. Because of the incompatibility with the producible jerk, it is impossible in this case to cope with the joint rate constraint.

When these classic formulations are used, the resulting constraints on $\ddot{q}_{|k}^c$ are activated only one time-step before reaching the considered limits (i.e. $[\mathbf{q}_M, \mathbf{q}_m]$, $[\dot{\mathbf{q}}_m, \dot{\mathbf{q}}_M]$, $[\ddot{\mathbf{q}}_m, \ddot{\mathbf{q}}_M]$ and $[\ddot{\mathbf{q}}_{|k}, \ddot{\mathbf{q}}_{|k}]$). In this case, no sufficient time may be available for the actuators to react and cope with the considered boundaries. Different incompatibility cases can appear and the optimization control problem may become unsolvable.

1.2.3.1 Incompatibility cases related to the joint rate constraint

Coping with a joint velocity constraint automatically imply bringing the articular acceleration $\ddot{q}_{|k}$ to zero when hitting a Max/min velocity limit. In this case, a compatibility problem may arise if no sufficient articular jerk can be produced by the actuators during the braking phase. Coping at the same time with joint rate limits and articular jerk limits may become impossible (see Fig. 1.3).

1.2.3.2 Incompatibility cases related to the joint position constraint

On the other hand, coping with a joint position constraint imply bringing both articular velocity $\dot{q}_{|k}$ and acceleration $\ddot{q}_{|k}$ to zero when hitting the Max/min position boundaries. In this case, two incompatibility cases may arise. The first is when no sufficient articular deceleration is available during the braking phase (1 control time-step) even if sufficient

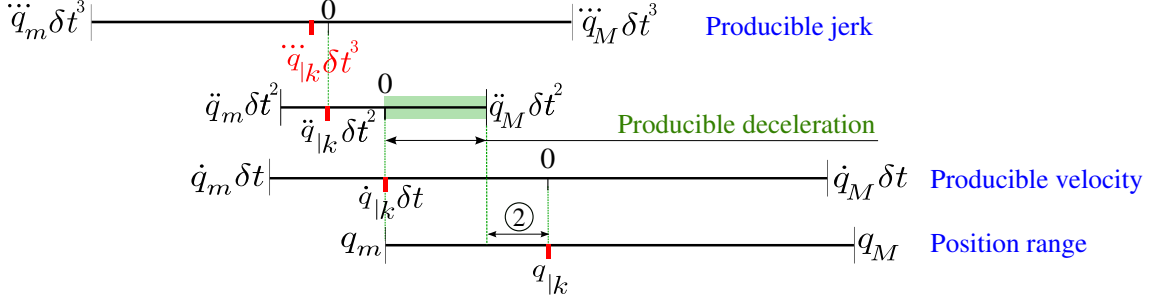


Figure 1.4: State $S_{|k}$ of an articular joint one time-step before reaching its lower position limit q_m . The range of producible deceleration $\ddot{q}_{|k}^c$ is not sufficient to allow forcing the articular velocity to zero at the next time-step when ($q_{|k}$ becomes equal to q_m). Because of the incompatibility with the deceleration capability, it is impossible in this case to satisfy the joint position constraint.

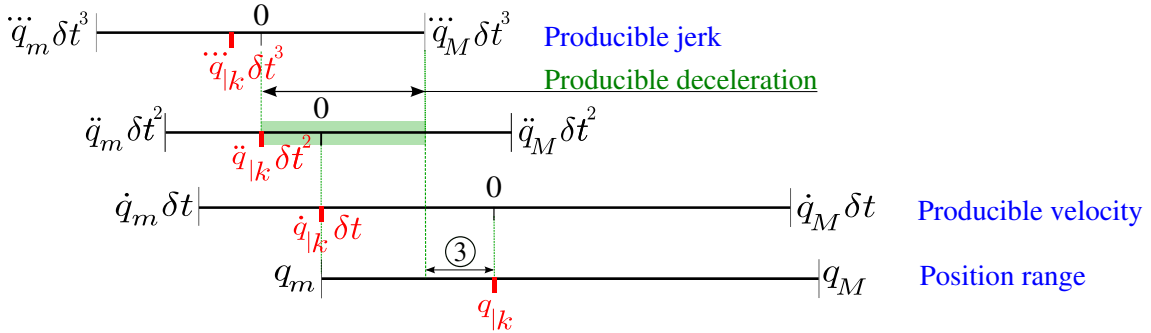


Figure 1.5: State $S_{|k}$ of an articular joint one time-step before reaching the minimum position limit q_m . The range of producible deceleration $\ddot{q}_{|k}^c$ is limited by the available jerk capability. It is not possible to force the articular velocity to zero for the next time-step (when $q_{|k}$ will be equal to q_m). Because of the incompatibility with jerk capabilities, it is impossible in this case to cope with the joint position constraint.

braking jerk can be produced (see Fig. 1.4). The second is when no sufficient jerk capabilities are available even if enough deceleration can be generated by the considered actuator (see Fig. 1.5).

1.2.4 Test case scenario for the experimental results

The controller previously described is implemented as a C++ Orocosp component [Soetens] on a virtual model of the Kuka LWR4 serial robot using XDE, a robotics-oriented physics simulation engine [Merlhiot 12]. The same test case scenario will be used as a basis for testing all the different joint constraints formulations. A comparison between the classic

and new formulations will be performed.

As a main activity, the robot performs a trajectory tracking task where its joints track desired articular positions (*discovered at every time-step*) (see Fig. 1.6). During its movement, the system is pushed to its physical limits (Max/min positions, velocities, accelerations and jerks). The LQP is solved in real-time at a period of 1 ms using Gurobi, a commercial optimization software [Gurobi Optimization Inc. 15]. Values used for the gains of the controller during simulation are $K_p = 400$, $K_d = 2\sqrt{K_p}$. For demonstration purposes, only the physical capabilities of the first joint (joint 0) will be constrained. Deceleration and jerk capabilities are considered constant in cartesian space.

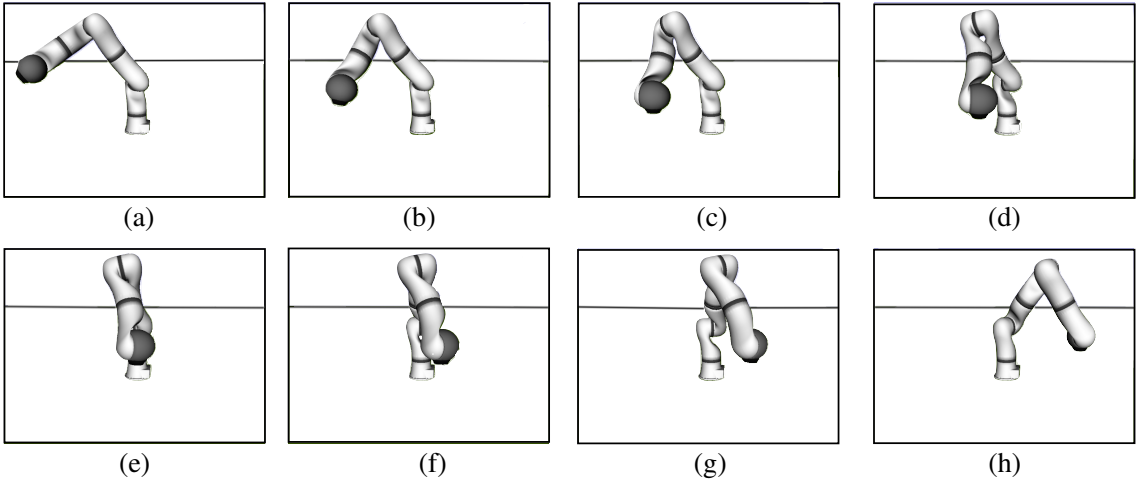


Figure 1.6: Screenshots of the test case scenario simulation with the KUKA LWR4 robot.

Fig. 1.7 shows the state of joint 0 as it reaches its desired position $q_0^* = 3.79 \text{ rad}^{16}$ within 3.5 s. During its movement, joint 0 reaches a maximum velocity of 2.57 rad.s^{-1} , a maximum acceleration of 3.15 rad.s^{-2} and a maximum jerk of -8.05 rad.s^{-3} .

1.3 Articular constraints: new formulations

In this section, the constraints incompatibility problems previously exposed are resolved. The formulation of joint rate constraints is modified to include the system's jerk capabilities. Joint position constraints are also reformulated to take into account both the

¹⁶The position domain for joint 0 on a real KUKA LWR4 is $[q_{0_m}, q_{0_M}] = [-2.97, 2.97] \text{ rad}$. A wider range is considered in simulation.

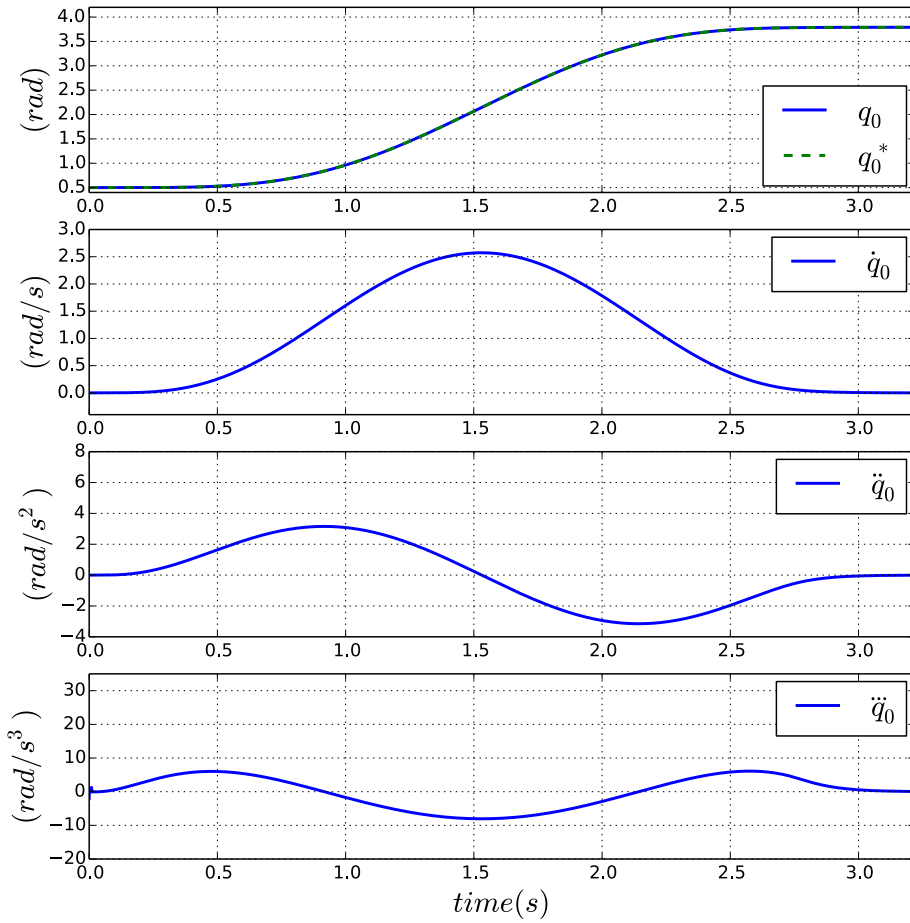


Figure 1.7: State S of joint 0 during the test case scenario; The movement of the joint is not constrained. Top to bottom: position, velocity, acceleration and jerk.

amounts of deceleration and jerk that can be generated by the actuators. Considering the reaction capabilities of the robot, the corresponding braking phases will start earlier and at the right moment to cope with the different joints physical limitations. For each incompatibility case, the state of the actuator during the induced¹⁷ braking phase is described then the new constraints formulations are derived. Finally, the new formulations are compared with the classic ones.

¹⁷Induced by the constraint to cope with the physical limitations of the actuators.

1.3.1 Joint velocity constraint incompatibility with jerk limits

As previously explained, these constraints (1.11b and 1.11d) may become incompatible if a joint gets close to one of its velocity limits too fast (see Fig. 1.3). In this case, the admissible jerk may not be sufficient to allow a fast variation of the articular torque and it becomes impossible to bring the articular acceleration to zero within only one control time-step duration. The only solution to preserve compatibility is to start braking with maximum jerk several time-steps (not just one) before reaching the velocity boundaries. The braking phase lasts therefore ($n_{1_N} \geq 1$) control time-steps.

Lets consider the braking phase for a joint hitting the maximum velocity limit \dot{q}_M . During this phase, the actuator is braking with constant jerk \ddot{q}_m until reaching the maximum velocity. The state S of the system during this braking phase can be described as following:

$$\begin{aligned} S_{|k+1} & \left\{ \begin{array}{l} \dot{q}_{|k+1} = \dot{q}_{|k} + \ddot{q}_{|k}\delta t, \\ \ddot{q}_{|k+1} = \ddot{q}_{|k} + \ddot{q}_m\delta t. \end{array} \right. \\ S_{|k+2} & \left\{ \begin{array}{l} \dot{q}_{|k+2} = \dot{q}_{|k+1} + \ddot{q}_{|k+1}\delta t, \\ \ddot{q}_{|k+2} = \ddot{q}_{|k+1} + \ddot{q}_m\delta t. \end{array} \right. \\ & \vdots \quad \vdots \\ S_{|k+n_1} & \left\{ \begin{array}{l} \dot{q}_{|k+n_1} = \dot{q}_{|k+n_1-1} + \ddot{q}_{|k+n_1-1}\delta t, \\ \ddot{q}_{|k+n_1} = \ddot{q}_{|k+n_1-1} + \ddot{q}_m\delta t. \end{array} \right. \end{aligned} \tag{1.12}$$

With: $\dot{\mathbf{q}}_{|k} \geq 0$, $\ddot{\mathbf{q}}_{|k} \geq 0$ and $\ddot{\mathbf{q}}_m \leq 0$. The joint velocity evolution in n_1 iterations is equal to the general form¹⁸ of the numerical sequence (1.12):

$$\dot{\mathbf{q}}_{|k+n_1} = \dot{\mathbf{q}}_{|k} + n_1 \ddot{\mathbf{q}}_{|k} \delta t + \frac{(n_1^2 - n_1)}{2} \ddot{\mathbf{q}}_m \delta t^2 \quad (1.13)$$

Finally, in case of a dynamic-level control, the condition $\dot{\mathbf{q}}_{|k+n_1} \leq \dot{\mathbf{q}}_M$ for all integer n_1 leads to:

$$\ddot{\mathbf{q}}_{|k}^c \leq \frac{(\dot{\mathbf{q}}_M - \dot{\mathbf{q}}_{|k})}{n_1 \delta t} - \frac{(n_1 - 1)}{2} \ddot{\mathbf{q}}_m \delta t \quad (1.14)$$

n_1 is the integer minimizing the right hand side of (1.14). By differentiating this expression w.r.t n_1 :

$$\left. \begin{array}{l} n_1 \geq 1 \\ \frac{-(\dot{\mathbf{q}}_M - \dot{\mathbf{q}}_{|k})}{n_1^2 \delta t} - \frac{\delta t}{2} \ddot{\mathbf{q}}_m = 0 \end{array} \right\} \Rightarrow n_1 = -\frac{\sqrt{-2 \ddot{\mathbf{q}}_m (\dot{\mathbf{q}}_M - \dot{\mathbf{q}}_{|k})}}{\ddot{\mathbf{q}}_m \delta t} \quad (1.15)$$

Following the same method for the lower velocity limit, the condition $\dot{\mathbf{q}}_{|k+n_2} \geq \dot{\mathbf{q}}_m$ for all integer $n_2 \geq 1$ becomes:

$$\ddot{\mathbf{q}}_{|k}^c \geq \frac{(\dot{\mathbf{q}}_m - \dot{\mathbf{q}}_{|k})}{n_2 \delta t} - \frac{(n_2 - 1)}{2} \ddot{\mathbf{q}}_M \delta t \quad (1.16)$$

With:

$$n_2 = \frac{\sqrt{-2 \ddot{\mathbf{q}}_M (\dot{\mathbf{q}}_m - \dot{\mathbf{q}}_{|k})}}{\ddot{\mathbf{q}}_M \delta t} \quad (1.17)$$

maximizing the right hand side of (1.16).

In this case, the reflected constraint on the acceleration control variable $\ddot{\mathbf{q}}_{|k}^c$ is of the form :

$$f_\beta(\dot{\mathbf{q}}_{|k}, \dot{\mathbf{q}}_m, \ddot{\mathbf{q}}_M, n_2) \leq \ddot{\mathbf{q}}_{|k}^c \leq f_\alpha(\dot{\mathbf{q}}_{|k}, \dot{\mathbf{q}}_M, \ddot{\mathbf{q}}_m, n_1) \quad (1.18)$$

f_β and f_α are as in (1.14) and (1.16).

¹⁸Computed using Maple

1.3.1.0.1 Simulation

For the first experiment, joint 0 is reaching its upper velocity limit \dot{q}_{M_0} . Only the classic formulation of the joint velocity constraint (1.11b) is implemented with the controller: (1.6), (1.7). The hard-coded constraint on articular jerk (1.11d) is not considered. Fig. 1.8

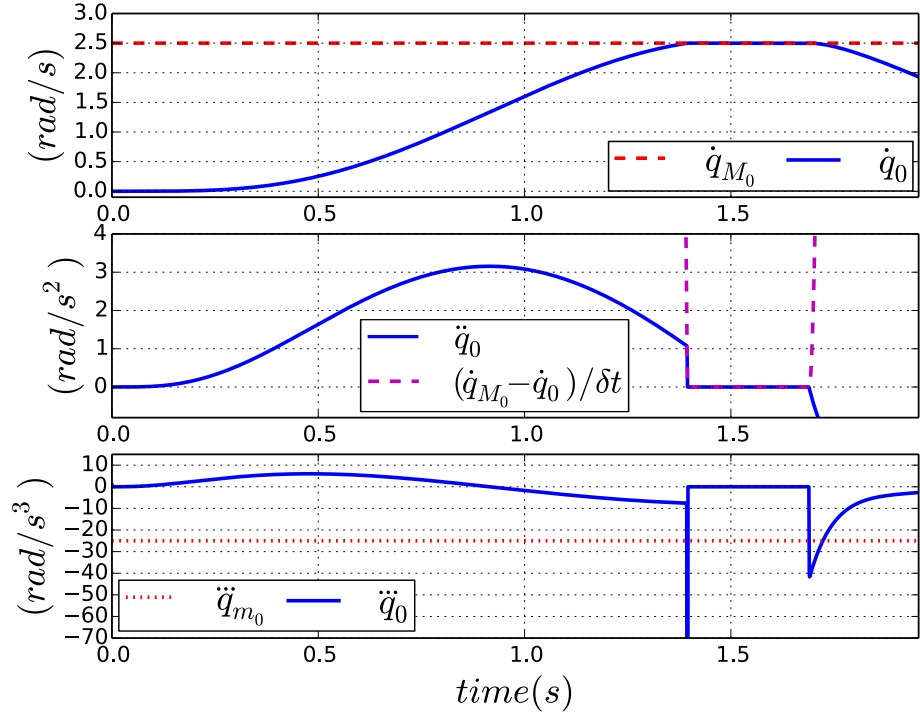


Figure 1.8: State S of joint 0 during the braking phase to cope with a maximum velocity limit. The classic articular velocity constraint formulation (1.11b) is used. Top to bottom: velocity, acceleration and jerk.

shows the state of joint 0 during a braking phase induced only one time-step = 1 ms before reaching \dot{q}_{M_0} . A high peak of jerk is created. In this case, if the hard-coded constraint on articular jerk (1.11d) is implemented, the control problem will become unsolvable. It is then clear that for a real system with limited jerk capabilities (e.g. $\ddot{q}_{M_0} = 25 \text{ rad.s}^{-3}$), coping with a velocity limit using the classic formulation of the constraint is simply impossible.

On the other hand, when the new formulation of the joint rate constraint (1.14) is used, the system starts braking several time-steps before reaching the velocity limit (see Fig. 1.9).

Joint 0 is capable of coping with both joint rate and jerk¹⁹ limits (see Fig. 1.10)). Activating the hard-coded constraint on jerk (1.11d) will not result into an infeasible control problem and therefore, incompatibility between the joint rate and jerk constraints is resolved.

¹⁹ $\ddot{\bar{q}}_{M_0} = 25 \text{ rad.s}^{-3}$)

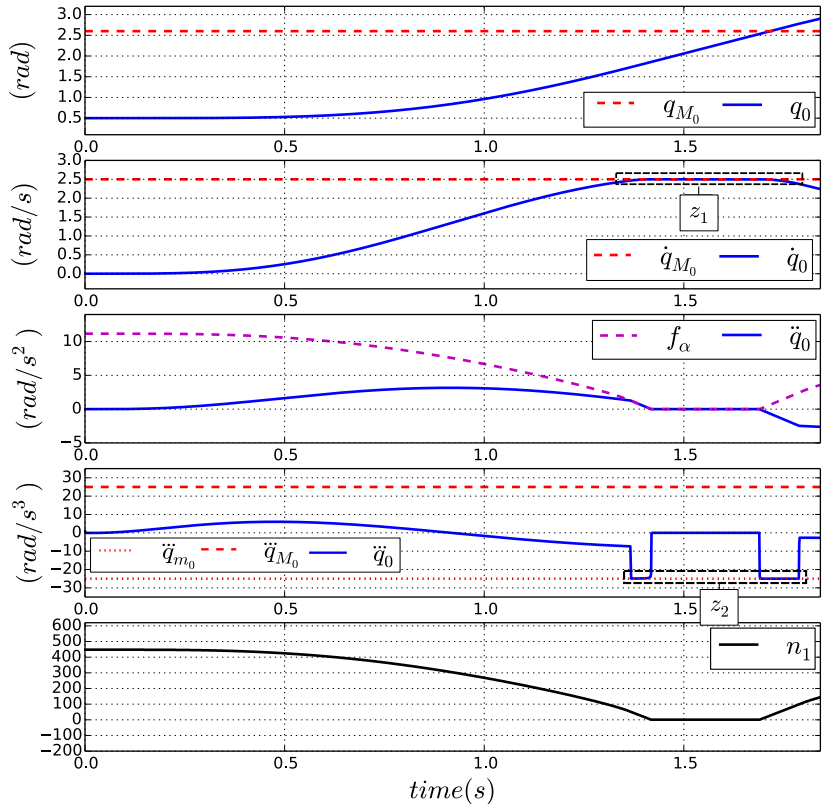


Figure 1.9: State S of joint 0 during the braking phase to cope with a maximum velocity limit. In this test, the new constraint formulation (1.14) that takes into account the jerk capability $\ddot{q}_{M_0} = 25 \text{ rad.s}^{-3}$ is used. Top to bottom: velocity, acceleration, jerk and n_1

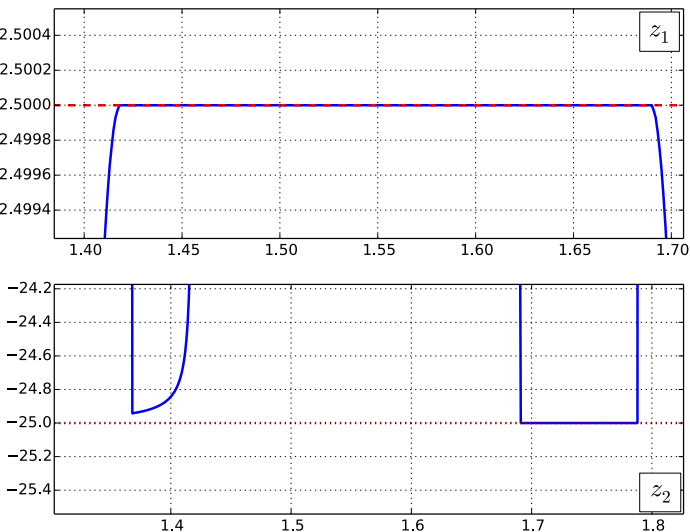


Figure 1.10: Zooms corresponding to Fig. 1.9.

1.3.2 Joint position constraint incompatibility with deceleration and/or jerk limits

The constraints on articular position (1.11a), acceleration (1.11c) and jerk (1.11d) may become incompatible if a joint gets close to one of its position limits too fast (see Fig. 1.4 and Fig. 1.5). In this case, the admissible deceleration and/or jerk may not be sufficient to allow a fast variation of the articular torque and it becomes impossible to bring both articular acceleration and velocity to zero within only one time-step duration. For example, the *complete* braking phase to cope with an upper position limit q_M is as following: the actuator starts jerking with maximum capability in the opposite direction. If maximum producible deceleration is reached, braking jerk is brought to zero and the *charged* deceleration is applied during several time-steps. The amount of deceleration in the joint is finally *de-charged* and brought to zero by jerking positively. At the end, the joint is stopped exactly on its position limit. As explained before, coping with a joint position constraint may fail because of incompatibilities with two other constraints: articular deceleration limits (1.8c) and jerk limits (1.8d). The resolution of these incompatibilities will be performed as following: First, independently from jerk capabilities, the expression of the position constraint (1.11a) is modified to include deceleration capabilities (e.g. \ddot{q}_m considering an upper position limit q_M). The joint will start braking using this deceleration during n_{3N} iterations before reaching q_M . The constraints on articular position (1.8a) and acceleration (1.8c) will be made compatible. The reflected constraint on the control variable $\ddot{q}_{|k}^c$ will be of the form:

$$f_\xi(\mathbf{q}_m, \ddot{\mathbf{q}}_M, n_4) \leq \ddot{q}_{|k}^c \leq f_\gamma(\mathbf{q}_M, \ddot{\mathbf{q}}_m, n_3) \quad (1.19)$$

Secondly, independently from deceleration capabilities, the expression of the position constraint (1.11a) is modified to include jerk capabilities (e.g. \dddot{q}_m considering an upper position limit q_M). Using this jerk, the joint will induce a braking movement during n_{5N} iterations so the constraints on articular position (1.8a) and jerk (1.8c) will become compatible. In this case, the reflected constraint on the control variable will be of the

form:

$$f_\theta(\mathbf{q}_m, \ddot{\mathbf{q}}_M, n_6) \leq \ddot{\mathbf{q}}_{|k}^c \leq f_\eta(\mathbf{q}_M, \ddot{\mathbf{q}}_m, n_5) \quad (1.20)$$

Because of undesired oscillations that may appear in the movement of the joint when using (1.20) to cope with a position limit, this formulation is modified as following to include at the same time the positive and negative jerk capabilities for a considered upper or lower position limit:

$$f_\mu(\mathbf{q}_m, \ddot{\mathbf{q}}_M, \ddot{\mathbf{q}}_m, n_8, n_{10}) \leq \ddot{\mathbf{q}}_{|k}^c \leq f_\lambda(\mathbf{q}_M, \ddot{\mathbf{q}}_m, \ddot{\mathbf{q}}_M, n_7, n_9) \quad (1.21)$$

Fourthly, an expression of the position constraint that takes into account at the same time both jerk and deceleration capabilities is formulated. Both constraints on articular acceleration (1.8c) and jerk (1.8d) will be made compatible with the constraint on articular position (1.8a). Reflected constraint on the control variable $\ddot{\mathbf{q}}_{|k}^c$ will be of the form:

$$f_\rho(\mathbf{q}_m, \ddot{\mathbf{q}}_M, \ddot{\mathbf{q}}_M, n_{12}, n_{14}) \leq \ddot{\mathbf{q}}_{|k}^c \leq f_\pi(\mathbf{q}_M, \ddot{\mathbf{q}}_m, \ddot{\mathbf{q}}_m, n_{11}, n_{13}) \quad (1.22)$$

Finally, using all the previous expressions, a formulation of the position constraint based on a **complete** description of the braking phase when coping with a Max/min position limit is proposed. This will include the deceleration *de-charging* sub-phase that is necessary to prevent any oscillations on the movement of the actuator. This new formulation takes into account both negative and positive jerk capabilities ($\ddot{\mathbf{q}}_m, \ddot{\mathbf{q}}_M$) in addition to the producible deceleration (e.g. $\ddot{\mathbf{q}}_m$ when coping with an upper position limit \mathbf{q}_M). Without any drawbacks²⁰, both constraints on articular deceleration (1.8c) and jerk (1.8d) will be made compatible with the articular position constraint (1.8a). Reflected constraint on the acceleration control variable will be of the form:

$$f_\chi(\mathbf{q}_m, \ddot{\mathbf{q}}_M, \ddot{\mathbf{q}}_M, \ddot{\mathbf{q}}_m, n_{16}, n_{18}, n_{20}) \leq \ddot{\mathbf{q}}_{|k}^c \leq f_\phi(\mathbf{q}_M, \ddot{\mathbf{q}}_m, \ddot{\mathbf{q}}_m, \ddot{\mathbf{q}}_M, n_{15}, n_{17}, n_{19}) \quad (1.23)$$

²⁰No oscillations on the movement of the joint.

$f_\xi, f_\gamma, f_\theta, f_\eta, f_\mu, f_\lambda, f_\rho, f_\pi, f_\chi, f_\phi$ will be defined in the upcoming subsections.

1.3.2.1 Joint position constraint incompatibility with deceleration limits

We consider the braking phase induced by a joint when stopping at its upper position limit \mathbf{q}_M . In this case, the maximum producible deceleration is $\ddot{\mathbf{q}}_m$. Jerk capabilities $\dddot{\mathbf{q}}_m$ are not considered. The state of the system during this phase can be described as following:

$$\begin{aligned} S_{|k+1} & \left\{ \begin{array}{l} \mathbf{q}_{|k+1} = \mathbf{q}_{|k} + \dot{\mathbf{q}}_{|k} \delta t, \\ \dot{\mathbf{q}}_{|k+1} = \dot{\mathbf{q}}_{|k} + \ddot{\mathbf{q}}_m \delta t. \end{array} \right. \\ S_{|k+2} & \left\{ \begin{array}{l} \mathbf{q}_{|k+2} = \mathbf{q}_{|k+1} + \dot{\mathbf{q}}_{|k+1} \delta t, \\ \dot{\mathbf{q}}_{|k+2} = \dot{\mathbf{q}}_{|k+1} + \ddot{\mathbf{q}}_m \delta t. \end{array} \right. \\ & \vdots \quad \vdots \\ S_{|k+n_3} & \left\{ \begin{array}{l} \mathbf{q}_{|k+n_3} = \mathbf{q}_{|k+n_3-1} + \dot{\mathbf{q}}_{|k+n_3-1} \delta t, \\ \dot{\mathbf{q}}_{|k+n_3} = \dot{\mathbf{q}}_{|k+n_3-1} + \ddot{\mathbf{q}}_m \delta t. \end{array} \right. \end{aligned} \tag{1.24}$$

With: $\mathbf{q}_{|k} \geq 0$, $\dot{\mathbf{q}}_{|k} \geq 0$ and $\ddot{\mathbf{q}}_m \leq 0$ (braking phase). The joint position evolution in $n_3 \geq 1$ iterations is equal to the general form of the numerical sequence (1.24):

$$\mathbf{q}_{|k+n_3} = \mathbf{q}_{|k} + n_3 \dot{\mathbf{q}}_{|k} \delta t + \frac{(n_3^2 - n_3)}{2} \ddot{\mathbf{q}}_m \delta t^2 \tag{1.25}$$

Finally, the condition $\mathbf{q}_{|k+n_3} \leq \mathbf{q}_M$ for all integer n_3 leads to:

$$\dot{\mathbf{q}}_{|k}^c \leq \underbrace{\frac{(\mathbf{q}_M - \mathbf{q}_{|k})}{n_3 \delta t} - \frac{(n_3 - 1)}{2} \ddot{\mathbf{q}}_m \delta t}_{f_{\gamma_{vel}}} \tag{1.26}$$

$\dot{q}_{|k}^c$ is the velocity control input in case the robot is controlled at the kinematic-level. The equivalent constraint on the acceleration control variable $\ddot{q}_{|k}^c$ (in case the robot is controlled at the dynamic-level) that generates the same²¹ braking profile can be written:

$$\ddot{q}_{|k}^c \leq \frac{(\mathbf{q}_M - \mathbf{q}_{|k})}{n_3 \delta t^2} - \frac{\dot{q}_{|k}}{\delta t} - \frac{(n_3 - 1)}{2} \ddot{q}_m \quad (1.27)$$

With:

$$n_3 = \frac{-\sqrt{-2\ddot{q}_m(\mathbf{q}_M - \mathbf{q}_{|k})}}{\ddot{q}_m \delta t} \quad (1.28)$$

the integer minimizing the right-hand side of (1.27).

Following the same reasoning for the lower position limit, when reflected on the acceleration control variable, the condition $\mathbf{q}_{|k+n_4} \geq \mathbf{q}_m$ for all integer $n_4 \geq 1$ leads to:

$$\ddot{q}_{|k}^c \geq \frac{(\mathbf{q}_m - \mathbf{q}_{|k})}{n_4 \delta t^2} - \frac{\dot{q}_{|k}}{\delta t} - \frac{(n_4 - 1)}{2} \ddot{q}_M \quad (1.29)$$

With:

$$n_4 = \frac{\sqrt{-2\ddot{q}_M(\mathbf{q}_m - \mathbf{q}_{|k})}}{\ddot{q}_M \delta t} \quad (1.30)$$

maximizing the right hand side of (1.29). f_ξ and f_γ are respectively equivalent to the right hand sides of (1.29) and (1.27).

1.3.2.1.1 Simulation

For this experiment, the controller is implemented with the new formulation of the position constraint (1.27) that takes into account the available deceleration capability ($\ddot{q}_{m_0} = -100 \text{ rad.s}^{-2}$). In this case, joint 0 is moving towards its maximum allowed position q_{M_0} . Fig. 1.11 shows the state of joint 0 as a braking phase is induced at the

²¹This can easily be proven as following: with a velocity control input $\dot{q}_{|k}^c$, articular velocity at the next time-step is $\dot{q}_{|k+1} = \dot{q}_{|k}^c$. On the other hand, in case of a dynamic level control input: $\dot{q}_{|k+1} = \dot{q}_{|k} + \ddot{q}_{|k}^c \delta t$. The relation between kinematic and dynamic control inputs that result in the same articular movement is: $\dot{q}_{|k} + \ddot{q}_{|k}^c \delta t = \dot{q}_{|k}^c$.

right time using the maximum available deceleration to cope with the upper position limit. As the articular jerk limits are not considered in this formulation of the position constraint, a jerk peak is seen at the beginning of the braking phase when the constraint (1.27) is activated. When this new formulation is used, including the hard-coded acceleration/deceleration constraint (1.11c) in the controller will not result into an infeasible control problem. Incompatibility between the articular position and deceleration constraints is resolved.

On the other hand, it has been impossible to cope with this same position limit using the classic formulation of the articular position constraint (1.11a). Much more deceleration capabilities (1.11c) are needed for a braking phase that is induced only one time-step before joint 0 reaches q_{M_0} .

Fig. 1.13 demonstrates how the starting time of the braking phase is automatically adapted to the amount of available deceleration. For example, when the deceleration capability \ddot{q}_{m_0} is reduced and fixed at -3 rad.s^{-2}). The braking phase starts earlier and lasts longer.

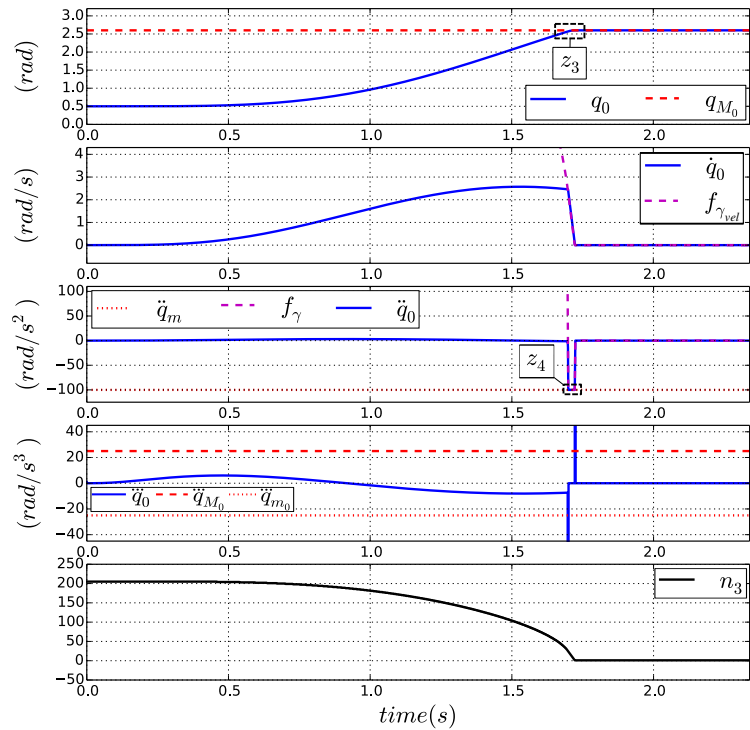


Figure 1.11: State S of joint 0 during the braking phase to cope with a maximum position limit M_0 ; The new constraint formulation (1.27) that takes into account the deceleration capability $\ddot{q}_{m_0} = -100 \text{ rad.s}^{-2}$ is used. Top to bottom: position, velocity, acceleration, jerk and n_3

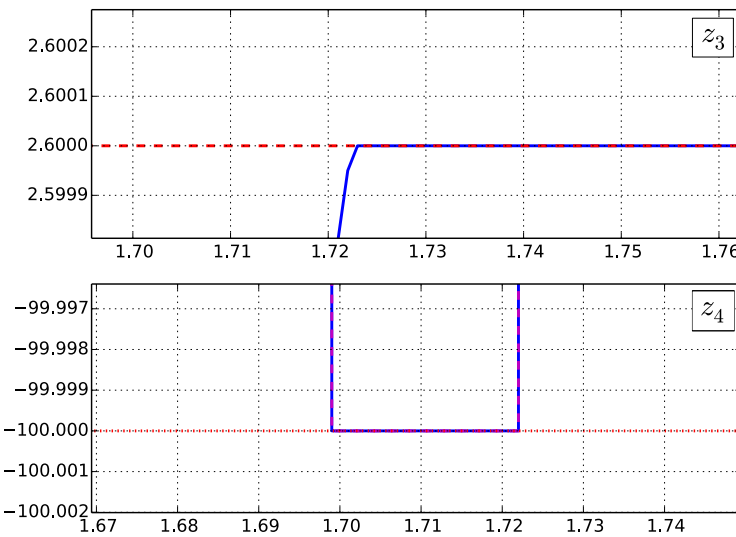
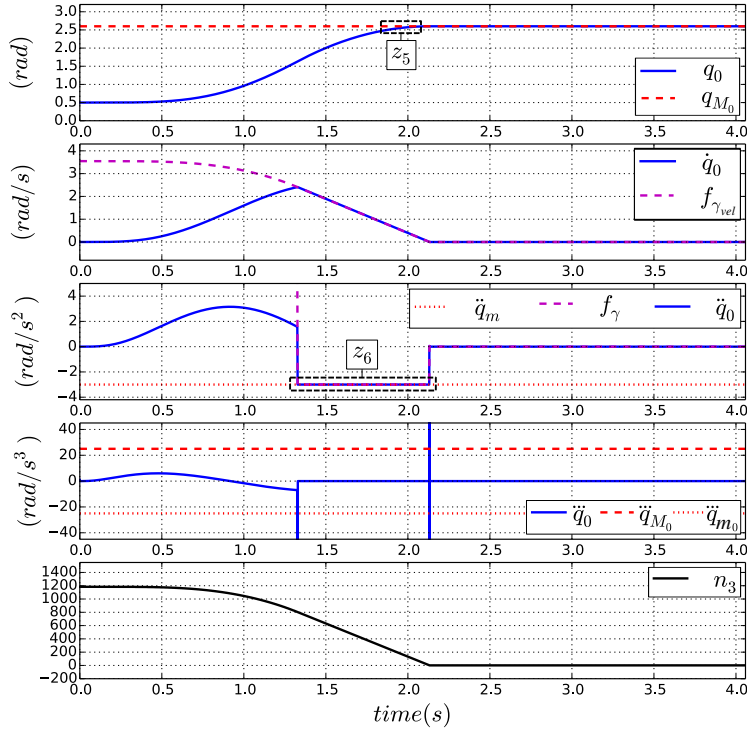


Figure 1.12: Zooms corresponding to Fig. 1.11.



28

Figure 1.13: State S of joint 0 during the braking phase to cope with a maximum position limit; The new constraint formulation (1.27) that takes into account the deceleration capability $\ddot{q}_{m_0} = -3 \text{ rad.s}^{-2}$ is used. Top to bottom: position, velocity, acceleration, jerk and n_3 .

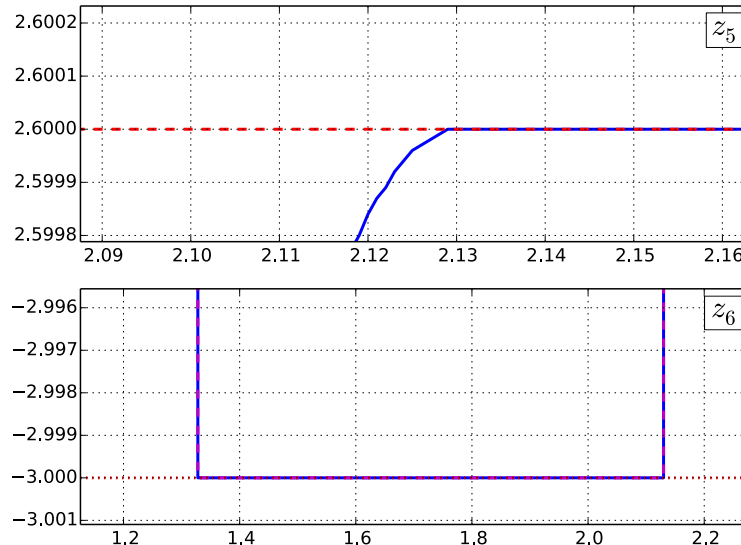


Figure 1.14: Zooms corresponding to Fig. 1.13.

1.3.2.2 Joint position constraint incompatibility with jerk limits

We consider the braking phase for a joint moving towards its upper position limit q_M . In this case, only the lower limit \ddot{q}_m of jerk capabilities is considered. Maximum producible deceleration \ddot{q}_m is not taken into account. The state S of the system during the induced braking phase can be described as following:

$$\begin{aligned} S_{|k+1} & \left\{ \begin{array}{l} q_{|k+1} = q_{|k} + \dot{q}_{|k}\delta t, \\ \dot{q}_{|k+1} = \dot{q}_{|k} + \ddot{q}\delta t, \\ \ddot{q}_{|k+1} = \ddot{q}_{|k} + \ddot{q}_m\delta t \end{array} \right. \\ S_{|k+2} & \left\{ \begin{array}{l} q_{|k+2} = q_{|k+1} + \dot{q}_{|k+1}\delta t, \\ \dot{q}_{|k+2} = \dot{q}_{|k+1} + \ddot{q}_{|k+1}\delta t, \\ \ddot{q}_{|k+2} = \ddot{q}_{|k+1} + \ddot{q}_m\delta t \end{array} \right. \\ & \vdots \quad \vdots \\ S_{|k+n_5} & \left\{ \begin{array}{l} q_{|k+n_5} = q_{|k+n_5-1} + \dot{q}_{|k+n_5-1}\delta t, \\ \dot{q}_{|k+n_5} = \dot{q}_{|k+n_5-1} + \ddot{q}_{|k+n_5-1}\delta t, \\ \ddot{q}_{|k+n_5} = \ddot{q}_{|k+n_5-1} + \ddot{q}_m\delta t \end{array} \right. \end{aligned} \tag{1.31}$$

With: $q_{|k} \geq 0$, $\dot{q}_{|k} \geq 0$ and $\ddot{q}_m \leq 0$. The joint position evolution within n_5 iterations is equal to the general form²² of the numerical sequence (1.31):

$$q_{|k+n_5} = q_{|k} + n_5 \dot{q}_{|k}\delta t + \frac{(n_5^2 - n_5)}{2} \ddot{q}_{|k}\delta t^2 + \left(\frac{n_5^3}{6} - \frac{n_5^2}{2} + \frac{n_5}{3} \right) \ddot{q}_m \delta t^3 \tag{1.32}$$

²²Computed using Maple.

Finally, the condition $\mathbf{q}_{|k+n_5} \leq \mathbf{q}_M$ for all integer n_5 leads to:

$$\ddot{\mathbf{q}}_{|k}^c \leq \frac{2(\mathbf{q}_M - \mathbf{q}_{|k})}{(n_5^2 - n_5)\delta t^2} - \frac{2\dot{\mathbf{q}}_{|k}}{(n_5 - 1)\delta t} - \frac{(\frac{n_5^2}{3} - n_5 + \frac{2}{3})}{(n_5 - 1)} \ddot{\mathbf{q}}_m \delta t \quad (1.33)$$

n_5 is the integer minimizing the right hand side of (1.33); It can be computed analytically.

By differentiating this expression w.r.t n_5 :

$$\left\{ \begin{array}{l} n_5 \geq 3, \\ -(\frac{1}{3}\ddot{\mathbf{q}}_m \delta t^3)n_5^4 + (\frac{2}{3}\ddot{\mathbf{q}}_{|m} \delta t^3)n_5^3 \\ +(2\dot{\mathbf{q}}_{|k} \delta t - \frac{1}{3}\ddot{\mathbf{q}}_m \delta t^3)n_5^2 \\ +4(\mathbf{q}_M - \mathbf{q}_{|k})n_5 - 2(\mathbf{q}_M - \mathbf{q}_{|k}) = 0 \end{array} \right. \quad (1.34)$$

n_5 is the rounded-up real root of (1.34).

Following the same reasoning for the lower position limit, the condition $\mathbf{q}_{|k+n_6} \geq \mathbf{q}_m$ for all integer $n_6 \geq 3$ can be reflected on the acceleration control variable as following:

$$\ddot{\mathbf{q}}_{|k}^c \geq \frac{2(\mathbf{q}_m - \mathbf{q}_{|k})}{(n_6^2 - n_6)\delta t^2} - \frac{2\dot{\mathbf{q}}_{|k}}{(n_6 - 1)\delta t} - \frac{(\frac{n_6^2}{3} - n_6 + \frac{2}{3})}{(n_6 - 1)} \ddot{\mathbf{q}}_M \delta t \quad (1.35)$$

With:

$$\left\{ \begin{array}{l} n_6 \geq 3, \\ -(\frac{1}{3}\ddot{\mathbf{q}}_M \delta t^3)n_6^4 + (\frac{2}{3}\ddot{\mathbf{q}}_{|M} \delta t^3)n_6^3 \\ +(2\dot{\mathbf{q}}_{|k} \delta t - \frac{1}{3}\ddot{\mathbf{q}}_M \delta t^3)n_6^2 \\ +4(\mathbf{q}_m - \mathbf{q}_{|k})n_6 - 2(\mathbf{q}_m - \mathbf{q}_{|k}) = 0 \end{array} \right. \quad (1.36)$$

n_6 is the rounded up real root of (1.36) that maximizes the right-hand side of (1.35). f_θ and f_η are respectively equivalent to the right hand sides of (1.35) and (1.33).

Algorithm 1 Compute n_5, n_6, f_θ and f_η

Require: $q_M, q_m, q_{|k}, \dot{q}_{|k}, \ddot{q}_M, \ddot{q}_m, \delta t$

- 1: $f_{\theta_{max}} \leftarrow \ddot{q}_m$ ▷ temporary lower bound of $\ddot{q}_{|k}^c$
- 2: $f_{\eta_{min}} \leftarrow \ddot{q}_M$ ▷ temporary upper bound of $\ddot{q}_{|k}^c$
- 3: **for** ($i = 3 \rightarrow N^a$) **do**
- 4: $n_5^* \leftarrow i$ $n_6^* \leftarrow i$
- 5: $f_\theta^* \leftarrow f_\theta(q_m, \ddot{q}_M, q_{|k}, \dot{q}_{|k}, \ddot{q}_M, n_6^*)$
- 6: $f_\eta^* \leftarrow f_\eta(q_M, \ddot{q}_m, q_{|k}, \dot{q}_{|k}, \ddot{q}_m, n_5^*)$
- 7: **if** ($f_\theta^* \geq f_{\theta_{max}}$) **then**
- 8: $f_{\theta_{max}} \leftarrow f_\theta^*$ $n_6 \leftarrow n_6^*$
- 9: **end if**
- 10: **if** ($f_\eta^* \leq f_{\eta_{min}}$) **then**
- 11: $f_{\eta_{min}} \leftarrow f_\eta^*$ $n_5 \leftarrow n_5^*$
- 12: **end if**
- 13: **end for**
- 14: $f_\theta \leftarrow f_{\theta_{max}}$ $f_\eta \leftarrow f_{\eta_{min}}$
- 15: **return** $n_5, n_6, f_\theta, f_\eta$

^a N can be fixed heuristically, it must however be \geq to the solutions of (1.34) and (1.36).

Algorithm 1 shows how n_5, n_6, f_θ and f_η can be computed numerically.

1.3.2.2.1 simulation

For this experiment, the controller is implemented with the new formulation of position constraint (1.33) that takes into account the available jerk capability ($\ddot{q}_{m_0} = -25 \text{ rad.s}^{-3}$). We also include the right-hand side of the hard-coded constraint on jerk (1.11d) ($\ddot{q}_{0|k} \leq \ddot{q}_{M_0} = 25 \text{ rad.s}^{-3}$). Joint 0 is moving towards its upper position limit q_{M_0} .

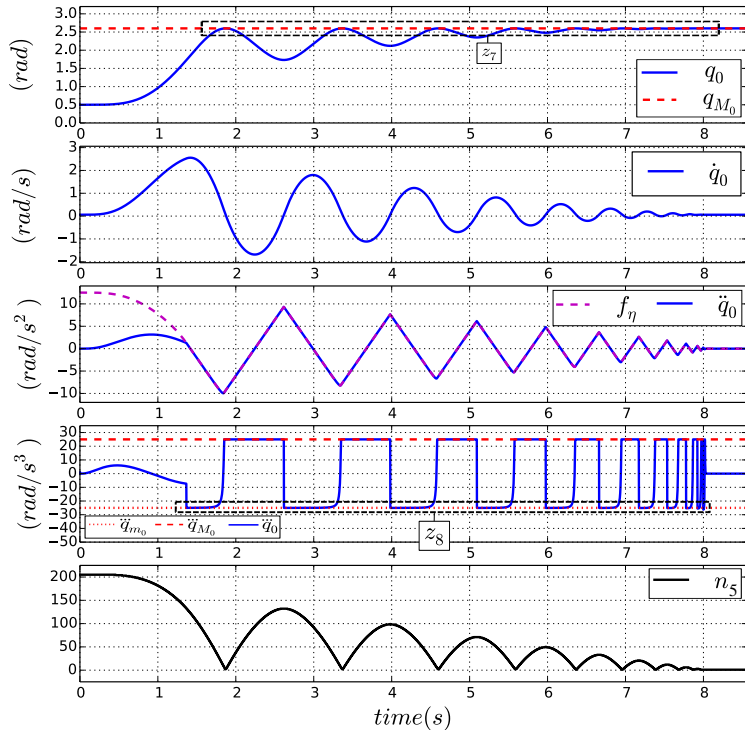
Fig. 1.15 illustrates how joint 0 starts braking with maximum negative jerk until its position limit is reached. The amount of *charged* deceleration should then be brought to 0. However, because of the hard-coded constraint on jerk, the amount of deceleration in the joint cannot be *de-charged* instantaneously. The joint position is then forced to move away from q_{M_0} and oscillates until completely *de-charging* the amount of deceleration it contains.

On the other hand, in case of an actuator with higher jerk capabilities, the decaying oscillations will be reduced (see Fig. 1.17 with $\ddot{q}_{m_0} = -2500 \text{ rad.s}^{-3}$). This makes the

proposed new formulation of position constraint more practical as the maximum amplitude of oscillations is significantly reduced (e.g. from 0.8 rad in Fig. 1.15 to 0.025 rad in Fig. 1.17).

The main reason for these oscillations is the non **complete** description of the braking phase in (1.31). Indeed, the *deceleration de-charging with positive jerk* sub-phase was not considered.

Also, as it appears in Fig. 1.16 and Fig. 1.18, the lower jerk limit is not completely satisfied. This is mainly due to the *discrete* description of the state of the joint during the braking phase (1.31). In this case, activating the hard-coded constraint on negative jerk ($\ddot{q}_{0|k} \geq \ddot{q}_{m_0} = -25 \text{ rad.s}^{-3}$, (1.11d)) will result into an infeasible control problem.



33

Figure 1.15: State S of joint 0 during the braking phase to cope with a maximum position limit q_{M_0} ; The new constraint formulation (1.33) that takes into account the jerk capability $\ddot{q}_{m_0} = -25 \text{ rad.s}^{-3}$ is used. Top to bottom: position, velocity, acceleration, jerk and n_5 .

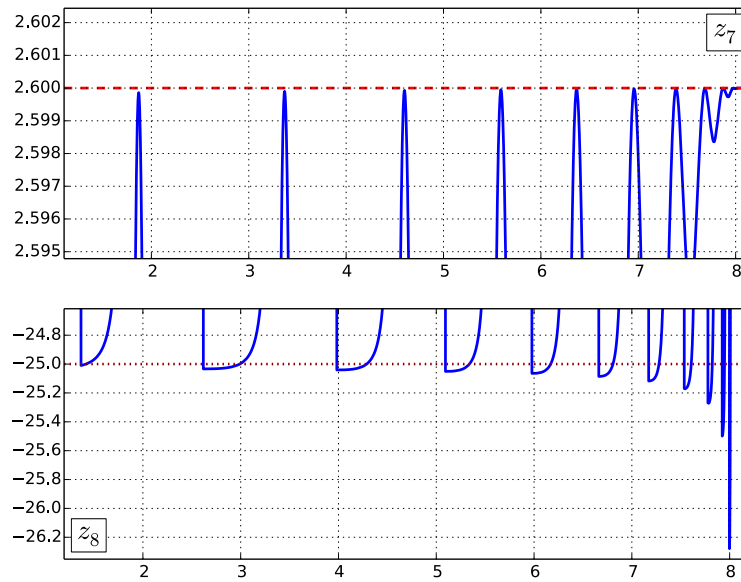
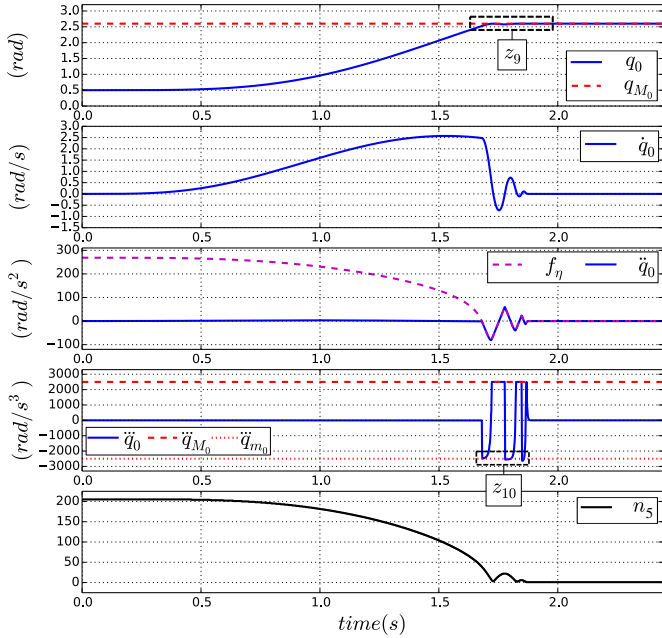


Figure 1.16: Zooms corresponding to Fig. 1.15.



34

Figure 1.17: State S of joint 0 during the braking phase to cope with a maximum position limit; The new constraint formulation (1.33) that takes into account the jerk capability $\ddot{q}_{m_0} = -2500 \text{ rad.s}^{-3}$. Top to bottom: position, velocity, acceleration, jerk and n_5 .

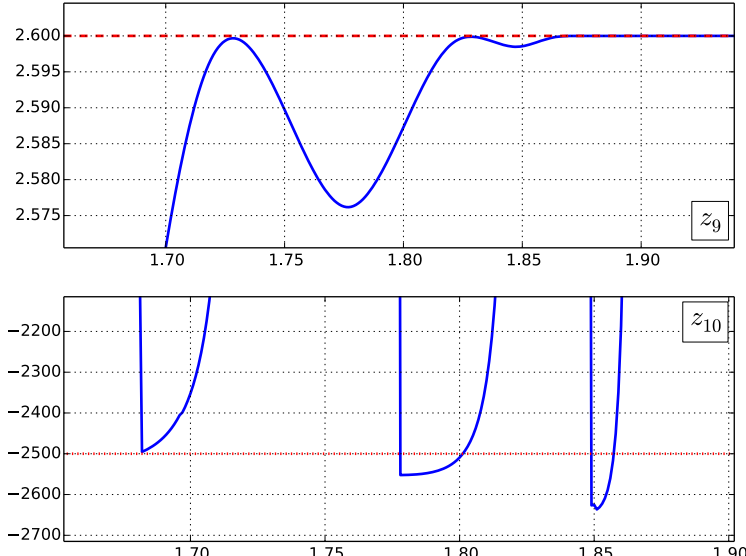


Figure 1.18: Zooms corresponding to Fig. 1.17.

1.3.2.3 Joint position constraint incompatibility with jerk limits, complete braking phase

As previously explained, To palliate the oscillations on the movement of joint 0 when coping with its position limit, a more **complete** description of the braking phase must be used. The same movement of joint 0 hitting its upper position limit is considered. This time, the new formulation of articular position constraint will include both lower \ddot{q}_m and upper \ddot{q}_M jerk limits. The induced braking phase will be as following: joint 0 will start jerking during n_{7N} iterations in the opposite direction forcing itself to decelerate. The reached deceleration is then *released* by jerking positively in the direction of the position limit during n_{9N} iterations. Maximum producible deceleration \ddot{q}_m is not considered. The state S of the system during this braking phase can be described as following:

$$\begin{aligned}
 S_{|k+1} & \left\{ \begin{array}{l} q_{|k+1} = q_{|k} + \dot{q}_{|k} \delta t, \\ \dot{q}_{|k+1} = \dot{q}_{|k} + \ddot{q} \delta t, \\ \ddot{q}_{|k+1} = \ddot{q}_{|k} + \ddot{q}_m \delta t \\ \vdots \quad \vdots \end{array} \right. & \left. \right\} & \text{Equivalent to (1.31)} \\
 S_{|k+n_7} & \left\{ \begin{array}{l} q_{|k+n_7} = q_{|k+n_7-1} + \dot{q}_{|k+n_7-1} \delta t, \\ \dot{q}_{|k+n_7} = \dot{q}_{|k+n_7-1} + \ddot{q}_{|k+n_7-1} \delta t, \\ \ddot{q}_{|k+n_7} = \ddot{q}_{|k+n_7-1} + \ddot{q}_m \delta t \end{array} \right. & \left. \right\} \\
 S_{|k+n_7+1} & \left\{ \begin{array}{l} q_{|k+n_7+1} = q_{|k+n_7} + \dot{q}_{|k+n_7} \delta t, \\ \dot{q}_{|k+n_7+1} = \dot{q}_{|k+n_7} + \ddot{q} \delta t, \\ \ddot{q}_{|k+n_7+1} = \ddot{q}_{|k+n_7} + \ddot{q}_M \delta t \\ \vdots \quad \vdots \end{array} \right. & \left. \right\} & \text{Equivalent to (1.31)} \\
 S_{|k+n_7+n_9} & \left\{ \begin{array}{l} q_{|k+n_7+n_9} = q_{|k+n_7+n_9-1} + \dot{q}_{|k+n_7+n_9-1} \delta t, \\ \dot{q}_{|k+n_7+n_9} = \dot{q}_{|k+n_7+n_9-1} + \ddot{q}_{|k+n_7+n_9-1} \delta t, \\ \ddot{q}_{|k+n_7+n_9} = \ddot{q}_{|k+n_7+n_9-1} + \ddot{q}_M \delta t \end{array} \right. & \left. \right\} &
 \end{aligned} \tag{1.37}$$

With: $\mathbf{q}_{|k} \geq 0$, $\dot{\mathbf{q}}_{|k} \geq 0$, $\ddot{\mathbf{q}}_m \leq 0$ and $\ddot{\mathbf{q}}_M \geq 0$. The joint position evolution in $(n_7 + n_9)$ iterations is equal to the general form of the numerical sequence (1.37):

$$\mathbf{q}_{|k+n_7+n_9} = \mathbf{q}_{|k+n_7} + n_9 \dot{\mathbf{q}}_{|k+n_7} \delta t + \frac{(n_9^2 - n_7)}{2} \ddot{\mathbf{q}}_{|k+n_7} \delta t^2 + \left(\frac{n_9^3}{6} - \frac{n_9^2}{2} + \frac{n_9}{3} \right) \ddot{\mathbf{q}}_M \delta t^3 \quad (1.38)$$

$\mathbf{q}_{|k+n_7}$ and $\dot{\mathbf{q}}_{|k+n_7}$ are respectively equivalent to (1.32) and (1.13). And:

$$\ddot{\mathbf{q}}_{|k+n_7} = \ddot{\mathbf{q}}_{|k} + n_7 \ddot{\mathbf{q}}_m \delta t \quad (1.39)$$

When developed, (1.38) is written:

$$\begin{aligned} \mathbf{q}_{|k+n_7+n_9} = & \mathbf{q}_{|k} + (n_7 + n_9) \dot{\mathbf{q}}_{|k} \delta t + \left[(n_7 n_9) + \frac{(n_7^2 - n_7) + (n_9^2 - n_9)}{2} \right] \ddot{\mathbf{q}}_{|k} \delta t^2 \\ & + \left[\frac{n_7(n_9^2 - n_9) + n_9(n_7^2 - n_7)}{2} + \left(\frac{n_7^3}{6} - \frac{n_7^2}{2} + \frac{n_7}{3} \right) \right] \ddot{\mathbf{q}}_m \delta t^3 \\ & + \left(\frac{n_9^3}{6} - \frac{n_9^2}{2} + \frac{n_9}{3} \right) \ddot{\mathbf{q}}_M \delta t^3 \end{aligned} \quad (1.40)$$

Finally, the condition $\mathbf{q}_{|k+n_7+n_9} \leq \mathbf{q}_M$ for all integers (n_7, n_9) leads to:

$$\begin{aligned} \ddot{\mathbf{q}}_{|k}^c \leq & \frac{(\mathbf{q}_M - \mathbf{q}_{|k})}{\left[(n_7 n_9) + \frac{(n_7^2 - n_7) + (n_9^2 - n_9)}{2} \right] \delta t^2} + \frac{(n_7 + n_9) \dot{\mathbf{q}}_{|k}}{\left[(n_7 n_9) + \frac{(n_7^2 - n_7) + (n_9^2 - n_9)}{2} \right] \delta t} \\ & + \frac{\left[\frac{n_7(n_9^2 - n_9) + n_9(n_7^2 - n_7)}{2} + \left(\frac{n_7^3}{6} - \frac{n_7^2}{2} + \frac{n_7}{3} \right) \right] \ddot{\mathbf{q}}_m \delta t}{\left[(n_7 n_9) + \frac{(n_7^2 - n_7) + (n_9^2 - n_9)}{2} \right]} \\ & + \frac{\left(\frac{n_9^3}{6} - \frac{n_9^2}{2} + \frac{n_9}{3} \right) \ddot{\mathbf{q}}_M \delta t}{\left[(n_7 n_9) + \frac{(n_7^2 - n_7) + (n_9^2 - n_9)}{2} \right]} \end{aligned} \quad (1.41)$$

(n_7, n_9) are the two integers minimizing the right-hand side of (1.41). Following the same reasoning for the lower position limit, the condition $\mathbf{q}_{|k+n_8+n_{10}} \geq \mathbf{q}_m$ can be reflected on

the acceleration control variable as follows:

$$\begin{aligned} \ddot{\mathbf{q}}_{|k}^c \geq & \frac{(\mathbf{q}_m - \mathbf{q}_{|k})}{[(n_8 n_{10}) + \frac{(n_8^2 - n_8) + (n_{10}^2 - n_{10})}{2}] \delta t^2} + \frac{(n_8 + n_{10}) \dot{\mathbf{q}}_{|k}}{[(n_8 n_{10}) + \frac{(n_8^2 - n_8) + (n_{10}^2 - n_{10})}{2}] \delta t} \\ & + \frac{[\frac{n_8(n_{10}^2 - n_{10}) + n_{10}(n_8^2 - n_8)}{2} + (\frac{n_8^3}{6} - \frac{n_8^2}{2} + \frac{n_8}{3})] \ddot{\mathbf{q}}_M \delta t}{[(n_8 n_{10}) + \frac{(n_8^2 - n_8) + (n_{10}^2 - n_{10})}{2}]} \\ & + \frac{(\frac{n_{10}^3}{6} - \frac{n_{10}^2}{2} + \frac{n_{10}}{3}) \ddot{\mathbf{q}}_m \delta t}{[(n_8 n_{10}) + \frac{(n_8^2 - n_8) + (n_{10}^2 - n_{10})}{2}]} \end{aligned} \quad (1.42)$$

(n_8, n_{10}) are the two integers maximizing the right-hand side of (1.41). f_μ and f_λ are respectively equivalent to the right hand sides of (1.42) and (1.41).

Algorithm 2 Compute $n_7, n_8, n_9, n_{10}, f_\mu$ and f_λ

Require: $q_M, q_m, q|_k, \dot{q}|_k, \ddot{q}_M, \ddot{q}_m, \delta t$

```

1:  $f_{\mu_{max}} \leftarrow \ddot{q}_m$                                 ▷ temporary lower bound of  $\ddot{q}|_k^c$ 
2:  $f_{\lambda_{min}} \leftarrow \ddot{q}_M$                             ▷ temporary upper bound of  $\ddot{q}|_k^c$ 
3: for ( $i = 1 \rightarrow N^a$ ) do
4:    $n_8^* \leftarrow i$        $n_7^* \leftarrow i$ 
5:   if ( $\ddot{q}|_k \geq 0$ ) then  $n_9^* \leftarrow n_7^* - \left\lfloor \frac{\ddot{q}|_k}{\ddot{q}_m \delta t} \right\rfloor$      $n_{10}^* \leftarrow n_8^* + \left\lceil \frac{\ddot{q}|_k}{\ddot{q}_M \delta t} \right\rceil$ 
6:   if ( $\ddot{q}|_k < 0$ ) then
7:      $n_9^* \leftarrow n_7^* + \left\lfloor \frac{\ddot{q}|_k}{\ddot{q}_M \delta t} \right\rfloor$      $n_{10}^* \leftarrow n_8^* - \left\lceil \frac{\ddot{q}|_k}{\ddot{q}_m \delta t} \right\rceil$ 
8:     if ( $n_7^* \leq 1$ ) then  $n_9^* \leftarrow \left\lfloor \frac{\ddot{q}|_k}{\ddot{q}_M \delta t} \right\rfloor$ 
9:     if ( $n_8^* \leq 1$ ) then  $n_{10}^* \leftarrow \left\lceil \frac{\ddot{q}|_k}{\ddot{q}_m \delta t} \right\rceil$ 
10:    end if
11:    if ( $n_7^* \leq 1$ ) then  $n_7^* \leftarrow 1$ 
12:    if ( $n_8^* \leq 1$ ) then  $n_8^* \leftarrow 1$ 
13:    if ( $n_9^* \leq 2$ ) then  $n_9^* \leftarrow 2$ 
14:    if ( $n_{10}^* \leq 2$ ) then  $n_{10}^* \leftarrow 2$ 
15:     $f_\mu^* \leftarrow f_\mu(q_m, \ddot{q}_M, q|_k, \dot{q}|_k, \ddot{q}_m, n_8^*, n_{10}^*)$ 
16:     $f_\lambda^* \leftarrow f_\lambda(q_M, \ddot{q}_m, q|_k, \dot{q}|_k, \ddot{q}_M, n_7^*, n_9^*)$ 
17:    if ( $f_\mu^* \geq f_{\mu_{max}}$ ) then
18:       $f_{\mu_{max}} \leftarrow f_\mu^*$      $n_8 \leftarrow n_8^*$      $n_{10}^b \leftarrow n_{10}^*$ 
19:    end if
20:    if ( $f_\lambda^* \leq f_{\lambda_{min}}$ ) then
21:       $f_{\lambda_{min}} \leftarrow f_\lambda^*$      $n_7 \leftarrow n_7^*$      $n_9^a \leftarrow n_9^*$ 
22:    end if
23:  end for
24:   $f_\mu \leftarrow f_{\mu_{max}}$      $f_\lambda \leftarrow f_{\lambda_{min}}$ 
25: return  $n_7, n_8, n_9, n_{10}, f_\mu, f_\lambda$ 

```

^a N is fixed heuristically, it must however be \geq to the total number of iterations needed to perform the braking movement described in (1.37).

^b For calculation stability in the computation of f_μ and f_λ , (n_9^*, n_{10}^*) are used as real numbers (even if previously defined as numbers of iterations). The same for n_9 and n_{10} .

Algorithm 2 shows how $n_7, n_8, n_9, n_{10}, f_\mu$ and f_λ can be computed numerically.

1.3.2.3.1 Simulation

For this experiment, the controller is implemented with the new formulation of the position constraint (1.41) that takes into account both positive and negative jerk capabilities ($[\ddot{q}_{m_0}, \ddot{q}_{M_0}] = [-25, 25] \text{ rad.s}^{-3}$). In this case, joint 0 is also moving towards its upper position limit q_{M_0} .

Fig. 1.19 depicts how joint 0 starts braking with maximum negative then positive jerk until reaching its position limit; The amount of *charged* deceleration is then released and brought to 0. We also highlight that no oscillations appear when using this more complete description of the braking phase to formulate the position constraint.

On the other hand, we underline an exceeding of 0.013 rad.s^{-3} over the jerk limit \ddot{q}_{m_0} (see Fig. 1.20). Also, as it appears in the joint jerk profile, the positive jerk capability is not fully used when de-charging the accumulated deceleration. This is caused by the *discrete* description of the state of joint 0 during its braking phase (1.37).

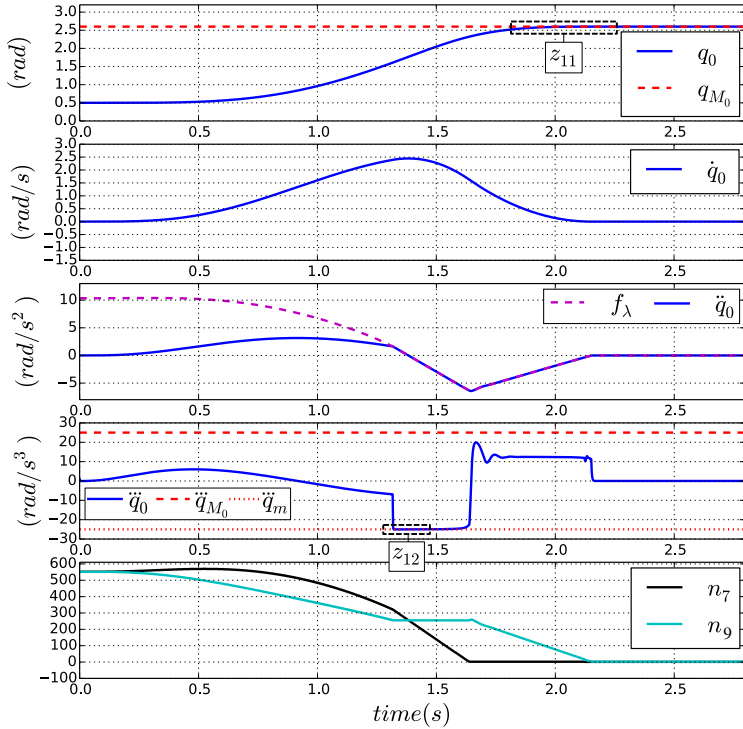


Figure 1.19: State S of joint 0 during the braking phase to cope with a maximum position limit q_{M_0} ; The new constraint formulation (1.41) that takes into account both positive and negative jerk capabilities $[\ddot{q}_{m_0}, \ddot{q}_{M_0}] = [-25, 25] \text{ rad.s}^{-3}$ is used. Top to bottom: position, velocity, acceleration, jerk and (n_7, n_9) .

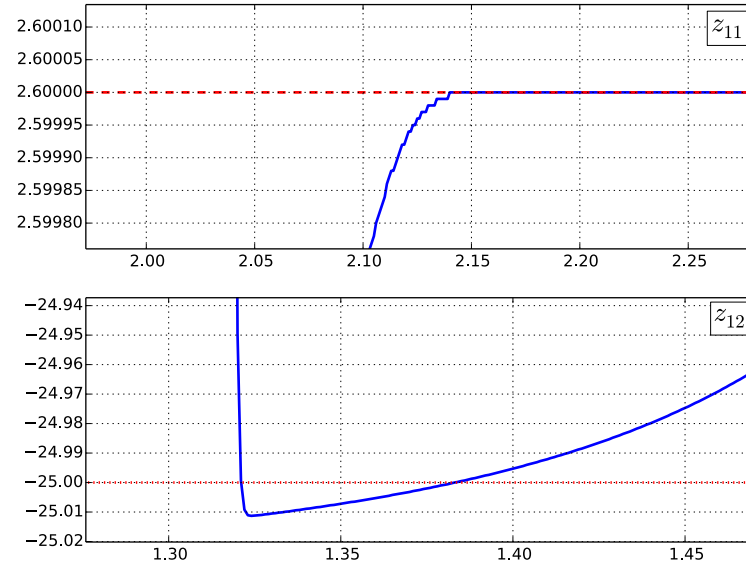


Figure 1.20: Zooms corresponding to Fig. 1.19.

1.3.2.4 Joint position constraint incompatibility with both deceleration and jerk limits

In all the previously introduced new formulations, jerk and deceleration capabilities have been independently considered for the mathematical expressions of articular position constraints when coping with an upper joint limit q_M . As already explained, these capabilities ($\ddot{q}_m, \ddot{\ddot{q}}_m, \ddot{\ddot{q}}_M$) should appear together in the expression of the position constraint. Indeed, during the braking phase induced to stop a joint at its upper limit, the joint starts jerking negatively in the opposite direction during n_{11_N} iterations. If *maximum deceleration is reached*, the joint stops jerking and the *charged* deceleration is applied for n_{13_N} iterations. Finally, the amount of deceleration in the joint is *de-charged* and released during several time-steps by jerking positively towards the position limit.

In the following example, for pedagogical reasons, the braking phase to cope with a maximum position limit is considered without the *deceleration de-charging* sub-phase. The **complete** braking phase that we just described will be used for the final formulation of the articular position constraint. The state S of the system during $(n_{11_N} + n_{13_N})$ iterations can be described as following:

$$\left. \begin{array}{l}
S_{|k+1} \left\{ \begin{array}{ll} \mathbf{q}_{|k+1} & = \mathbf{q}_{|k} + \dot{\mathbf{q}}_{|k} \delta t, \\ \dot{\mathbf{q}}_{|k+1} & = \dot{\mathbf{q}}_{|k} + \ddot{\mathbf{q}}_{|k} \delta t, \\ \ddot{\mathbf{q}}_{|k+1} & = \ddot{\mathbf{q}}_{|k} + \ddot{\mathbf{q}}_m \delta t \\ \vdots & \vdots \end{array} \right. \\ S_{|k+n_{11}} \left\{ \begin{array}{ll} \mathbf{q}_{|k+n_{11}} & = \mathbf{q}_{|k+n_{11}-1} + \dot{\mathbf{q}}_{|k+n_{11}-1} \delta t, \\ \dot{\mathbf{q}}_{|k+n_{11}} & = \dot{\mathbf{q}}_{|k+n_{11}-1} + \ddot{\mathbf{q}}_{|k+n_{11}-1} \delta t, \\ \ddot{\mathbf{q}}_{|k+n_{11}} & = \ddot{\mathbf{q}}_{|k+n_{11}-1} + \ddot{\mathbf{q}}_m \delta t \end{array} \right. \\ S_{|k+n_{11}+1} \left\{ \begin{array}{ll} \mathbf{q}_{|k+n_{11}+1} & = \mathbf{q}_{|k+n_{11}} + \dot{\mathbf{q}}_{|k+n_{11}} \delta t, \\ \dot{\mathbf{q}}_{|k+n_{11}+1} & = \dot{\mathbf{q}}_{|k+n_{11}} + \ddot{\mathbf{q}}_m \delta t, \\ \vdots & \vdots \end{array} \right. \\ S_{|k+n_{11}+n_{13}} \left\{ \begin{array}{ll} \mathbf{q}_{|k+n_{11}+n_{13}} & = \mathbf{q}_{|k+n_{11}+n_{13}-1} + \dot{\mathbf{q}}_{|k+n_{11}+n_{13}-1} \delta t, \\ \dot{\mathbf{q}}_{|k+n_{11}+n_{13}} & = \dot{\mathbf{q}}_{|k+n_{11}+n_{13}-1} + \ddot{\mathbf{q}}_m \delta t, \end{array} \right. \end{array} \right\} \text{Equivalent to (1.31)} \quad (1.43)$$

The articular position evolution is equal to the general form of the numerical sequence (1.43):

$$\mathbf{q}_{|k+n_{11}+n_{13}} = \mathbf{q}_{|k+n_{11}} + n_{13} \dot{\mathbf{q}}_{|k+n_{11}} \delta t + \frac{(n_{13}^2 - n_{13})}{2} \ddot{\mathbf{q}}_m \delta t^2 \quad (1.44)$$

With: $\mathbf{q}_{|k+n_{11}}$ and $\dot{\mathbf{q}}_{k+n_{11}}$ respectively equivalent to (1.32) and (1.13). When developed, (1.44) is written:

$$\begin{aligned} \mathbf{q}_{|k+n_{11}+n_{13}} &= \mathbf{q}_{|k} + (n_{11} + n_{13})\dot{\mathbf{q}}_{|k}\delta t \\ &\quad + \left(\frac{n_{11}^2 - n_{11}}{2} + n_{11}n_{13}\right)\ddot{\mathbf{q}}_{|k}\delta t^2 \\ &\quad + \left[\left(\frac{n_{11}^3}{6} - \frac{n_{11}^2}{2} + \frac{n_{11}}{3}\right) + \frac{n_{13}(n_{11}^2 - n_{11})}{2}\right]\ddot{\mathbf{q}}_m\delta t^3 \\ &\quad + \frac{(n_{13}^2 - n_{13})}{2}\ddot{\mathbf{q}}_m\delta t^2 \end{aligned} \quad (1.45)$$

With: $\mathbf{q}_{|k} \geq 0$, $\dot{\mathbf{q}}_{|k} \geq 0$, $\ddot{\mathbf{q}}_m \leq 0$ and $\ddot{\mathbf{q}}_m \leq 0$. The condition $\mathbf{q}_{|k+n_{11}+n_{13}} \leq \mathbf{q}_M$ for all integers (n_{11}, n_{13}) in case of a dynamic-level control leads to:

$$\begin{aligned} \ddot{\mathbf{q}}_{|k}^c &\leq \frac{(\mathbf{q}_M - \mathbf{q}_{|k})}{\left(\frac{n_{11}^2 - n_{11}}{2} + n_{11}n_{13}\right)\delta t^2} - \frac{(n_{11} + n_{13})}{\left(\frac{n_{11}^2 - n_{11}}{2} + n_{11}n_{13}\right)\delta t}\dot{\mathbf{q}}_{|k} \\ &\quad - \frac{\left[\frac{n_{11}^3}{6} - \frac{n_{11}^2}{2} + \frac{n_{11}}{3} + \frac{n_{13}(n_{11}^2 - n_{11})}{2}\right]\ddot{\mathbf{q}}_m\delta t}{\left(\frac{n_{11}^2 - n_{11}}{2} + n_{11}n_{13}\right)} \\ &\quad - \frac{(n_{13}^2 - n_{13})}{(n_{11}^2 - n_{11} + 2n_{11}n_{13})}\ddot{\mathbf{q}}_m \end{aligned} \quad (1.46)$$

In case the control is performed at the kinematic-level, the constraint can be reflected on $\dot{\mathbf{q}}_{|k}^c$ as following:

$$\begin{aligned} \dot{\mathbf{q}}_{|k}^c &\leq \frac{(\mathbf{q}_M - \mathbf{q}_{|k})}{(n_{11} + n_{13})\delta t} - \frac{\left[\frac{(n_{11}^2 - n_{11})}{2} + n_{11}n_{13}\right]\ddot{\mathbf{q}}_{|k}\delta t}{(n_{11} + n_{13})} \\ &\quad - \frac{\left[\frac{(n_{11}^3)}{6} + \frac{(n_{11}^2)}{2} + \frac{(n_{11})}{3} + \frac{n_{13}(n_{11}^2 - n_{11})}{2}\right]\ddot{\mathbf{q}}_m\delta t^2}{(n_{11} + n_{13})} \\ &\quad - \frac{(n_{13}^2 - n_{13})}{2(n_{11} + n_{13})}\ddot{\mathbf{q}}_m\delta t \end{aligned} \quad (1.47)$$

(n_{11}, n_{13}) are the two integers minimizing the right-hand side of (1.46). Following the same reasoning for the lower position limit, for all integers (n_{12}, n_{14}) , the constraint

$\mathbf{q}_{|k+n_{12}+n_{14}} \geq \mathbf{q}_m$ can be reflected on the acceleration control variable as following:

$$\begin{aligned}\ddot{\mathbf{q}}_{|k}^c &\geq \frac{(\mathbf{q}_m - \mathbf{q}_{|k})}{\left(\frac{n_{12}^2 - n_{12}}{2} + n_{12}n_{14}\right)\delta t^2} \\ &- \frac{\left[\frac{n_{12}^3}{6} - \frac{n_{12}^2}{2} + \frac{n_{12}}{3} + \frac{n_{14}(n_{12}^2 - n_{12})}{2}\right]\ddot{\mathbf{q}}_M\delta t}{\left(\frac{n_{12}^2 - n_{12}}{2} + n_{12}n_{14}\right)} \\ &- \frac{(n_{12} + n_{14})}{\left(\frac{n_{12}^2 - n_{12}}{2} + n_{12}n_{14}\right)\delta t}\dot{\mathbf{q}}_{|k} - \frac{(n_{14}^2 - n_{14})}{(n_{12}^2 - n_{12} + 2n_{12}n_{14})}\ddot{\mathbf{q}}_M\end{aligned}\quad (1.48)$$

(n_{12}, n_{14}) are the two integers maximizing the right-hand side of (1.48). f_ρ and f_π are respectively equivalent to the right hand sides of (1.46) and (1.48).

Algorithm 3 Compute $n_{11}, n_{12}, n_{13}, n_{14}, f_\rho$ and f_π

Require: $q_M, q_m, q|_k, \ddot{q}|_k, \ddot{q}_M, \ddot{q}_m, \ddot{\ddot{q}}_M, \ddot{\ddot{q}}_m, \delta t$

```

1:  $f_{\rho_{max}} \leftarrow \ddot{q}_m$ 
2:  $f_{\pi_{min}} \leftarrow \ddot{q}_M$ 
3: for ( $i_1 = 3 \rightarrow N_1^a$ ) do
4:    $n_{11}^* \leftarrow 3$ 
5:    $n_{12}^* \leftarrow 3$ 
6:   for ( $i_2 = 1 \rightarrow N_2^a$ ) do
7:      $n_{13}^* \leftarrow i_2$ 
8:      $n_{14}^* \leftarrow i_2$ 
9:      $f_\rho^* \leftarrow f_\rho(q_m, q|_k, \ddot{q}|_k, \ddot{q}_M, \ddot{q}_m, n_{12}^*, n_{14}^*)$ 
10:     $f_\pi^* \leftarrow f_\pi(q_M, q|_k, \ddot{q}|_k, \ddot{q}_m, \ddot{q}_m, n_{11}^*, n_{13}^*)$ 
11:    if ( $f_\rho^* \geq f_{\rho_{max}}$ ) then
12:       $f_{\rho_{max}} \leftarrow f_\rho^*$ 
13:       $n_{12} \leftarrow n_{12}^*$ 
14:       $n_{14} \leftarrow n_{14}^*$ 
15:    end if
16:    if ( $f_\pi^* \leq f_{\pi_{min}}$ ) then
17:       $f_{\pi_{min}} \leftarrow f_\pi^*$ 
18:       $n_{11} \leftarrow n_{11}^*$ 
19:       $n_{13} \leftarrow n_{13}^*$ 
20:    end if
21:  end for
22: end for
23:  $f_\rho \leftarrow f_{\rho_{max}}$ 
24:  $f_\pi \leftarrow f_{\pi_{min}}$ 
25: return  $n_{11}, n_{12}, n_{13}, n_{14}, f_\rho, f_\pi$ 

```

^a N_1 and N_2 are fixed heuristically, they must however be \geq to the number of iterations needed to perform the braking movement described in (1.43).

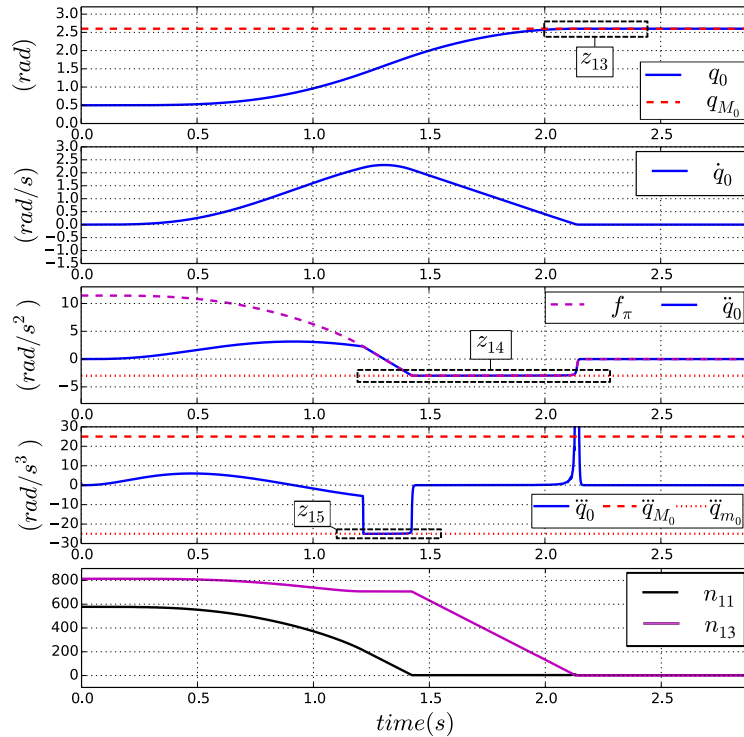
Algorithm 3 shows how $n_{11}, n_{13}, n_{12}, n_{14}, f_\rho$ and f_π can be computed numerically.

1.3.2.4.1 Simulation

For this experiment, the controller is implemented with the new formulation of position constraint (1.46) that takes into account both jerk ($\ddot{\ddot{q}}_{m_0} = -25 \text{ rad.s}^{-3}$) and deceleration capabilities \ddot{q}_{m_0} . In Fig. 1.15, the amplitude of deceleration corresponding to the first oscillation reaches -10 rad.s^{-2} . To demonstrate the interest of using the new formula-

tion, \ddot{q}_{m_0} is diminished to -3 rad.s^{-2} . We consider the same movement for joint 0 hitting its upper position limit q_{M_0} . No hard-coded constraints on the articular jerk (1.11d) are implemented.

Fig. 1.21 illustrates how joint 0 starts braking with negative jerk until maximum deceleration is reached. This deceleration is then used to stop the joint at its position limit. As no hard-coded constraints on jerk are activated, deceleration is *de-charged* almost instantaneously and a high peak of jerk is created. Otherwise, decaying oscillations would also appear as in Fig. 1.15. We also underline an exceeding of (0.013 rad.s^{-3}) over the minimum jerk limit. On the other hand, the deceleration limit is well satisfied (see Fig. 1.21).



47

Figure 1.21: State S of joint 0 during the braking phase to cope with a maximum position limit q_{M_0} ; The new constraint formulation (1.46) that takes into account both deceleration and jerk capabilities $\ddot{q}_{m_0} = -25 \text{ rad.s}^{-3}$, $\ddot{q}_{m_0} = -3 \text{ rad.s}^{-2}$ is used. Top to bottom: position, velocity, acceleration, jerk and (n_{11}, n_{13})

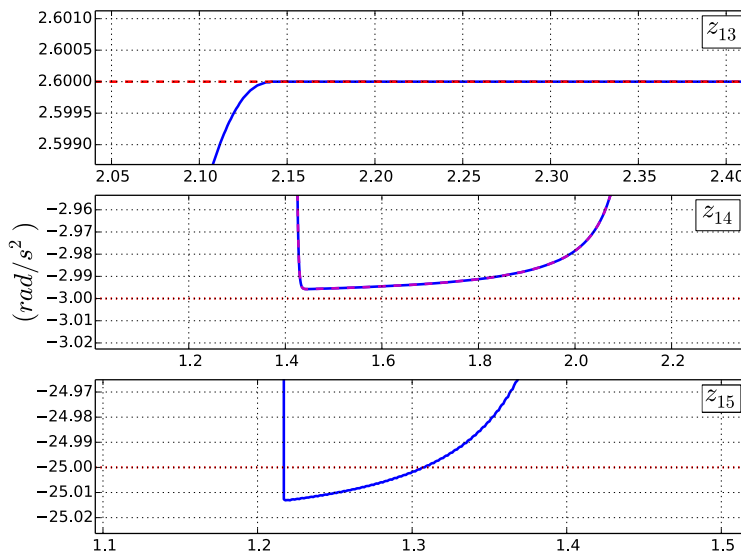


Figure 1.22: Zooms corresponding to Fig. 1.21.

1.3.2.5 Joint position constraint incompatibility with both jerk and deceleration limits, complete braking phase

Finally, a fully **complete** description of the braking phase is used to extract the last formulation of the position constraint. When coping with an upper position limit, this braking phase is as following: the joint starts jerking negatively in the opposite direction during n_{15_N} iterations until reaching the maximum deceleration. This deceleration is then applied during n_{17_N} iterations then *de-charged* during n_{19_N} time-steps by jerking positively. The state S of the system during the $(n_{15_N} + n_{17_N} + n_{19_N})$ time-steps can be described as following:

$$\begin{aligned}
S_{|k+1} \left\{ \begin{array}{lcl} q_{|k+1} & = & q_{|k} + \dot{q}_{|k} \delta t, \\ \dot{q}_{|k+1} & = & \dot{q}_{|k} + \ddot{q}_{|k} \delta t, \\ \ddot{q}_{|k+1} & = & \ddot{q}_{|k} + \ddot{q}_m \delta t \\ \vdots & & \vdots \end{array} \right. & \left. \right\} \text{Equivalent to (1.31)} \\
S_{|k+n_{15}} \left\{ \begin{array}{lcl} q_{|k+n_{15}} & = & q_{|k+n_{15}-1} + \dot{q}_{|k+n_{15}-1} \delta t, \\ \dot{q}_{|k+n_{15}} & = & \dot{q}_{|k+n_{15}-1} + \ddot{q}_{|k+n_{15}-1} \delta t, \\ \ddot{q}_{|k+n_{15}} & = & \ddot{q}_{|k+n_{15}-1} + \ddot{q}_m \delta t \end{array} \right. & \left. \right\} \\
S_{|k+n_{15}+1} \left\{ \begin{array}{lcl} q_{|k+n_{15}+1} & = & q_{|k+n_{15}} + \dot{q}_{|k+n_{15}} \delta t, \\ \dot{q}_{|k+n_{15}+1} & = & \dot{q}_{|k+n_{15}} + \ddot{q}_m \delta t, \\ \vdots & & \vdots \end{array} \right. & \left. \right\} \text{Equivalent to (1.24) (1.49)} \\
S_{|k+n_{15}+n_{17}} \left\{ \begin{array}{lcl} q_{|k+n_{15}+n_{17}} & = & q_{|k+n_{15}+n_{17}-1} + \dot{q}_{|k+n_{15}+n_{17}-1} \delta t, \\ \dot{q}_{|k+n_{15}+n_{17}} & = & \dot{q}_{|k+n_{15}+n_{17}-1} + \ddot{q}_m \delta t, \end{array} \right. & \left. \right\} \\
S_{|k+n_{15}+n_{17}+1} \left\{ \begin{array}{lcl} q_{|k+n_{15}+n_{17}+1} & = & q_{|k+n_{15}+n_{17}} + \dot{q}_{|k+n_{15}+n_{17}} \delta t, \\ \dot{q}_{|k+n_{15}+n_{17}+1} & = & \dot{q}_{|k+n_{15}+n_{17}} + \ddot{q}_{|k+n_{15}+n_{17}} \delta t, \\ \ddot{q}_{|k+n_{15}+n_{17}+1} & = & \ddot{q}_{|k+n_{15}+n_{17}} + \ddot{q}_M \delta t \\ \vdots & & \vdots \end{array} \right. & \left. \right\} \text{Equivalent to (1.31)} \\
S_{|k+n_{15}+n_{17}+n_{19}} \left\{ \begin{array}{lcl} q_{|k+n_{15}+n_{17}+n_{19}} & = & q_{|k+n_{15}+n_{17}+n_{19}-1} + \dot{q}_{|k+n_{15}+n_{17}+n_{19}-1} \delta t, \\ \dot{q}_{|k+n_{15}+n_{17}+n_{19}} & = & \dot{q}_{|k+n_{15}+n_{17}+n_{19}-1} + \ddot{q}_{|k+n_{15}+n_{17}+n_{19}-1} \delta t, \\ \ddot{q}_{|k+n_{15}+n_{17}+n_{19}} & = & \ddot{q}_{|k+n_{15}+n_{17}+n_{19}-1} + \ddot{q}_M \delta t \end{array} \right. & \left. \right\}
\end{aligned}$$

The articular position evolution in $(n_{15} + n_{17} + n_{19})$ iterations is equal to the general form of the numerical sequence (1.49):

$$\begin{aligned}\mathbf{q}_{|k+n_{15}+n_{17}+n_{19}} = & \mathbf{q}_{|k+n_{15}+n_{17}} + n_{19}\dot{\mathbf{q}}_{|k+n_{15}+n_{17}}\delta t \\ & + \frac{(n_{19}^2 - n_{19})}{2}\ddot{\mathbf{q}}_{|k+n_{15}+n_{17}}\delta t^2 \\ & + \left(\frac{n_{19}^3}{6} - \frac{n_{19}^2}{2} + \frac{n_{19}}{3}\right)\ddot{\mathbf{q}}_M\delta t^3\end{aligned}\quad (1.50)$$

With:

$$\left\{ \begin{aligned}\mathbf{q}_{|k+n_{15}+n_{17}} = & \mathbf{q}_{|k+n_{15}} + n_{17}\dot{\mathbf{q}}_{|k+n_{15}}\delta t + \frac{(n_{17}^2 - n_{17})}{2}\ddot{\mathbf{q}}_m\delta t^2, \\ = & \mathbf{q}_{|k} + (n_{15} + n_{17})\dot{\mathbf{q}}_{|k}\delta t + [(n_{15}n_{17}) + \frac{(n_{15}^2 - n_{15})}{2}]\ddot{\mathbf{q}}_{|k}\delta t^2 \\ & + \frac{(n_{17}^2 - n_{17})}{2}\ddot{\mathbf{q}}_m\delta t^2 \\ & + [\frac{n_{17}(n_{15}^2 - n_{15})}{2} + \left(\frac{n_{15}^3}{6} - \frac{n_{15}^2}{2} + \frac{n_{15}}{3}\right)]\ddot{\mathbf{q}}_m\delta t^3,\end{aligned}\quad (1.51)\right.$$

$$\begin{aligned}\dot{\mathbf{q}}_{|k+n_{15}+n_{17}} = & \dot{\mathbf{q}}_{|k+n_{15}} + n_{17}\ddot{\mathbf{q}}_m\delta t \\ = & \dot{\mathbf{q}}_{|k} + n_{15}\ddot{\mathbf{q}}_{|k}\delta t + \frac{(n_{15}^2 - n_{15})}{2}\ddot{\mathbf{q}}_m\delta t^2 + n_{17}\ddot{\mathbf{q}}_m\delta t,\end{aligned}$$

$$\left. \ddot{\mathbf{q}}_{|k+n_{15}+n_{17}} = \ddot{\mathbf{q}}_{|k} + \ddot{\mathbf{q}}_m\delta t\right.$$

$\mathbf{q}_{|k+n_{15}}$, $\mathbf{q}_{|k+n_{15}+n_{17}}$ and $\dot{\mathbf{q}}_{|k+n_{15}}$ are respectively equivalent to (1.32), (1.45) and (1.13).

When developed, (1.50) becomes:

$$\begin{aligned}\mathbf{q}_{|k+n_{15}+n_{17}+n_{19}} &= \mathbf{q}_{|k} + (n_{15} + n_{17} + n_{19})\dot{\mathbf{q}}_{|k}\delta t \\ &\quad + [n_{15}(n_{17} + n_{19}) + \frac{(n_{15}^2 - n_{15}) + (n_{19}^2 - n_{19})}{2}]\ddot{\mathbf{q}}_{|k}\delta t^2 \\ &\quad + [\frac{(n_{17} + n_{19}) + (n_{15}^2 - n_{15})}{2} + (\frac{n_{15}^3}{6} - \frac{n_{15}^2}{2} + \frac{n_{15}}{3})]\ddot{\mathbf{q}}_m\delta t^3 \quad (1.52) \\ &\quad + [(n_{17}n_{19}) + \frac{(n_{17}^2 - n_{17}) + (n_{19}^2 - n_{19})}{2}]\ddot{\mathbf{q}}_m\delta t^2 \\ &\quad + (\frac{n_{19}^3}{6} - \frac{n_{19}^2}{2} + \frac{n_{19}}{3})\ddot{\mathbf{q}}_M\delta t^3\end{aligned}$$

With: $\mathbf{q}_{|k} \geq 0$, $\dot{\mathbf{q}}_{|k} \geq 0$, $\ddot{\mathbf{q}}_m \leq 0$, $\ddot{\mathbf{q}}_m \leq 0$ and $\ddot{\mathbf{q}}_M \geq 0$. The condition $\mathbf{q}_{|k+n_{15}+n_{17}+n_{19}} \leq \mathbf{q}_M$ for all integers (n_{15}, n_{17}, n_{19}) leads to:

$$\begin{aligned}\ddot{\mathbf{q}}_{|k}^c &\leq \frac{(\mathbf{q}_M - \mathbf{q}_{|k})}{[n_{15}(n_{17} + n_{19}) + \frac{(n_{15}^2 - n_{15}) + (n_{19}^2 - n_{19})}{2}]\delta t^2} \\ &\quad - \frac{(n_{15} + n_{17} + n_{19})\dot{\mathbf{q}}_{|k}}{[n_{15}(n_{17} + n_{19}) + \frac{(n_{15}^2 - n_{15}) + (n_{19}^2 - n_{19})}{2}]\delta t} \\ &\quad - \frac{[\frac{(n_{17} + n_{19}) + (n_{15}^2 - n_{15})}{2} + (\frac{n_{15}^3}{6} - \frac{n_{15}^2}{2} + \frac{n_{15}}{3})]\ddot{\mathbf{q}}_m\delta t}{[n_{15}(n_{17} + n_{19}) + \frac{(n_{15}^2 - n_{15}) + (n_{19}^2 - n_{19})}{2}]} \quad (1.53) \\ &\quad - \frac{[(n_{17}n_{19}) + \frac{(n_{17}^2 - n_{17}) + (n_{19}^2 - n_{19})}{2}]\ddot{\mathbf{q}}_m}{[n_{15}(n_{17} + n_{19}) + \frac{(n_{15}^2 - n_{15}) + (n_{19}^2 - n_{19})}{2}]} \\ &\quad - \frac{[(\frac{n_{19}^3}{6} - \frac{n_{19}^2}{2} + \frac{n_{19}}{3})]\ddot{\mathbf{q}}_M\delta t}{[n_{15}(n_{17} + n_{19}) + \frac{(n_{15}^2 - n_{15}) + (n_{19}^2 - n_{19})}{2}]}\end{aligned}$$

(n_{15}, n_{17}, n_{19}) are the integers minimizing the right-hand side of (1.53). Following the same reasoning for the lower position limit, the condition $\mathbf{q}_{|k+n_{16}+n_{18}+n_{20}} \geq \mathbf{q}_m$ can be

reflected on the acceleration control variable as following:

$$\begin{aligned}
 \ddot{\mathbf{q}}_{|k}^c &\geq \frac{(\mathbf{q}_m - \mathbf{q}_{|k})}{[n_{16}(n_{18} + n_{20}) + \frac{(n_{16}^2 - n_{16}) + (n_{20}^2 - n_{20})}{2}]\delta t^2} \\
 &- \frac{(n_{16} + n_{18} + n_{20})\dot{\mathbf{q}}_{|k}}{[n_{16}(n_{18} + n_{20}) + \frac{(n_{16}^2 - n_{16}) + (n_{20}^2 - n_{20})}{2}]\delta t} \\
 &- \frac{[\frac{(n_{18} + n_{20}) + (n_{16}^2 - n_{16})}{2} + (\frac{n_{16}^3}{6} - \frac{n_{16}^2}{2} + \frac{n_{16}}{3})]\ddot{\mathbf{q}}_M \delta t}{[n_{16}(n_{18} + n_{20}) + \frac{(n_{16}^2 - n_{16}) + (n_{20}^2 - n_{20})}{2}]} \\
 &- \frac{[(n_{18}n_{20}) + \frac{(n_{18}^2 - n_{18}) + (n_{20}^2 - n_{20})}{2}]\ddot{\mathbf{q}}_M}{[n_{16}(n_{18} + n_{20}) + \frac{(n_{16}^2 - n_{16}) + (n_{20}^2 - n_{20})}{2}]} \\
 &- \frac{[(\frac{n_{20}^3}{6} - \frac{n_{20}^2}{2} + \frac{n_{20}}{3})]\ddot{\mathbf{q}}_m \delta t}{[n_{16}(n_{18} + n_{20}) + \frac{(n_{16}^2 - n_{16}) + (n_{20}^2 - n_{20})}{2}]}
 \end{aligned} \tag{1.54}$$

(n_{16}, n_{18}, n_{20}) are the integers maximizing the right-hand side of (1.54). f_χ and f_ϕ are respectively equivalent to the right hand sides of (1.53) and (1.54).

Algorithm 4 Compute $n_{15}, n_{16}, n_{17}, n_{18}, n_{19}, n_{20}, f_\chi$ and f_ϕ

Require: $q_M, q_m, q|_k, \dot{q}|_k, \ddot{q}_M, \ddot{q}_m, \ddot{\ddot{q}}_M, \ddot{\ddot{q}}_m, \delta t$

- 1: $f_{\chi_{max}} \leftarrow \ddot{q}_m \quad f_{\phi_{min}} \leftarrow \ddot{q}_M$
- 2: **for** ($i_1 = 1 \rightarrow N_1^a$) **do**
- 3: | $n_{16}^* \leftarrow i_1 \quad n_{15}^* \leftarrow i_1$
- 4: | **for** ($i_2 = 0 \rightarrow N_2^a$) **do**
- 5: | | $n_{18}^* \leftarrow i_2 \quad n_{17}^* \leftarrow i_2$
- 6: | | **if** ($\ddot{q}|_k \geq 0$) **then**
- 7: | | | $n_{20_{\mathbb{R}+}}^* \leftarrow n_{16} - \left| \frac{\ddot{q}|_k}{\ddot{\ddot{q}}_m \delta t} \right| \quad n_{19_{\mathbb{R}+}}^* \leftarrow n_{15} + \left| \frac{\ddot{q}|_k}{\ddot{\ddot{q}}_M \delta t} \right|$
- 8: | | | **end if**
- 9: | | | **if** ($\ddot{q}|_k < 0$) **then**
- 10: | | | | $n_{20_{\mathbb{R}+}}^* \leftarrow n_{16} + \left| \frac{\ddot{q}|_k}{\ddot{\ddot{q}}_M \delta t} \right| \quad n_{19_{\mathbb{R}+}}^* \leftarrow n_{15} - \left| \frac{\ddot{q}|_k}{\ddot{\ddot{q}}_m \delta t} \right|$
- 11: | | | | **if** ($n_{16}^* \leq 1$) **then** $n_{20_{\mathbb{R}+}}^* \leftarrow \left| \frac{\ddot{q}|_k}{\ddot{\ddot{q}}_m \delta t} \right|$
- 12: | | | | **if** ($n_{15}^* \leq 1$) **then** $n_{19_{\mathbb{R}+}}^* \leftarrow \left| \frac{\ddot{q}|_k}{\ddot{\ddot{q}}_M \delta t} \right|$
- 13: | | | | **end if**
- 14: | | | **if** ($n_{15}^* \leq 1$) **then** $n_{15}^* \leftarrow 1$
- 15: | | | **if** ($n_{16}^* \leq 1$) **then** $n_{16}^* \leftarrow 1$
- 16: | | | **if** ($n_{19_{\mathbb{R}+}}^* \leq 2$) **then** $n_{19_{\mathbb{R}+}}^* \leftarrow 2$
- 17: | | | **if** ($n_{20_{\mathbb{R}+}}^* \leq 2$) **then** $n_{20_{\mathbb{R}+}}^* \leftarrow 2$
- 18: | | | $f_\chi^* \leftarrow f_\chi(q_m, q|_k, \dot{q}|_k, \ddot{q}_M, \ddot{q}_m, \ddot{\ddot{q}}_m, n_{15}^*, n_{17}^*, n_{19}^*)$
- 19: | | | $f_\phi^* \leftarrow f_\phi(q_M, q|_k, \dot{q}|_k, \ddot{q}_m, \ddot{\ddot{q}}_m, \ddot{\ddot{q}}_M, n_{16}^*, n_{18}^*, n_{20}^*)$
- 20: | | | **if** ($f_\chi^* \geq f_{\chi_{max}}$) **then**
- 21: | | | | $f_{\chi_{max}} \leftarrow f_\chi^* \quad n_{16} \leftarrow n_{16}^* \quad n_{18} \leftarrow n_{18}^* \quad n_{20}^b \leftarrow n_{20_{\mathbb{R}+}}^*$
- 22: | | | | **end if**
- 23: | | | **if** ($f_\phi^* \leq f_{\phi_{min}}$) **then**
- 24: | | | | $f_{\phi_{min}} \leftarrow f_\phi^* \quad n_{15} \leftarrow n_{15}^* \quad n_{17} \leftarrow n_{17}^* \quad n_{19}^b \leftarrow n_{19_{\mathbb{R}+}}^*$
- 25: | | | | **end if**
- 26: | | | **end for**
- 27: **end for**
- 28: $f_\chi \leftarrow f_{\chi_{max}} \quad f_\phi \leftarrow f_{\phi_{min}}$
- 29: **return** $n_{15}, n_{16}, n_{17}, n_{18}, n_{19}, n_{20}, f_\chi, f_\phi$

^a N_1 and N_2 are fixed heuristically, they must however be \geq to the number of iterations needed to perform the braking movement described in (1.49).

^b for calculation stability in the computation of f_χ and f_ϕ , (n_{19}^*, n_{20}^*) are used as real numbers (even if previously defined as numbers of iterations). The same for n_{19} and n_{20} .

Algorithm 4 shows how $n_{15}, n_{16}, n_{17}, n_{18}, n_{19}, n_{20}, f_\chi$ and f_ϕ can be computed numeri-

cally.

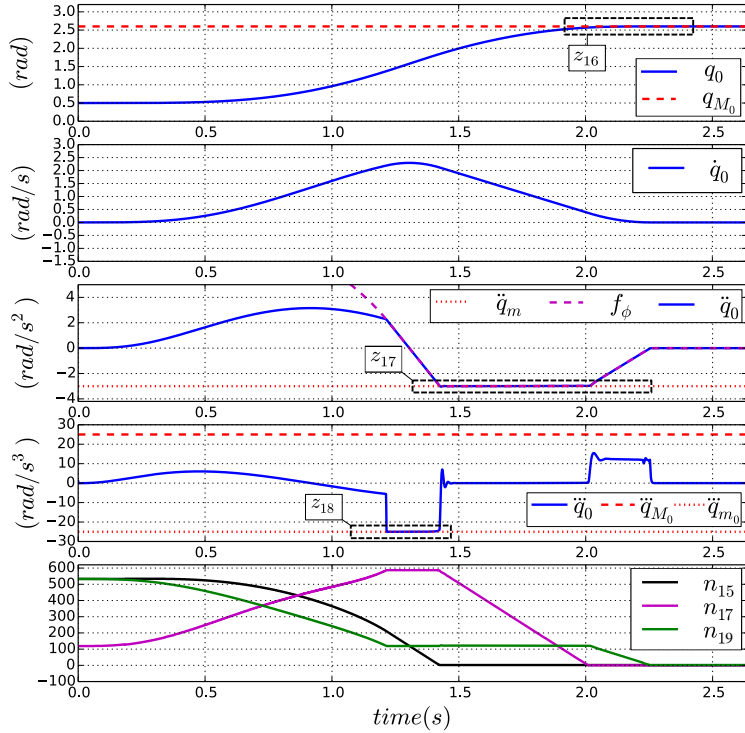
1.3.2.5.1 Simulation

For this experiment, the controller is implemented with the last **complete** formulation of the articular position constraint (1.53) that takes into account both positive and negative jerk capabilities, $[\ddot{q}_{m_0}, \ddot{q}_{M_0}] = [-25, 25] \text{ rad.s}^{-3}$; In addition to the deceleration capability ($\ddot{q}_{m_0} = -3 \text{ rad.s}^{-2}$). As before, joint 0 is moving towards its maximum position limit q_{M_0} . No hard-coded constraints on the articular acceleration (1.11c) nor jerk (1.11d) are considered.

Fig. 1.23, illustrates the braking phase induced by joint 0 when coping with its position limit. the joint starts jerking negatively until maximum deceleration is reached. This deceleration is used for several time-steps then de-charged and brought to 0 by jerking positively. The joint is stopped exactly at its upper position limit. The jerk profile in Fig. 1.24 shows an exceeding of (0.013 rad.s^{-3}) over the lower jerk limit and an other one of (0.035 rad.s^{-2}) over the deceleration limit. As before, this is mainly due to the *discrete* description of the braking phase.

Fig. 1.25 illustrates the induced braking phase in case the lower deceleration limit \ddot{q}_{m_0} is fixed at -100 rad.s^{-2} . Consequently, the second braking *sub-phase*²³ disappears resulting into an equivalent behaviour as for (1.41) in Fig. 1.19.

²³We distinguish 3 sub-phases during the **complete** braking movement: constant negative jerk, constant deceleration then constant positive jerk (Considering an upper position limit).



55

Figure 1.23: State S of joint 0 during the braking phase to cope with a maximum position limit q_{M_0} ; The new constraint formulation (1.53) that takes into account the deceleration capability $\ddot{q}_{m_0} = -3 \text{ rad.s}^{-2}$ in addition to the positive and negative jerk limits $[\ddot{\ddot{q}}_{m_0}, \ddot{\ddot{q}}_{M_0}] = [-25, 25] \text{ rad.s}^{-3}$ is used. Top to bottom: position, velocity, acceleration, jerk and (n_{15}, n_{17}, n_{19}) .

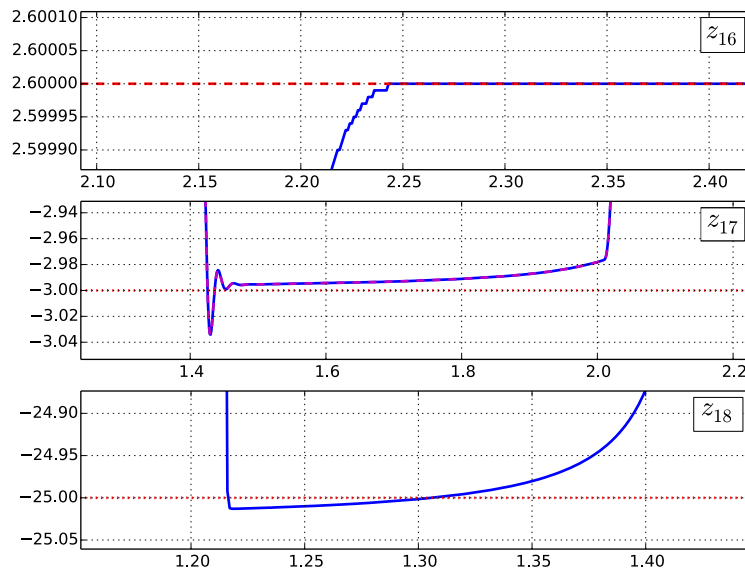


Figure 1.24: Zooms corresponding to Fig. ??.

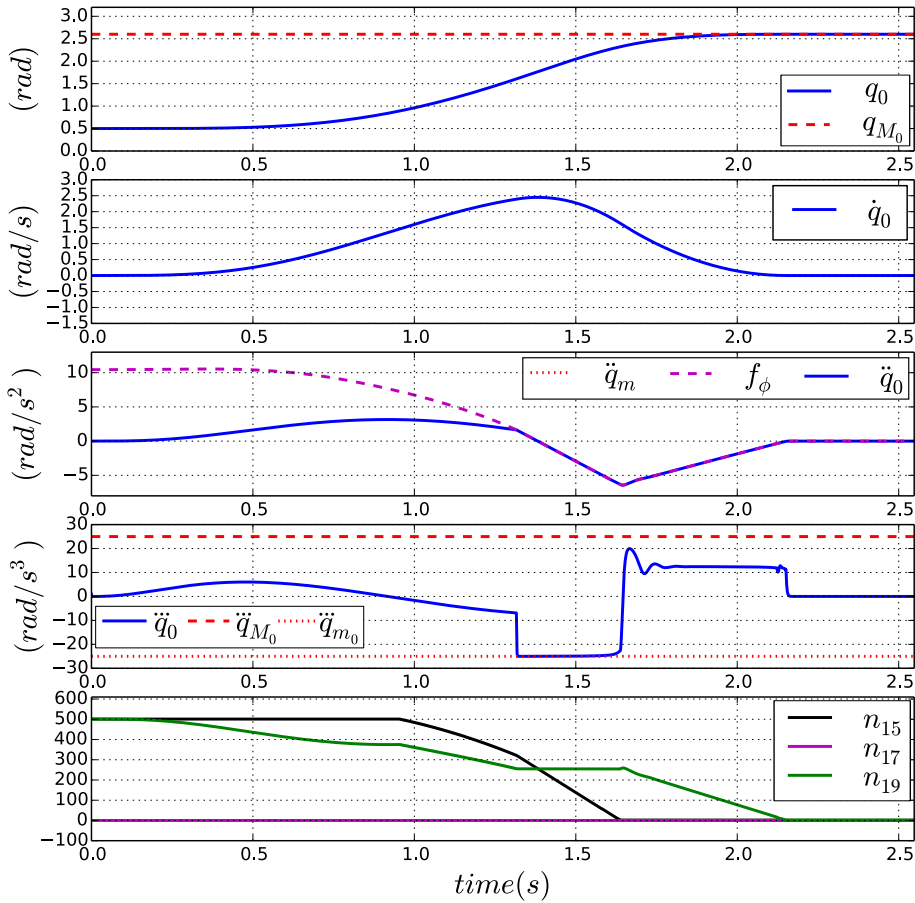


Figure 1.25: State S of joint 0 during the braking phase to cope with a maximum position limit q_{M_0} ; The new constraint formulation (1.53) that takes into account the deceleration capability $\ddot{q}_{m_0} = -100 \text{ rad.s}^{-2}$ in addition to the positive and negative jerk limits $[\ddot{q}_{m_0}, \ddot{q}_{M_0}] = [-25, 25] \text{ rad.s}^{-3}$ is used. Top to bottom: position, velocity, acceleration, jerk and (n_{15}, n_{17}, n_{19}).

1.4 Final bounds on the acceleration control variable

All articular constraints on position, velocity, acceleration and jerk are reflected on the acceleration control variable. Therefore, the final acting bounds on $\ddot{q}_{|k}^c$ are computed using the following algorithm:

Algorithm 5 Compute f_ψ and f_ω

Require: $f_\alpha, f_\beta, f_\lambda, f_\mu, \ddot{q}_M, \ddot{q}_m, \ddot{\ddot{q}}_M, \ddot{\ddot{q}}_m, \delta t$

- 1: $f_\psi \leftarrow \ddot{q}_M$
- 2: $f_\omega \leftarrow \ddot{q}_m$
- 3: $f_\psi^* \leftarrow \min(f_\alpha(\dot{q}_M, \ddot{q}_m), f_\lambda(q_M, \ddot{q}_m, \ddot{q}_M, \ddot{\ddot{q}}_M), \ddot{q}_M, (\ddot{q}_{|k} + \ddot{q}_M \delta t))$
- 4: $f_\omega^* \leftarrow \max(f_\beta(\dot{q}_m, \ddot{q}_M), f_\mu(q_m, \ddot{q}_M, \ddot{q}_m, \ddot{\ddot{q}}_m), \ddot{q}_m, (\ddot{q}_{|k} + \ddot{q}_m \delta t))$
- 5: **if** $(|f_\psi^* - \ddot{q}_{|k}^c| \leq \epsilon^a)$ **then**
- 6: | $f_\psi \leftarrow f_\psi^*$
- 7: **end if**
- 8: **if** $(|f_\omega^* - \ddot{q}_{|k}^c| \leq \epsilon)$ **then**
- 9: | $f_\omega \leftarrow f_\omega^*$
- 10: **end if**
- 11: **return** f_ψ, f_ω

^a e.g. $\epsilon = 1$

The final bounds on $\ddot{q}_{|k}^c$ are of the form:

$$f_\omega \leq \ddot{q}_{|k}^c \leq f_\psi \quad (1.55)$$

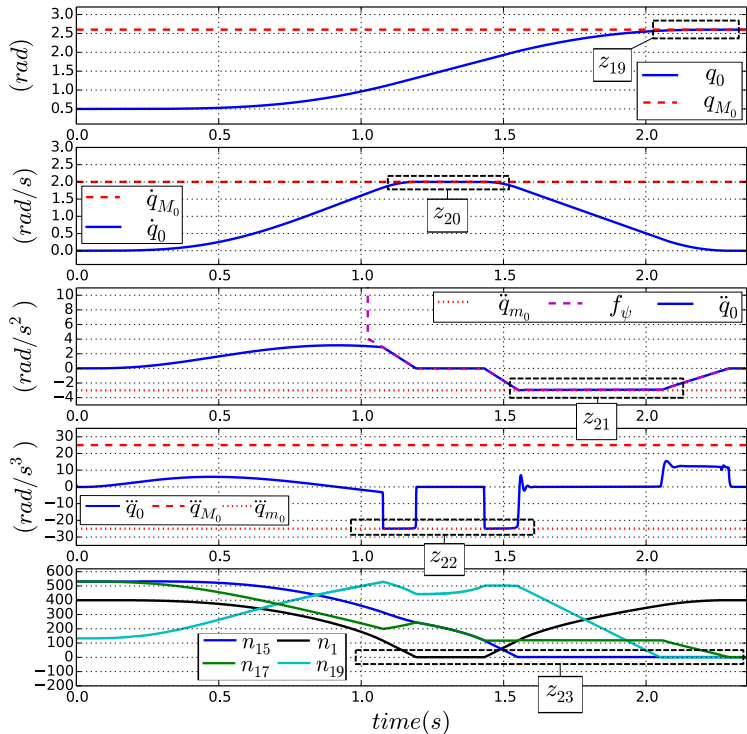
Algorithm 5 shows how f_ω and f_ψ can be computed numerically.

1.4.0.5.2 Simulation

For this final experiment, the controller is implemented with the constraint (1.55) that takes into account all the articular limitations of the actuators of the robot. The joint capabilities are imposed as following: $[q_{m_0}, q_{M_0}] = [-2.6, 2.6] \text{ rad}$, $[\dot{q}_{m_0}, \dot{q}_{M_0}] = [-2, 2] \text{ rad.s}^{-1}$, $[\ddot{q}_{m_0}, \ddot{q}_{M_0}] = [-3^{24}, 100] \text{ rad.s}^{-2}$ and $[\ddot{\ddot{q}}_{m_0}, \ddot{\ddot{q}}_{M_0}] = [-25, 25] \text{ rad.s}^{-3}$. As for the previous experiments, joint 0 is moving towards its maximum position limit q_{M_0} .

Fig. 1.26 and Fig. 1.27 show how joint 0 is capable of coping at the same time with all its limitations. Constraints on the articular position, velocity, acceleration and jerk all respected during the movement of the joint and viability for the state of the robot is guaranteed at every time-step.

²⁴To ensure compatibility between the hard-coded constraint on acceleration (1.8c) and the new formulation of position constraint (1.53), \ddot{q}_{m_0} is diminished to 2.95 for the computation of f_ψ in Algorithm 5.



58

Figure 1.26: State S of joint 0 when coping with both maximum position and velocity limits; Using the final articular constraint formulation (1.55) that takes into account all the limitations of the joint. Top to bottom: position, velocity, acceleration, jerk and $(n_1, n_{15}, n_{17}, n_{19})$.

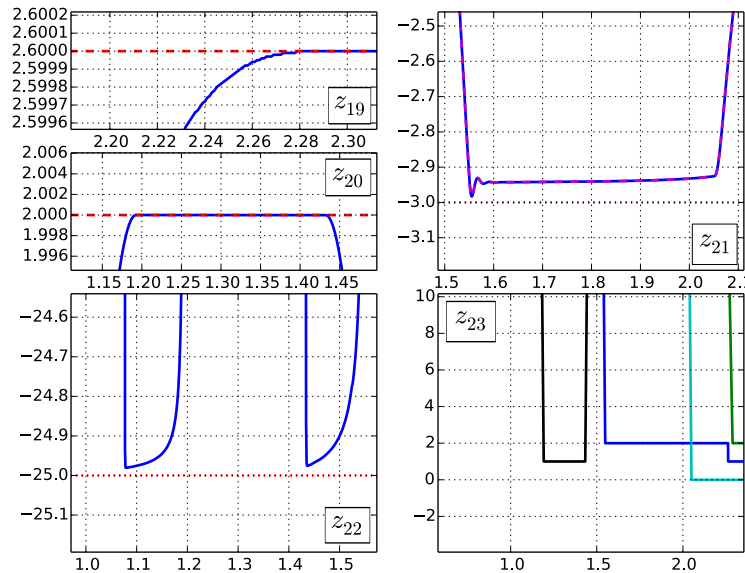


Figure 1.27: Zooms corresponding to Fig. 1.26.

1.5 Conclusion

This chapter discussed the problem of ensuring viability for a robotic system that is reactively controlled at the dynamic-level and whose joints have limited positions, velocities, accelerations and jerks. As it is impossible to respect all the constraints related to these limitations using the classic known formulations, new mathematical expressions that include the reaction capabilities of the robot have been proposed.

For joint rate constraints, the new formulation take into account the actuators jerk capabilities. For position constraints, both producible articular deceleration and jerk are included in the new formulation. Finally, mathematical expressions for the upper and lower bounds reflected on the dynamic control input and that consider all the physical limitations of the robot and that ensure every time-step the existence of a solution to the optimization control problem are presented. Performed simulations on a 7-degree-of-freedom KUKA LWR4 arm clearly show the interest of using the proposed new formulations in comparison to the classic ones to guarantee the satisfaction of the different joint bounds.

The only drawback with the new introduced formulations is the computational load linked to the heuristic method with which the *number of time-steps needed for the induced braking phases to cope with the considered limits* is computed. Fixing N , N_1 and N_2 in Algorithm 2, 3 and 4 to high²⁵ values (e.g. 10000²⁶) and running all these algorithms at the same time for all the joints of the robot can rapidly become computationally heavy. In a more practical way, maximum values for N , N_1 and N_2 can be computed as solutions to the following problems:

- What is the number of time-steps needed for a joint actuator in an initial state of *maximum* acceleration to bring this acceleration to zero considering the amount of jerk it can produce.
- What is the number of time-steps needed for a joint actuator moving at *maximum* velocity and *maximum* acceleration to completely stop considering the amount of deceleration and jerk it can produce.

²⁵To guarantee finding the right values for the n_i parameters.

²⁶10000 time-steps durations with a control sample time of 1 ms are equal to 10 s

The maximum solution between these two problems is the biggest number of time-steps regarding the worst case braking movement that can be induced by the considered actuator.

Finally, in the upcoming chapters, to deal with safety issues during human-robot interaction, new constraints expressed in operational space are introduced and implemented in the controller of the robot. Problems regarding incompatibility with this type of constraints will be discussed.

Chapter 2

Energy based control for safe human-robot physical interaction

Abstract

In this chapter, we propose physically meaningful energy related safety indicators for robots sharing their workspace with humans. Based on these indicators, safety criteria are introduced as constraints in the control algorithm. The first constraint depending on the distance between the robot and a nearby obstacle is used to limit the amount of kinetic energy dissipated in case of a collision. After the establishment of physical contact, the second constraint is used to modulate contact forces by limiting the amount of potential energy generated within the obstacle-robot system. The control algorithm is formulated as an optimization problem and computes every time-step the needed actuation torques for a KUKA LWR4 manipulator given some task to be performed, the introduced constraints and the physical limitations of the system to cope with. The overall framework tested in simulation allows a robot to safely interact with its environment.

2.1 Introduction

Service and intervention robotics, as well as more traditional industrial robotics applications, are evolving in a direction where the workspace of the robot is very likely to be shared with humans. This may induce deliberate¹ and non-intentional physical interactions. Safety in this context becomes a critical issue to be dealt with [Alami 06].

To ensure safe human-robot interactions, several approaches have been explored in the robotics literature. At the hardware level, the mechanical design can be optimized to reduce the apparent inertia of the robot [Zinn 04] and compliant components can be introduced to allow smoother contacts and less severe impacts [Haddadin 12b]. Torque sensing at the joint level also provides a way to actively control the impedance of the robot. The Kuka-DLR lightweight robot [Bischoff 10], [Loughlin 07], [Hirzinger 01] has been specifically designed to meet these challenges.

Different control approaches using internal and external force/torque sensors have been developed to handle safety during pre and post impact/contact phases [Ebert 02], [Lumelsky 93], [Ikuta 03]. Haddadin in [Haddadin 08] and De Luca in [De Luca 06] present different strategies to reduce the effect of undesired impacts. A collision detection parameter based on the estimated external torque is introduced and used to scale down the link inertia obtaining a “lighter” robot that “flees” from the collision area. An other strategy is the use of the disturbance input to slow the robot until zero velocity then pushing it back along its original path. Heizmann and Zelinsky in [Heinzmann 03] propose a safety criterion based on the *potential impact force* to filter the control torque of the system. The introduced controller scheme allows one to consider two potential contact points at the same time for a real-time implementation. As the degree of potential injury is directly related to the mass and velocity of the colliding objects, the controller proposed in [Haddadin 12a] takes into account the reflected robot inertia along a collision direction to decide about the maximum operational point velocity. The bounds on this velocity are based on experimental results relating mass, velocity, geometry and medically observable soft tissue injury by systematic drop-testing experiments with pig abdominal wall sample. By making use of the redundancy property of a KUKA/DLR lightweight arm,

¹For example if the robot can be both used in an autonomous mode or in a co-manipulation mode.



Figure 2.1: View of a user sharing its workspace with the KUKA LWR manipulator. The kinetic energy of the system is modulated as a function of the distance between the human operator and the end-effector of the robot in order to best perform the task of the robot while ensuring safety.

[De Luca 08] proposes a physical interaction strategy that is able to react safely to collisions while continuing to execute as much possible of the original task. Kinetic energy has already been discussed in [Haddadin 08] and [Haddadin 12a] as a good representation of the risk of injury. It is used in the work presented in This chapter to synthesize a physically meaningful safety indicator. This indicator can also include elastic potential energy associated with the controller in phases where the robots physically interacts with its environment. The kinetic energy part of the proposed criteria is used to constrain the dynamic behaviour of the KUKA LWR4 serial robot in the direction of a considered obstacle². The imposed constraint accounts for the breaking capabilities of the robot and is modulated as a function of the distance between the robot and the human operator.

In order to properly account for the safety constraint, the control problem is expressed as a Linearly Constrained Quadratic Program (LQP) [Boyd 04]. The computation of the adequate actuation torques needed to perform a trajectory tracking in operational space is subject to several linear inequality constraints accounting for the physical limitations of the robot (joint limits, joint velocity and torque saturations) as well as for limit values on the energy-based safety indicators. The proposed control framework is expected to

²All along the manuscript, "obstacle" is used as a generic term for any external element of the environment, e. g. a human operator.

decrease impact forces due to collisions and also contact forces by constraining the kinetic energy of the robot. Contact forces induced by deliberate physical interactions can be limited through a constraint on the elastic potential energy of the controller. Using the same framework, contact with the environment can be enabled, modulated and disabled by a straightforward modification of physically meaningful control parameters. Fig. 2.1 illustrates a typical workspace-sharing scenario for the proposed controller.

This chapter is organised as following: In section 2, the proposed safety indicators are formulated for both pre-collision and physical-contact phases. In section 3, the associated safety criteria, namely the maximum allowed values for the introduced safety indicators are presented. The controller is described in Section 4: task related objectives are formulated and the expressions of the energy related constraints needed for safe human-robot interaction are provided. In Section 5, an experimental scenario is introduced in simulation using a KUKA LWR4 serial robot, based on which the possibilities offered by the proposed controller are illustrated and discussed. Finally, Section 6 summarizes the contribution and provides an overview of the future work.

2.2 Interaction forces and safety indicators

In this section, safety indicators quantifying the degree of danger³ represented by the robot towards a nearby human operator are introduced. These indicators must be physically meaningful, related to the control input and computable in real-time. During human-robot interaction, the degree of danger is mainly caused by two parameters: the impact force created in case of a collision and the contact forces existing after the establishment of physical contact. The most generic way to include and express these forces is to use an energetic formulation. Indeed, energy is a universal entity that can describe all the physical phenomena occurring during human-robot interaction⁴. Therefore, it is used in the presented work to synthesize two indicators whose value is related to the impact and contact forces. Safety criteria, namely bounds on the maximum values of these indicators are then derived. The energy based criteria are finally used to constrain the

³risk induced by a collision or physical contact

⁴physical and non physical

dynamic behaviour of a KUKA LWR4 serial robot during its interaction with a human operator.

2.2.1 Kinetic energy

The generated impact force in case of a collision can be written as a function of the dissipated energy and the shock absorption distance :

$$\begin{aligned} \int_u F_{impact} du &= E_{dissipated} \\ &= E_c^{hum} + E_c^{rob}, \end{aligned} \tag{2.1}$$

F_{impact} is the generated impact force at the collision, u the shock absorption distance and $E_{dissipated}$ the dissipated energy which is equal to the sum of kinetic energy E_c of both the human operator and the robot.

On the one hand, the left side parameters of the shock absorption equation (2.1) are not directly related to the actuation torque. Moreover, it is impossible to have an accurate model of the human body-robot impedance⁵. As a matter of fact, the use of the impact force or of the shock absorption distance as a safety indicator is neither desirable nor possible. On the other hand, the dissipated energy is closely related to the impact force and can be directly related to the actuation torque and thus controlled in order to reduce the impact of a collision.

At a given time, very few assumptions can be made on the state of energy of the human operator and on its future evolution. As a consequence, the retained safety indicator S_c is robot-centred. E_c^{rob} is directly related to the impact force and can be expressed using the actuation torque. It is therefore to be considered for the formulation of the first safety indicator:

$$S_c = E_C^{i,j} = \frac{1}{2} m(\mathbf{q})_{i,j}^{eq} v_{i,j}^2 \tag{2.2}$$

⁵This model would have to be individual and body-part specific.

With: $1/m(\mathbf{q})_{i,j}^{eq} = J(\mathbf{q})_C^{i,j} M(\mathbf{q})^{-1} J(\mathbf{q})_C^{i,jT}$. $m(\mathbf{q})_{i,j}^{eq}$ being the equivalent mass of the robot segment i in the direction of obstacle j expressed in the cartesian space [Khatib 95]. $M(\mathbf{q})$ is the joint space inertia matrix of the robot and \mathbf{q} its joint space configuration. $v_{i,j} = J(\mathbf{q})_C^{i,j} \dot{\mathbf{q}}$ is the relative velocity of the closest point C belonging to the robot segment i in the direction of obstacle⁶ j . $J(\mathbf{q})_C^{i,j}$ is the Jacobian of the robot segment i expressed at point C and projected along the distance vector towards obstacle j .

To ensure safety for both the robot and any nearby obstacle, the introduced indicator must be considered for each (robot segment i , obstacle j) pair, *i.e.* for n_o obstacles and a robot composed of n_b mobile bodies, $n_o \times n_b$ safety indicators are needed. An other solution is to consider a safety indicator related to the real-time closest points C and o respectively on the robot and human operator. The main drawback in this case will be the resulting discontinuities in the value of the indicator. Within the framework of this chapter, and without loss of generality, a single obstacle O is considered and the only mobile body of the robot considered for safety is the end-effector (EE). Indeed, it is the last segment of the fixed base serial robot (KUKA LWR4) that holds the practical load and consequently deploys the maximum kinetic energy. The kinetic energy based safety indicator can thus be written:

$$S_c = E_{c|k}^{EE,O} = \frac{1}{2} m(\mathbf{q})^{eq} v^2, \quad (2.3)$$

With: $m(\mathbf{q})^{eq} = m(\mathbf{q})_{EE,O}^{eq}$ and $v = v_{EE}^{EE,O}$. This indicator represents the energy that will be dissipated by the end-effector of the robot and the human operator in case of a collision.

2.2.2 Potential energy

After the establishment of physical contact, contact forces are created as a consequence of the potential energy generated within the human-robot system. The contact force $\mathbf{F}_{C|k}$

⁶All along the paper, "obstacle" is used as a generic term for any external element of the environment, *e. g.* a human operator.

pulling the contact point in the direction of its desired trajectory⁷ is derived from the potential energy $E_{p|k}$:

$$\mathbf{F}_{C|k} = -\nabla E_{p|k} \quad (2.4)$$

Therefore :

$$E_{p|k} = - \int_{\mathbf{x}_{C|k}^*}^{\mathbf{x}_{C|k}} \mathbf{F}_{C|k} d\mathbf{x} = \int_{\mathbf{x}_{C|k}}^{\mathbf{x}_{C|k}^*} \mathbf{F}_{C|k} d\mathbf{x} = \mathbf{F}_{C|k} \left\| \mathbf{X}_{C|k}^* - \mathbf{X}_{C|k} \right\|_{C,*} \quad (2.5)$$

With :

$$\mathbf{F}_{C|k} = m(\mathbf{q})_{C,*}^{eq} \ddot{\mathbf{X}}_{C|k}^{C,*} \quad (2.6)$$

$C, *$ represents the directing vector between the contact point C (on the considered segment i) and its desired position $*$. $\ddot{\mathbf{X}}_{C|k}^{C,*} = J(\mathbf{q}|k)_C^{C,*} \dot{\mathbf{q}}|k + J(\mathbf{q}|k)_C^{C,*} \ddot{\mathbf{q}}|k^c$ is the cartesian acceleration of the contact point C along the $C, *$ distance vector. $\ddot{\mathbf{q}}|k^c$ is the acceleration control variable corresponding to the generated torque $\tau|k^c$ (considering a dynamic controller).

$E_{p|k}$ is directly related to the contact forces and can be expressed using the actuation parameters (articular acceleration/torque). It is therefore used for the formulation of the safety indicator during physical-contact. The retained safety indicator $S_{p_{contact}}$ is robot centred and can be expressed as following :

$$S_{p_{contact}} = E_{p|k} = \mathbf{F}_{C|k} \left\| \mathbf{X}_{C|k}^* - \mathbf{X}_{C|k} \right\|_{C,*} \quad (2.7)$$

In case of a physical contact occurring at the level of the end-effector, $S_{p_{contact}}$ can be written:

$$S_{p_{contact}} = E_{p|k}^{EE,*} = m(\mathbf{q})_{EE,*}^{eq} \ddot{\mathbf{X}}_{C|k}^{EE,*} \left\| \mathbf{X}_{C|k}^* - \mathbf{X}_{C|k} \right\|_{EE,*} \quad (2.8)$$

Finally, $S_{p_{contact}}$ represents the amount of potential energy generated within the human-robot system during physical contact. This same potential energy when released⁸ is transformed into kinetic energy.

⁷considering a trajectory tracking task

⁸In case physical contact is released.

2.2.3 Relation between kinetic and potential energies

During free⁹ movements of the robot, the equivalent force:

$$\mathbf{F}_{C|k} = m(\mathbf{q})_{C,*}^{eq} \left\| \ddot{\mathbf{X}}_{C|k} \right\| \quad (2.9)$$

derived from the potential energy $E_{p|k}$, pulls the potential collision point C along its trajectory from its current position $\mathbf{X}_{C|k}$ to its future position $\mathbf{X}_{C|k+1}$. $E_{p|k}$ results from feeding the desired cartesian position, velocity and feed-forward acceleration¹⁰ to the controller. As Newton's third law of motion is satisfied, we can write :

$$2 \operatorname{sign}(\ddot{\mathbf{X}}_{C|k})^{11} \left\| \ddot{\mathbf{X}}_{C|k} \right\| \left\| \mathbf{X}_{C|k+1} - \mathbf{X}_{C|k} \right\|_{C,*} = v_{C|k+1}^2 - v_{C|k}^2 \quad (2.10)$$

$v_{C|k+1}$ and $v_{C|k}$ are respectively the current and following cartesian velocities of the end-effector expressed at C . Multiplying both sides of (2.10) by $\frac{1}{2}m(\mathbf{q})_{C,*}^{eq}$ results in:

$$\operatorname{sign}(\ddot{\mathbf{X}}_{C|k})m(\mathbf{q})_{C,*}^{eq} \left\| \ddot{\mathbf{X}}_{C|k} \right\| \left\| \mathbf{X}_{C|k+1} - \mathbf{X}_{C|k} \right\|_{C,*} = \frac{1}{2}m(\mathbf{q})_{C,*}^{eq} (v_{C|k+1}^2 - v_{C|k}^2) \quad (2.11)$$

Which is equivalent is equivalent to :

$$E_{p|k}^{C,*} = E_{c|k+1}^{C,*} - E_{c|k}^{C,*} \Leftrightarrow E_{c|k+1}^{C,*} = E_{c|k}^{C,*} + E_{p|k}^{C,*} \quad (2.12)$$

Meaning that, the kinetic energy of the robot expressed at the potential collision point C at time-step $k + 1$ is equal to its kinetic energy at the current time-step k plus the injected potential energy $E_{p|k}^{C,*}$. $\mathbf{X}_{C|k}$ and $\mathbf{X}_{C|k+1}$ are respectively the current and future real cartesian positions of C . $\ddot{\mathbf{X}}_{C|k} = \dot{\mathbf{J}}(\mathbf{q}|k)_C \dot{\mathbf{q}}|k + J(\mathbf{q}|k)_C \ddot{\mathbf{q}}^c|k$ is its cartesian acceleration. $\|\mathbf{A}\|_{i,j}$ is the norm of vector \mathbf{A} projected along the i, j direction. According to (2.12), the injected potential energy $E_{p|k}^{C,*}$, when released, modifies the kinetic energy of the robot in the right direction to accomplish the trajectory tracking task. Therefore, the kinetic energy of the system $E_{c|n}$ at a given time-step $k = n$ can be expressed as the sum of all

⁹Without any physical interaction with the environment

¹⁰We consider a trajectory tracking task in cartesian space. The desired position, velocity and feed-forward acceleration are generated using a trajectory generator.

¹¹Positive towards the obstacle and negative in the opposite direction.

the previously injected potential energies $E_{p|k}$:

$$E_{c|k} = \sum_{n=1}^{k-1} E_{p|n} \quad (2.13)$$

As the desired trajectory for the end-effector is discretized, every time step, only a small amount of potential energy $E_{p|k}$ is *injected* then promptly transformed into kinetic one during the movement of the robot. The modulation of this *injected* potential energy can directly influence the resulting kinetic energy of the system and therefore the impact force \mathbf{F}_{impact} . Thus, it can also be used as a safety indicator during the free movements of the robot. When expressed at the end-effector EE , the injected potential energy in the direction of a considered obstacle O is written :

$$S_{p_{free}} = E_{p|k}^{EE,O} = m(\mathbf{q})_{EE,O}^{eq} \ddot{\mathbf{X}}_{C|k}^{EE,O} \left\| \mathbf{X}_{C|k+1} - \mathbf{X}_{C|k} \right\|_{EE,O} \quad (2.14)$$

Notice that the expression of this *potential energy based safety indicator* during the free movements of the robot is different from the expression of the indicator during physical contacts (2.8). Indeed, the two points in cartesian space between which the two potential energies are considered are different. For $S_{p_{contact}}$, the potential energy generated within the human-robot system during physical contact is considered between the current position of the robot end-effector $X_{|k}$ and its current desired position $X_{|k}^*$. Indeed, the contact forces derived from this potential energy depends directly on the distance between these two points. On the other hand, for $S_{p_{free}}$, during the free movements of the robot, the potential energy modifies the kinetic energy of the system between the current position of the end-effector $X_{|k}$ and its position at the next time-step $X_{|k+1}$. The distance between these two points is then used for the expression of the safety indicator during the pre-collision phase.

2.3 Safety limit values

2.3.1 Safety limit value for the pre-collision safety indicator

For S_c , the safety criterion represents the maximum amount E_{climit} of kinetic energy allowed to be dissipated during a human-robot collision. The first safety criterion can be written $S_c \leq E_{climit}$ and must always be satisfied. Given the nature of S_c , such a constraint if imposed at the control level, may have two consequences: a limitation of the velocity of the end-effector in the direction of the obstacle and a modification of its apparent mass in the same direction. However, when no human operator is present at a close distance from the robot, it is not necessary to saturate the developed kinetic energy. Therefore, to prevent over limiting the dynamic of the system, the idea is as following: When the human operator is far from the robot, the system can be as dynamic as possible to accomplish its main task (maximum kinetic energy E_{cmax} allowed). As the operator starts walking towards the robot, a constraint E_{climit} depending on the distance between the robots end-effector and the person is placed on the kinetic energy of the system. The robot is forced into a safe dynamic behaviour. At this time, if any physical contact is engaged, the resulting impact force will be harmless.

E_{climit} should then depend on the amount of kinetic energy that is considered to be safe just before the occurrence of a contact/collision but also be a function of the distance d between the end-effector of the robot and the considered human operator (see Fig. 2.2).

$$S_c = E_c^{EE,O} = \frac{1}{2} \text{sign}(v^{EE,O}) m(\mathbf{q})_{EE,O}^{eq} v^{EE,O^2} \leq E_{climit} = E_{c_{safe}} + f(d) \quad (2.15)$$

The value of $E_{c_{safe}}$ depends on the contact zone, the shape of the tool/load carried by the end-effector, its apparent mass and the maximum allowed velocity [Haddadin 12a]. It also depends on the nature of the interaction authorized between the robot and its surrounding environment. Thus, if any contact between the robot and the human operator is forbidden, putting $E_{c_{safe}} = 0 \rightarrow v = 0$ forces the end-effector to stop at a distance $d = d_{safe}$ from the considered obstacle. When contact is permitted: $E_{c_{safe}} > 0$ is the maximum value of kinetic energy allowed for the robot just before collision. $f(d)$ is a

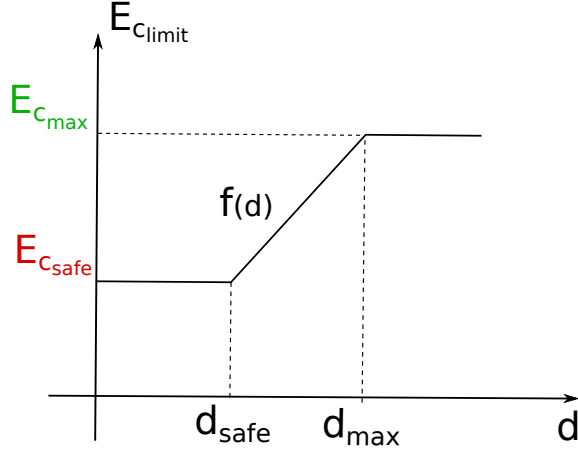


Figure 2.2: Evolution of the kinetic energy constraint depending on the distance d between the end-effector and the obstacle.

weighting function depending on the distance d between the end-effector and the considered obstacle (see Fig. 2.2). Based on the previous statements, three working zones, illustrated in Figure 2.3, are defined for the dynamic behaviour of the robot :

1. A safe zone for $d < d_{safe}$ in which the kinetic energy must be at most $E_{c_{safe}}$;
2. A working zone for $d_{safe} < d < d_{max}$ where the kinetic energy of the system is constrained as the human operator is moving towards the robot;
3. A third zone for $d > d_{max}$ in which maximum dynamic performances are allowed for the system.

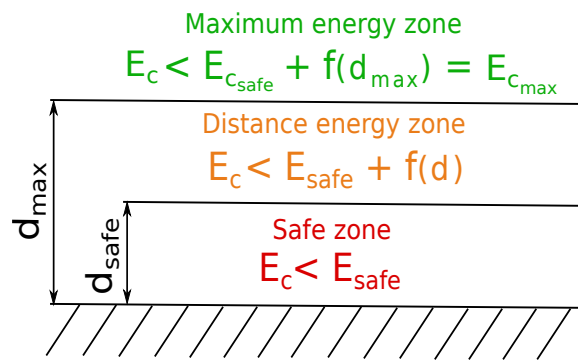


Figure 2.3: Energy zones for the dynamic behaviour of the robot.

When the relative distance between the robot and the human operator is decreasing, the system must be able to develop sufficient braking capabilities (torque and jerk) to satisfy

the imposed cartesian constraint on its kinetic energy; And this during two phases: First at the activation of the constraint, producible torque and jerk must be considered for the induced braking movement that makes the robot's kinetic energy cope with E_{climit} ; The second is when the kinetic energy is already sticking to the maximum allowed energy E_{climit} . Thus, the variation of the weighting function $f(d)$ must also account for the reaction capabilities of the robot at every time-step.

From the Work-Energy theorem, the amount of work exerted on the robot during the braking phase is equal to the variation of its kinetic energy. Moreover, this work can be expressed as a product between the *equivalent braking force* F_{eq} applied on the end-effector and the braking distance:

$$\begin{aligned} W &= \Delta E_c \\ &= F_{eq}(d - d_{safe}) \\ &= E_{climit}(d) - E_{climit}(d_{safe}) \\ &= f(d) - f(d_{safe}). \end{aligned} \tag{2.16}$$

The term f represents the maximum energy that can be dissipated during the braking phase. By choosing this function to be linear inside the distance energy working zone (see Figure 2.2), it can be written:

$$f(d) = K(d - d_{safe}). \tag{2.17}$$

The smaller the braking distance, the higher the slope coefficient of the weighting function $f(d)$ must be. K represents the equivalent braking force applied on the end-effector in the direction of the obstacle. It depends on the available braking torque $\tau_{braking}$, jerk capabilities and the Jacobian $J(\mathbf{q})_{EE}$ of the end-effector projected in the direction of the considered obstacle:

$$\tau_{braking} = J(\mathbf{q})_{EE}^{EE,O^T} K. \tag{2.18}$$

For every time-step, the instantaneous equivalent braking force in cartesian space can be computed as following :

$$\arg \max_K \|K\|^2, \quad (2.19)$$

s.t:

$$\begin{cases} \tau_{braking} = J(\mathbf{q})_{EE}^{EE,O^T} K, \\ \tau_M \leq \tau_{braking} \leq \tau_m \end{cases} \quad (2.20a)$$

$$(2.20b)$$

$\tau_{braking}$ and K are the optimization variables. τ_M, τ_m are the maximum and minimum producible torque.

For (2.17), K must be guaranteed over all the braking distance d . However, $\tau_{braking}$ and $J(\mathbf{q})_{EE}^{EE,O}$ can only be considered constant locally; The computation of K depends then on the future configurations of the robot along the braking distance d . Given the non linear nature of robotic manipulators, predicting the evolution of K is a complex problem. In the worst case, its value is very close to 0 and to ensure safety, E_{climit} should always be equal to E_{csafe} , strongly limiting the dynamic performances of the robot. On the other hand, using actuators capable of deploying high braking torques/jerks allows to significantly decrease the braking distance d . In this case, a local estimation of $\tau_{braking}$ and $J(\mathbf{q})_{EE}^{EE,O}$ will be a good approximation. Given the global objectives of this work, an average value of $K (> 0)$ is considered all over the workspace of the robot.

2.3.1.1 Pre collision safety criterion extension

The safety criterion previously introduced considers the squared relative velocity between the end-effector and a nearby obstacle. Therefore, there is no differentiation between the case where the robot is going towards the obstacle and where it is moving away from it. In a forbidden contact situation ($E_{csafe} = 0$), $v = 0$ is imposed which forbids the robot from going towards the obstacle but also from moving away from it. To avoid constraining the motion of the robot in the opposite direction of the obstacle, the

safety indicator can be signed :

$$S_c = \frac{1}{2} \text{sign}(v) m(\mathbf{q})^{eq} v^2, \quad (2.21)$$

with $\text{sign}(v) = 1$ when the end-effector is getting closer to the considered obstacle.

The safety criterion can be finally written:

$$S_c \leq E_{c_{safe}} + K(d - d_{safe}), \quad (2.22)$$

with S_c defined by (2.21). As previously explained, an other method to constrain the kinetic energy of the robot is to limit the amount of potential energy *injected* during the free movement of the robot. This potential energy changes the kinetic energy of the robot from $E_{c|k}^{EE,O}$ to $E_{c|k+1}^{EE,O}$.

$$E_{c|k+1}^{EE,O} - E_{c|k}^{EE,O} = E_{p|k}^{EE,O} \Rightarrow E_{c|k}^{EE,O} + E_{p|k}^{EE,O} = E_{c|k+1}^{EE,O} \leq E_{climit} \quad (2.23)$$

Based on (2.12), the constraint on kinetic energy expressed as a constraint on the *injected* potential energy can be written:

$$S_c = E_{c|k+1}^{EE,O} = \underbrace{E_{c|k}^{EE,O}}_{\text{measured}} + S_{pfree} \leq E_{climit} \Leftrightarrow S_{pfree} \leq \underbrace{E_{c_{safe}} + K(d - d_{safe})}_{E_{climit}} - \underbrace{E_{c|k}^{EE,O}}_{\text{measured}} \quad (2.24)$$

With: $S_{pfree} = E_{p|k}^{EE,O} = m(\mathbf{q})^{eq}_{EE,O} \dot{\mathbf{X}}_{EE|k}^{EE,O} \left\| \mathbf{X}_{EE|k+1} - \mathbf{X}_{EE|k} \right\|_{EE,O}$. The kinetic energy is tracked then saturated when reaching its allowed limit.

2.3.2 Safety limit value for the physical contact safety indicator

For $S_{p_{contact}}$, the safety criterion represents the maximum amount E_{plimit} of potential energy allowed to be generated within the human-robot system during physical contact. The value of E_{plimit} depends on several aspects: The desired degree of passivity of the robot, the maximum allowed contact forces, if a spring-damper like behaviour is desired and more importantly the degree of danger in case physical contact is released. Indeed, in such a situation, the stored potential energy E_{plimit} is to be rapidly transformed into

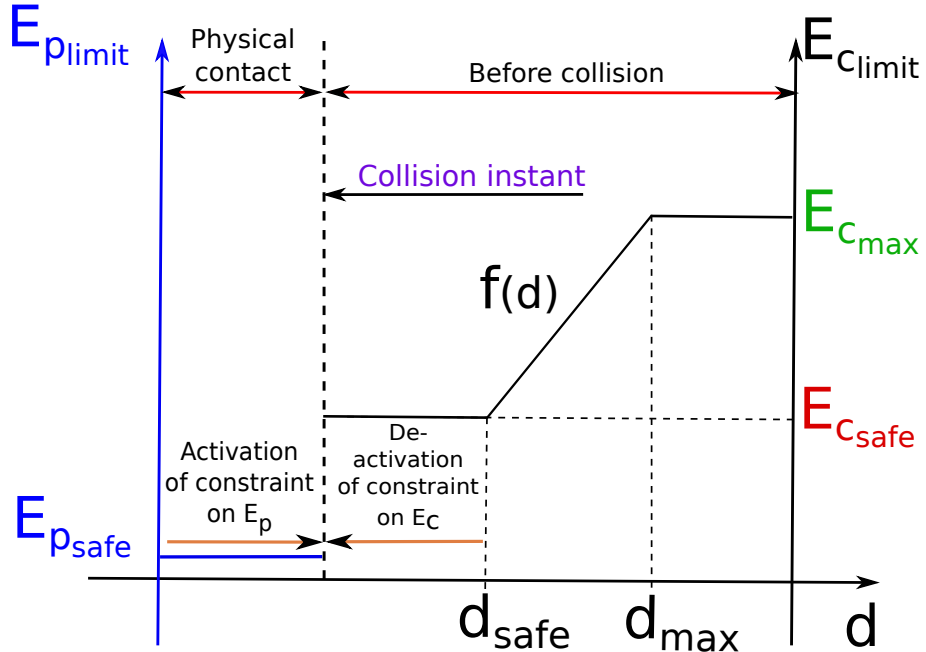


Figure 2.4: Evolution of the constraint on kinetic and potential energy depending on the distance d between the end-effector of the robot and the considered obstacle.

kinetic energy and if any collision occurs, the resulting impact force F_{impact} may be harmful. Therefore, the maximum value acceptable for $E_{p_{limit}} = E_{p_{safe}}$ should never be superior to $E_{c_{safe}}$:

$$S_{p_{contact}} \leq E_{p_{limit}} = E_{p_{safe}} \quad (2.25)$$

With: $0 \leq E_{p_{safe}} \leq E_{c_{safe}}$

2.3.3 Energies constraints activation/deactivation

Constraints on kinetic (2.15) and potential (2.25) energies can be implemented into a control optimization scheme as following: Before physical contact and during the approach of the human operator, only the constraint on kinetic energy (??) is considered. At collision, a safe amount of kinetic energy is dissipated creating a non hazardous impact force. Collision is detected, the constraint on S_c removed then simultaneously, the constraint on potential energy (2.25) is added to the controller (see Fig. 2.4). At the establishment of

physical contact, potential energy within the human-robot system increases to reach its maximum allowed value $E_{p_{limit}} = E_{p_{safe}}$. Depending on this value, the robot is more or less passive and can be moved easily. When physical contact is released, the constraint on potential energy is removed and the one on kinetic energy (2.15) can be reintroduced.

2.3.4 Task energy profile

In case of a trajectory tracking task, the amount of injected potential energy $E_{p|k}$ described in (2.13) can be measured at every time-step. As soon as $E_{p|k}$ is injected, the pulling force derived from it is created to drive the robot along its discretized trajectory. Because of this discretization, every time-step, only a small amount of potential energy is injected and transformed into kinetic one. For a repetitive trajectory tracking task, the energy profile $E_{p_{profile}}(t)$ ¹² can be initially registered during the free movement of the robot. Finally this profile can be used to constrain the instantaneous amount of potential energy the system is allowed to contain at every time-step. Therefore, in case of a collision/contact¹³, this constraint prevents the generation of high values of potential energy¹⁴ and thus of hazardous contact forces between the robot and its environment. To resume :

- Every repetitive trajectory tracking task has its own energy profile¹⁵.
- This energy profile is altered in case of any contact with the environment (more energy is charged in the system).
- A constrain on the instantaneously allowed amount of potential energy prevents the robot from crushing any obstacle during physical contact.

The constraint on the energy profile of a trajectory tracking task can be expressed at any potential collision point C . At the end-effector it is written:

$$S_{p_{profile}} = m(\mathbf{q}|k)_{EE,*}^{eq} \dot{\mathbf{X}}_{EE|k}^{EE,*} \left\| \mathbf{X}_{EE|k}^* - \mathbf{X}_{EE|k} \right\|_{EE,*} \leq E_{p_{limit}} = \underbrace{E_{p_{profile}}}_{measured} \quad (2.26)$$

¹²With: $E_{p_{profile}}(t = k\delta t) = E_{p|k}$

¹³Deliberate or accidental.

¹⁴The potential energy during physical contact is the extension of the potential energy *injected* in the robot during its free movement. $E_{p_{profile}}(t)$ can be used as $E_{p_{safe}}$ during physical contact.

¹⁵Just the needed amount of energy to accomplish the task.

Notice that the expression of $S_{p_{profile}}$ is the same as the expression of $S_{p_{contact}}$ ¹⁶ (2.8). However, the safety indicator related to the energy profile is defined for both *free movement* and *physical contact* phases. Using (2.26), the robot is prevented from deploying any additional energy than what is needed at time-step k for the accomplishment of its task. As it is activated only in case of collisions/physical contact with the environment, this constraint can always be included in the controller and used as a low-level security layer without altering the tracking performances related to the task. Even if collisions with the environment are not detected¹⁷, the robot will automatically comply to any external force preventing the generation of harmful contact forces.

When (2.26) is used to limit the potential energy injected every time-step in the system, (2.24) (or (2.3)) can be implemented in the controller at the same time and used to limit the deployed kinetic energy. Both constraints ((2.26) and (2.24)) or ((2.26) and (2.3)) are compatible and can be implemented *at the same time* in the optimization control scheme. On the other hand, in case E_{plimit} is fixed $< E_{p_{profile}}$, the performance of the trajectory tracking task will be deteriorated. Indeed, $E_{p_{profile}}$ is the amount of potential energy the system needs to transform into kinetic energy to accomplish its task in the most optimal way. At every time-step k , $E_{p_{profile}}$ can be computed as following :

$$E_{p_{profile}}(t = k\delta t) = m(\mathbf{q}_{|k})_{EE,*}^{eq} \ddot{\mathbf{X}}_{EE|k}^{EE,*} \left\| \mathbf{X}_{EE|k}^* - \mathbf{X}_{EE|k} \right\| \quad (2.27)$$

Or independently along the x , y and z axis in cartesian space:

$$\begin{cases} E_{p_{profile}}^x = m(\mathbf{q}_{|k})_x^{eq} \ddot{\mathbf{X}}_{x|k} \left\| \mathbf{X}_{x|k}^* - \mathbf{X}_{x|k} \right\|, \\ E_{p_{profile}}^y = m(\mathbf{q}_{|k})_y^{eq} \ddot{\mathbf{X}}_{y|k} \left\| \mathbf{X}_{y|k}^* - \mathbf{X}_{y|k} \right\|, \\ E_{p_{profile}}^z = m(\mathbf{q}_{|k})_z^{eq} \ddot{\mathbf{X}}_{z|k} \left\| \mathbf{X}_{z|k}^* - \mathbf{X}_{z|k} \right\|, \end{cases} \quad (2.28a)$$

$$\begin{cases} E_{p_{profile}}^x = m(\mathbf{q}_{|k})_x^{eq} \ddot{\mathbf{X}}_{x|k} \left\| \mathbf{X}_{x|k}^* - \mathbf{X}_{x|k} \right\|, \\ E_{p_{profile}}^y = m(\mathbf{q}_{|k})_y^{eq} \ddot{\mathbf{X}}_{y|k} \left\| \mathbf{X}_{y|k}^* - \mathbf{X}_{y|k} \right\|, \\ E_{p_{profile}}^z = m(\mathbf{q}_{|k})_z^{eq} \ddot{\mathbf{X}}_{z|k} \left\| \mathbf{X}_{z|k}^* - \mathbf{X}_{z|k} \right\|, \end{cases} \quad (2.28b)$$

$$\begin{cases} E_{p_{profile}}^x = m(\mathbf{q}_{|k})_x^{eq} \ddot{\mathbf{X}}_{x|k} \left\| \mathbf{X}_{x|k}^* - \mathbf{X}_{x|k} \right\|, \\ E_{p_{profile}}^y = m(\mathbf{q}_{|k})_y^{eq} \ddot{\mathbf{X}}_{y|k} \left\| \mathbf{X}_{y|k}^* - \mathbf{X}_{y|k} \right\|, \\ E_{p_{profile}}^z = m(\mathbf{q}_{|k})_z^{eq} \ddot{\mathbf{X}}_{z|k} \left\| \mathbf{X}_{z|k}^* - \mathbf{X}_{z|k} \right\|, \end{cases} \quad (2.28c)$$

Which allows enabling compliance to physical contact along the desired axis.

¹⁶That has been defined *only during physical contact* as the potential energy between the current position of the end-effector $\mathbf{X}_{|k}$ and its desired position $\mathbf{X}_{|k}^*$.

¹⁷In case of any problem with the collision detection algorithm.

2.4 Safe dynamic controller

In this section a dynamic control strategy that ensures safety for both the human operator and the robot is proposed. The objective is to compute the control torque τ^c in order to perform a trajectory tracking task while respecting a number of constraints at every time-step:

- Respect the introduced safety criteria to prevent harmful collisions and contacts,
- Respect the physical limits of the robotic system.

2.4.1 Task formulation

The objective function of the controller is defined as an error to be minimized. It could be for example an acceleration task if the robot has to perform a trajectory tracking, or a wrench task if the wrench applied on the environment needs to be controlled.

In the presented work, a trajectory tracking performance is considered. A cartesian acceleration task is defined as an error between the desired acceleration $\ddot{\mathbf{X}}^*$ and the expected acceleration $\ddot{\mathbf{X}}^c$ of the end-effector of the robot. Considering $\ddot{\mathbf{X}}^c = J(\mathbf{q}_{|k})_{EE} \ddot{\mathbf{q}}_{|k}^c + \dot{J}(\mathbf{q}_{|k})_{EE} \dot{\mathbf{q}}_{|k}$ (with $J(\mathbf{q}_{|k})_{EE}$ the Jacobian related to the end-effector), it can be written as a function of the control input $\tau_{|k}^c$ using the equation of motion of the system:

$$\ddot{\mathbf{X}}^c = J(\mathbf{q}_{|k}) M(\mathbf{q}_{|k})^{-1} \left(\tau_{|k}^c - \mathbf{b}(\mathbf{q}_{|k}, \dot{\mathbf{q}}_{|k}) \right) + \dot{J}(\mathbf{q}_{|k}) \dot{\mathbf{q}}_{|k}, \quad (2.29)$$

$\mathbf{b}(\mathbf{q}, \dot{\mathbf{q}})$ are the non linear terms of the equation of motion, namely gravity, Coriolis and centrifugal induced generalized forces. $\ddot{\mathbf{X}}^*$ can be computed with a PD controller and feed-forward acceleration term $\ddot{\mathbf{X}}_{ff}$ in order to track a desired trajectory \mathbf{X}^* and desired velocity $\dot{\mathbf{X}}^*$:

$$\ddot{\mathbf{X}}^* = \ddot{\mathbf{X}}_{ff} + K_p(\mathbf{X}^* - \mathbf{X}) + K_d(\dot{\mathbf{X}}^* - \dot{\mathbf{X}}) \quad (2.30)$$

where $K_p, K_d \in \mathbb{R}^+$ are the proportional and derivative gains. The acceleration task function to be minimized is finally written:

$$\mathbf{g}(\tau_{|k}^c, \ddot{\mathbf{X}}^c) = \ddot{\mathbf{X}}^* - \left(J(\mathbf{q}_{|k}) M(\mathbf{q}_{|k})^{-1} \left(\tau_{|k}^c - \mathbf{b}(\mathbf{q}_{|k}, \dot{\mathbf{q}}_{|k}) \right) + \dot{J}(\mathbf{q}_{|k}) \dot{\mathbf{q}}_{|k} \right). \quad (2.31)$$

2.4.2 Constraints formulation

2.4.2.1 Articular constraints

First, the physical limitations of the robot must be accounted for when solving the control problem. The computed control input $\tau_{|k}^c$ at instant k must be such that the considered limits are never violated. The actuators limitations are considered at the following levels: q , \dot{q} , \ddot{q} and \dddot{q} . Generally, these are expressed as inequality constraints and activated only one time-step in case the considered limits are reached; As explained into chapter 1, this can result into incompatibility problems that render the control problem impossible to solve. For e.g. no sufficient torque/jerk capabilities may be available to cope with an articular position or velocity limit within only one control time-step duration. Therefore, the modified articular constraints new formulations introduced in chapter 1 are used.

Inequality constraints corresponding to the articular physical limitations of the robot are written :

$$\left\{ \begin{array}{l} q_{|k+n_{15}+n_{17}+n_{19}} \leq q_M, \\ q_{|k+n_{16}+n_{18}+n_{20}} \geq q_m, \\ \dot{q}_{|k+n_1} \leq \dot{q}_M, \\ \dot{q}_{|k+n_2} \geq \dot{q}_m, \\ \tau_m \leq \tau_{|k}^c \leq \tau_M, \\ \ddot{q}_m \leq \ddot{q}_{|k+1} \leq \ddot{q}_M \end{array} \right. \quad \begin{array}{l} (2.32a) \\ (2.32b) \\ (2.32c) \\ (2.32d) \\ (2.32e) \\ (2.32f) \end{array}$$

$$\left\{ \begin{array}{l} q_{|k+n_{15}+n_{17}+n_{19}}, q_{|k+n_{16}+n_{18}+n_{20}} \\ \dot{q}_{|k+n_1}, \dot{q}_{|k+n_2} \\ \tau_{|k}^c \\ \ddot{q}_{|k+1} \end{array} \right. \quad \begin{array}{l} \text{as in (1.50)} \\ \text{and equivalent to (1.13).} \end{array}$$

To be easily accounted for, these constraints must be expressed as a function of the control variable $\ddot{q}_{|k}^c$. This can be done giving the state of the system at instant k and a discrete

linear approximation of the behaviour of the robot in joint space:

$$\left\{ \begin{array}{l} f_\chi(\mathbf{q}_m, \ddot{\mathbf{q}}_M, \ddot{\mathbf{q}}_M, \ddot{\mathbf{q}}_m, n_{16}, n_{18}, n_{20}) \leq \ddot{\mathbf{q}}_{|k}^c \leq f_\phi(\mathbf{q}_M, \ddot{\mathbf{q}}_m, \ddot{\mathbf{q}}_m, \ddot{\mathbf{q}}_M, n_{15}, n_{17}, n_{19}), \\ f_\beta(\dot{\mathbf{q}}_{|k}, \dot{\mathbf{q}}_m, \ddot{\mathbf{q}}_M, n_2) \leq \ddot{\mathbf{q}}_{|k}^c \leq f_\alpha(\dot{\mathbf{q}}_{|k}, \dot{\mathbf{q}}_M, \ddot{\mathbf{q}}_m, n_1), \end{array} \right. \quad (2.33a)$$

$$\boldsymbol{\tau}_m \leq \boldsymbol{\tau}_{|k}^c \leq \boldsymbol{\tau}_M, \quad (2.33b)$$

$$\ddot{\mathbf{q}}_m \delta t + \ddot{\mathbf{q}}_{|k} \leq \ddot{\mathbf{q}}_{|k}^c \leq \ddot{\mathbf{q}}_M \delta t + \ddot{\mathbf{q}}_{|k} \quad (2.33d)$$

With: f_χ, f_ϕ, f_β and f_α respectively equivalent to (1.53), (1.54), (1.14) and (1.16).

Finally, in addition to the articular constraints, the system is also subject to the linear constraints corresponding to its dynamic model :

$$M(\mathbf{q}_{|k}) \ddot{\mathbf{q}}_{|k}^c + \mathbf{b}(\mathbf{q}_{|k}, \dot{\mathbf{q}}_{|k}) = \boldsymbol{\tau}_{|k}^c \quad (2.34)$$

2.4.2.2 Energy related constraints

In an equivalent way, the safety indicators S_c and $S_{p_{free}}$, $S_{p_{contact}}$ and $S_{p_{profile}}$ can be expressed as a function of the control variable $\ddot{\mathbf{q}}_{|k}$.

First, based on (2.15), during free movements of the robot, S_c is expressed :

$$S_c = E_{c|k+1}^{EE,O} = \frac{1}{2} \text{sign}(v_{EE|k+1}^{EE,O}) m(\mathbf{q}_{|k})_{EE,O}^{eq} v_{EE|k+1}^{EE,O^2} \quad (2.35)$$

With:

$$\left\{ \begin{array}{l} v_{EE|k+1}^{EE,O} = J(\mathbf{q}_{|k})_{EE}^{EE,O} \dot{\mathbf{q}}_{|k+1}, \\ \dot{\mathbf{q}}_{|k+1} = \dot{\mathbf{q}}_{|k} + \ddot{\mathbf{q}}_{|k}^c \delta t \end{array} \right. \quad (2.36a)$$

$$\left\{ \begin{array}{l} v_{EE|k+1}^{EE,O} = J(\mathbf{q}_{|k})_{EE}^{EE,O} \dot{\mathbf{q}}_{|k+1}, \\ \dot{\mathbf{q}}_{|k+1} = \dot{\mathbf{q}}_{|k} + \ddot{\mathbf{q}}_{|k}^c \delta t \end{array} \right. \quad (2.36b)$$

Considering the second formulation of the kinetic energy of the system (2.24), S_c can also be written:

$$S_c = E_{c|k+1}^{EE,O} = \underbrace{E_{c|k}^{EE,O}}_{measured} + S_{p_{free}}^{18} = E_{c|k}^{EE,O} + m(\mathbf{q})_{EE,O}^{eq} \ddot{\mathbf{X}}_{EE|k}^{EE,O} \left\| \mathbf{X}_{EE|k+1} - \mathbf{X}_{EE|k} \right\|_{EE,O} \quad (2.37)$$

$$\text{With: } \ddot{\mathbf{X}}_{EE|k}^{EE,O} = \dot{J}(\mathbf{q}|k)_{EE}^{EE,O} \dot{\mathbf{q}}|k + J(\mathbf{q}|k)_{EE}^{EE,O} \ddot{\mathbf{q}}^c|k \quad (2.38)$$

$\mathbf{X}_{EE|k+1}$ is the future position of the end-effector. It can be estimated as following :

$$\mathbf{X}_{EE|k+1} = \mathbf{X}_{EE|k} + \underbrace{\dot{\mathbf{X}}_{EE|k}}_{measured} \delta t + \frac{1}{2} \underbrace{\ddot{\mathbf{X}}_{EE|k}}_{measured} \delta t^2 \quad (2.39)$$

On the other hand, during physical contact, $S_{p_{contact}}$ is expressed:

$$S_{p_{contact}} = m(\mathbf{q})_{EE,*}^{eq} \ddot{\mathbf{X}}_{EE|k}^{EE,*} \left\| \mathbf{X}_{EE|k}^* - \mathbf{X}_{EE|k} \right\|_{EE,*} \quad (2.40)$$

$$\text{With: } \ddot{\mathbf{X}}_{EE|k}^{EE,*} = \dot{J}(\mathbf{q}|k)_{EE}^{EE,*} \dot{\mathbf{q}}|k + J(\mathbf{q}|k)_{EE}^{EE,*} \ddot{\mathbf{q}}^c|k \quad (2.41)$$

Or independently along the x , y and z axis in cartesian space:

$$S_{p_{contact}}^x = m(\mathbf{q}|k)_x^{eq} \ddot{\mathbf{X}}_{x|k} \left\| \mathbf{X}_{x|k}^* - \mathbf{X}_{x|k} \right\|, \quad (2.42a)$$

$$S_{p_{contact}}^y = m(\mathbf{q}|k)_y^{eq} \ddot{\mathbf{X}}_{y|k} \left\| \mathbf{X}_{y|k}^* - \mathbf{X}_{y|k} \right\|, \quad (2.42b)$$

$$S_{p_{contact}}^z = m(\mathbf{q}|k)_z^{eq} \ddot{\mathbf{X}}_{z|k} \left\| \mathbf{X}_{z|k}^* - \mathbf{X}_{z|k} \right\|, \quad (2.42c)$$

Finally, constraints related to S_c and S_p that will be considered and tested¹⁹ using the presented optimization control scheme are as following :

- During the pre-collision phase:

¹⁸Here, $S_{p_{free}}$ is the injected potential energy expressed at the end-effector in the direction of the considered obstacle O during the free movement of the robot.

¹⁹In simulation and on the real robot

- Constraint on the kinetic energy (classic formulation) :

$$S_c = \frac{1}{2} \text{sign}(v_{EE|k+1}^{EE,O}) m(\mathbf{q}|_k)^{eq}_{EE,O} v_{EE|k+1}^{EE,O^2} \leq E_{c_{limit}} = E_{c_{safe}} + K(d - d_{safe}) \quad (2.43)$$

With $\text{sign}(v_{EE|k+1}^{EE,O})$ estimated by :

$$\text{sign}(v_{EE|k+1}^{EE,O}) = \text{sign}(v_{EE|k}^{EE,O} + \underbrace{\ddot{X}_{EE|k}^{EE,O} \delta t}_{\text{measured}}) \quad (2.44)$$

- Constraint on the kinetic energy (second formulation):

$$S_c = E_{c|k}^{EE,O} + S_{p_{free}} \leq E_{c_{limit}} = E_{c_{safe}} + K(d - d_{safe}) \quad (2.45)$$

Which transforms into:

$$m(\mathbf{q})_{EE,O}^{eq} \ddot{\mathbf{X}}_{EE|k}^{EE,O} \left\| \mathbf{X}_{EE|k+1} - \mathbf{X}_{EE|k} \right\|_{EE,O} \leq E_{c_{limit}} - \underbrace{E_{c|k}^{EE,O}}_{\text{measured}} \quad (2.46)$$

with $\mathbf{X}_{EE|k+1}$ estimated as in (2.39).

- During physical contact:

$$S_{p_{contact}} = m(\mathbf{q})_{EE,*}^{eq} \ddot{\mathbf{X}}_{EE|k}^{EE,*} \left\| \mathbf{X}_{EE|k}^* - \mathbf{X}_{EE|k} \right\|_{EE,*} \leq E_{p_{limit}} = E_{p_{safe}} \quad (2.47)$$

If decoupled along the x , y and z axis in cartesian space:

$$\begin{cases} S_{p_{contact}}^x = m(\mathbf{q}|_k)_x^{eq} \ddot{\mathbf{X}}_{x|k} \left\| \mathbf{X}_{x|k}^* - \mathbf{X}_{x|k} \right\| \leq E_{p_{safe}}^x, \end{cases} \quad (2.48a)$$

$$\begin{cases} S_{p_{contact}}^y = m(\mathbf{q}|_k)_y^{eq} \ddot{\mathbf{X}}_{y|k} \left\| \mathbf{X}_{y|k}^* - \mathbf{X}_{y|k} \right\| \leq E_{p_{safe}}^y, \end{cases} \quad (2.48b)$$

$$\begin{cases} S_{p_{contact}}^z = m(\mathbf{q}|_k)_z^{eq} \ddot{\mathbf{X}}_{z|k} \left\| \mathbf{X}_{z|k}^* - \mathbf{X}_{z|k} \right\| \leq E_{p_{safe}}^z \end{cases} \quad (2.48c)$$

Note: As expressed, (2.47) and (2.48) prevent the robot from generating harmful contact forces along the considered axis²⁰. With these constraints, contact forces are

²⁰Only in the positive direction of the axis.

diminished but the robot cannot be pushed in the opposite direction²¹. Therefore, it's the absolute value of potential energy that should be constrained. (2.47) and (2.48) are rewritten:

$$|S_{p_{contact}}| \leq E_{p_{safe}} \Leftrightarrow \begin{cases} S_{p_{contact}} \leq E_{p_{safe}}, \\ S_{p_{contact}} \geq -E_{p_{safe}} \end{cases} \quad (2.49a)$$

$$(2.49b)$$

And when decoupled :

$$\begin{cases} S_{p_{contact}}^x \leq E_{p_{safe}}^x, \\ S_{p_{contact}}^x \geq -E_{p_{safe}}^x, \end{cases} \quad (2.50a)$$

$$(2.50b)$$

$$\begin{cases} S_{p_{contact}}^y \leq E_{p_{safe}}^y, \\ S_{p_{contact}}^y \geq -E_{p_{safe}}^y, \end{cases} \quad (2.50c)$$

$$(2.50d)$$

$$\begin{cases} S_{p_{contact}}^z \leq E_{p_{safe}}^z, \\ S_{p_{contact}}^z \geq -E_{p_{safe}}^z, \end{cases} \quad (2.50e)$$

$$(2.50f)$$

- During both phases :

$$|S_{p_{profile}}| = \left| m(\mathbf{q})_{EE,*}^{eq} \ddot{\mathbf{X}}_{EE|k}^{EE,*} \| \mathbf{X}_{EE|k}^* - \mathbf{X}_{EE|k} \|_{EE,*} \right| \leq E_{p_{profile}}^{22} + \epsilon_{E_p} \quad (2.51)$$

Which can also be decoupled along the x , y and z axis in cartesian space.

$$\begin{cases} |S_{p_{profile}}^x| = \left| m(\mathbf{q}|_k)_x^{eq} \ddot{\mathbf{X}}_{x|k} \| \mathbf{X}_{x|k}^* - \mathbf{X}_{x|k} \| \right| \leq E_{p_{profile}}^x + \epsilon_{E_p}^x, \end{cases} \quad (2.52a)$$

$$\begin{cases} |S_{p_{profile}}^y| = \left| m(\mathbf{q}|_k)_y^{eq} \ddot{\mathbf{X}}_{y|k} \| \mathbf{X}_{y|k}^* - \mathbf{X}_{y|k} \| \right| \leq E_{p_{profile}}^y + \epsilon_{E_p}^y, \end{cases} \quad (2.52b)$$

$$\begin{cases} |S_{p_{profile}}^z| = \left| m(\mathbf{q}|_k)_z^{eq} \ddot{\mathbf{X}}_{z|k} \| \mathbf{X}_{z|k}^* - \mathbf{X}_{z|k} \| \right| \leq E_{p_{profile}}^z + \epsilon_{E_p}^z \end{cases} \quad (2.52c)$$

(2.51) or (2.52) can be implemented simultaneously with (2.43) or (2.45); It can also replace (2.50). ϵ_{E_p} is a constant used to compensate repeatability related variations of $E_{p_{profile}}$.

²¹Which is important regarding the safety of the operator during physical contact.

²²Measured during a free movement of the robot.

2.4.3 Controller formulation

The proposed controller computes the command torque by minimizing the norm of the cartesian acceleration task function expressed in the following quadratic form:

$$\arg \min_{\tau_{|k}^c} \left\| \mathbf{g} \left(\boldsymbol{\tau}_{|k}^c, \ddot{\mathbf{X}}^c \right) \right\|_{Q_t}^2 + \epsilon \|\boldsymbol{\tau}_{|k}^c\|_{Q_r}^2, \quad (2.53)$$

subject to (2.33), (2.34) and will be tested with: (2.43), (2.45), (2.47) and (2.51).

Note: Because of possible incompatibility problems with the energy based constraints²³, the *hard-coded* constraint on jerk (2.33d) will be removed from the controller when any energy based constraint is to be activated. Q_t and Q_r are positive semi-definite weighting matrices and $\|a\|_Q$ is the Q -weighted euclidean norm of a . In this case, Q_t and Q_r are identity matrices. $\epsilon \|\boldsymbol{\tau}_{|k}^c\|_{Q_r}^2$ with $\epsilon = 10^{-6}$ serves as a regularization task in order to ensure the uniqueness of the control solution and minimize the norm of the computed control torque. It can be shown that the quadratic forms composing the tasks expression can be written as a function of positive semidefinite matrix. Constraints expressed in (2.33), (2.43), (2.45), (2.51) and (2.47) are linear and can be written on the form: $Gx \leq h$ with: $x = [\boldsymbol{\tau}_{|k}^c, \ddot{\mathbf{q}}_{|k}^c]^T$. This LQP optimization problem is then convex and admits a unique global minimum.

2.5 Experimental results: Simulation

The controller described in Section 2.4 is implemented as a C++ Orocos component [[Soetens](#)] on a virtual model of the KUKA LWR4 serial robot using XDE, a robotics-oriented physics simulation engine [[Merlhiot 12](#)].

In this section, different behaviours that can be induced using different values of the algorithm parameters and the introduced energy based constraints are presented and discussed. First, a test case scenario used as a basis for all the different controller configurations is presented. An obstacle is introduced in the workspace of the robot and different interaction modes are simulated. Non physical interactions and collision tests

²³Incompatibilities may arise from the amount of jerk needed to cope with an energy based constraint. If this amount is superior to the articular capabilities of the system, the LQP becomes unsolvable.

are performed with and without constraints on the energy of the robot.

2.5.1 Test case scenario

As a main activity, the robot performs a repetitive pick and place movement²⁴ where it tracks a desired position and orientation in cartesian space (see Fig. 2.5). At the same time, its end-effector carries a load of 5 kg. The controller described in (2.53) is implemented without any energy related constraint. Only the linear constraints (2.33) corresponding to the articular limitations of the robot in addition to the equality constraints (2.34) corresponding to its dynamic model are considered. The LQP is solved at every time-step to compute the needed control torque $\tau_{|k}^c$. The problem is solved in real time using Gurobi, a commercial optimization software [Gurobi Optimization Inc. 15].

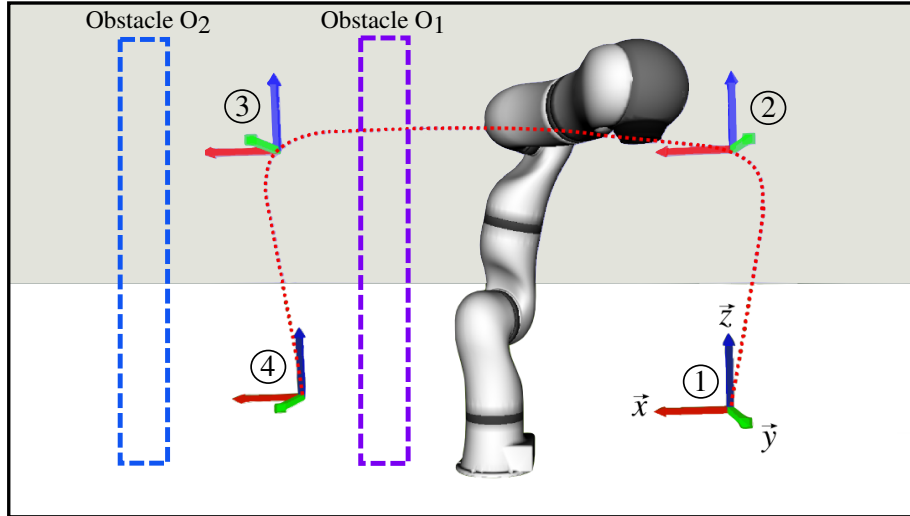


Figure 2.5: KUKA LWR4 serial robot within the XDE simulator near its considered obstacle. Case O_1 is when the obstacle intersects with the trajectory of the robot. Case O_2 is when the obstacle is nearby the robot but does not intersect with its trajectory

In this case, the movement of the robot is as dynamic as possible and the pick and place task is performed with maximum needed kinetic energy to track the desired X^* , \dot{X}^* and \ddot{X}_{ff} . Trajectory tracking performances can be observed in Fig. 2.6 and Fig. 2.7. Maximum tracking errors in cartesian space are as following: 1×10^{-3} m for position and

²⁴The trajectory for the pick and place movement is segmented into 3 segments: segment ①-②, ②-③ and ③-④. Trajectory for the next segment is not generated until the end-effector of the robot reaches the end of the current segment.

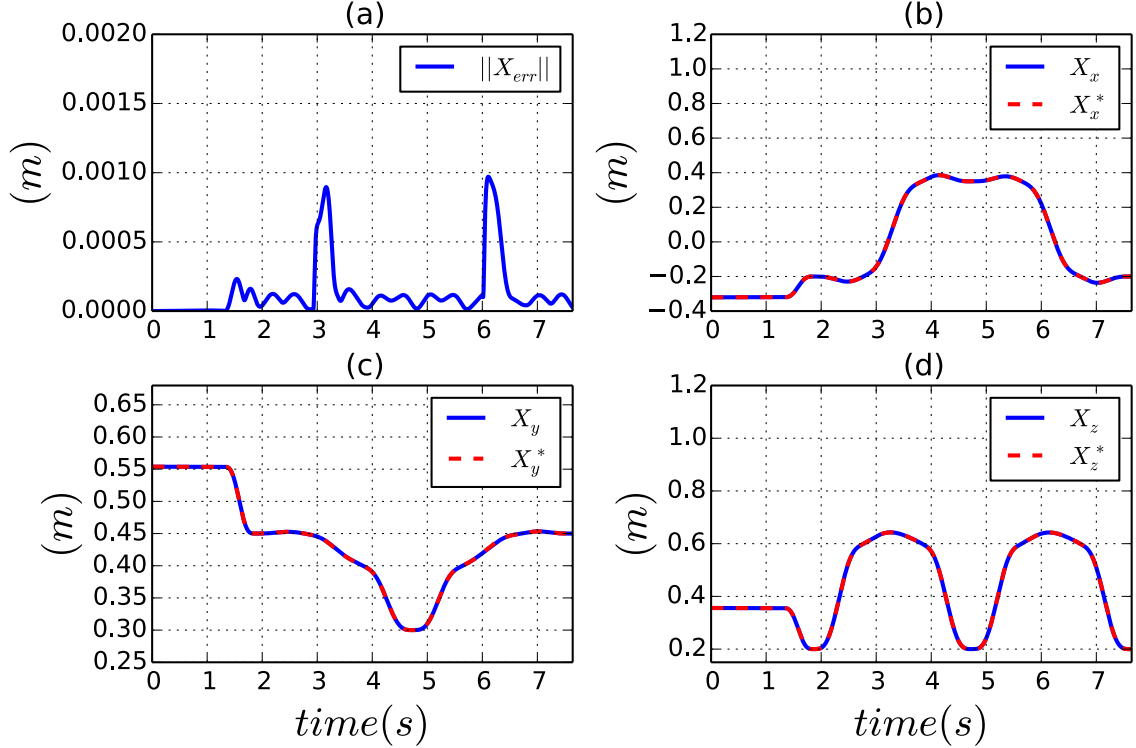


Figure 2.6: (a) Position tracking error for the end-effector along the x , y and z axis in cartesian space. (b), (c) and (d) are the real and desired position for the end-effector along the same axis.

$2.3 \times 10^{-2} \text{ rad}$ for orientation.

One of the main advantages of using a QP to compute the actuation torque is the ability to take into account the physical limitations of the system. Fig. 2.8 and Fig. 2.9 show how the limits on articular position, velocity, torque and also jerk are respected whenever a joint reaches its considered bounds. Along the movement of the robot, articular positions are within their max/min boundaries; And thanks to the new formulation of joint rate constraints ((2.32c) & (2.32d)), compatibility with articular jerk constraints (2.32f) is ensured. Indeed, when coping with a joint rate limit (see joint 0 in Fig. 2.8.b and Fig. 2.9.b), maximum producible jerk is used to bring the articular acceleration to zero²⁵.

The trajectory of the robot in this scenario does not intersect with any obstacle. During this *free* movement, a number of parameters related to the reaction capabilities of the robot and to the accomplished task are registered. Fig. 2.7.a illustrates the instantaneous

²⁵More details about this can be found in chapter 1.

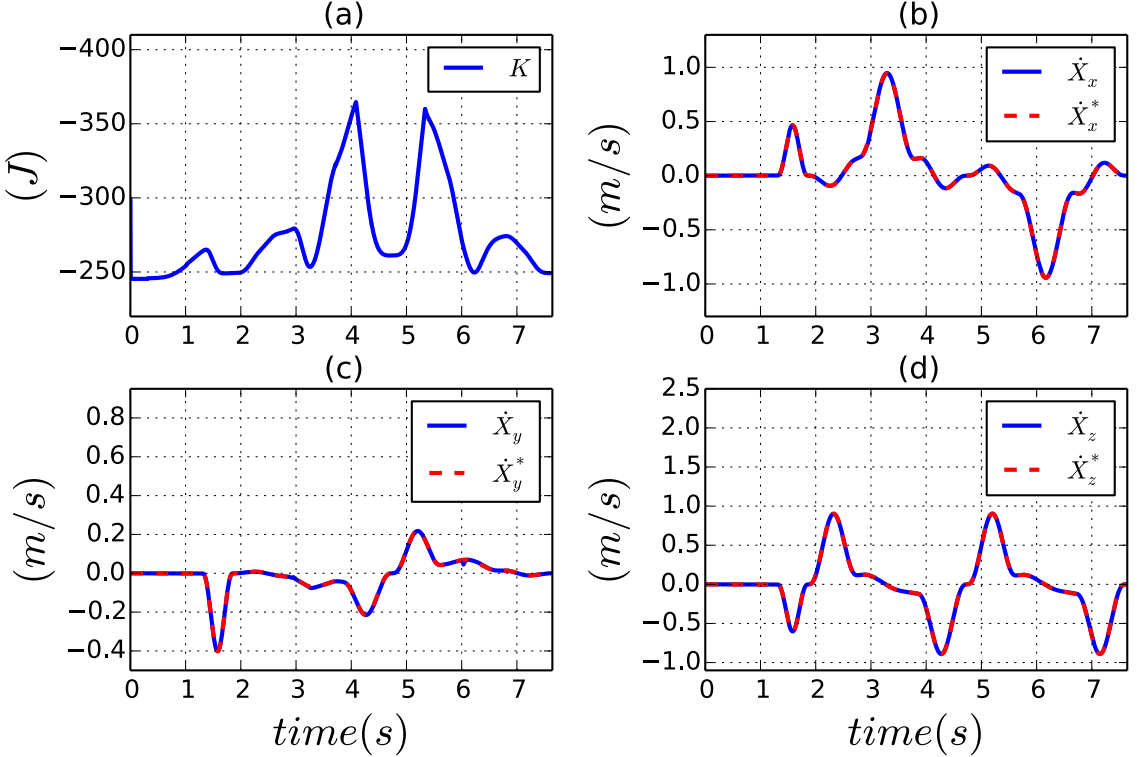


Figure 2.7: (a) Braking capability of the robot expressed at the end-effector in the opposite direction to the considered obstacle (case O_2 in Fig. ??). (b), (c) and (d) are the instantaneous real and desired velocity for the end-effector in cartesian space.

producible equivalent braking force in cartesian space expressed at the end-effector in the opposite direction to the nearby obstacle (case O_2 in Fig. 2.5). This force depends on the instantaneous articular configuration $q_{|k}$ and on the amount of torque producible by the actuators of the robot (2.19). The kinetic energy of the KUKA LWR4 expressed at its end-effector in the direction of the nearby considered obstacle (case O_2 in Fig. 2.5) is shown in Fig. 2.10.a. Maximum generated kinetic energy is 2.15 J; Which is equivalent to a 5 kg mass, moving at 0.92 m/s. At every time-step, the plotted kinetic energy is computed using two different methods :

$$S_c = E_{c|k}^{EE,O} = \frac{1}{2}m(\mathbf{q}_{|k})_{EE,O}^{eq}v_{EE|k}^{EE,O^2} \quad (2.54)$$

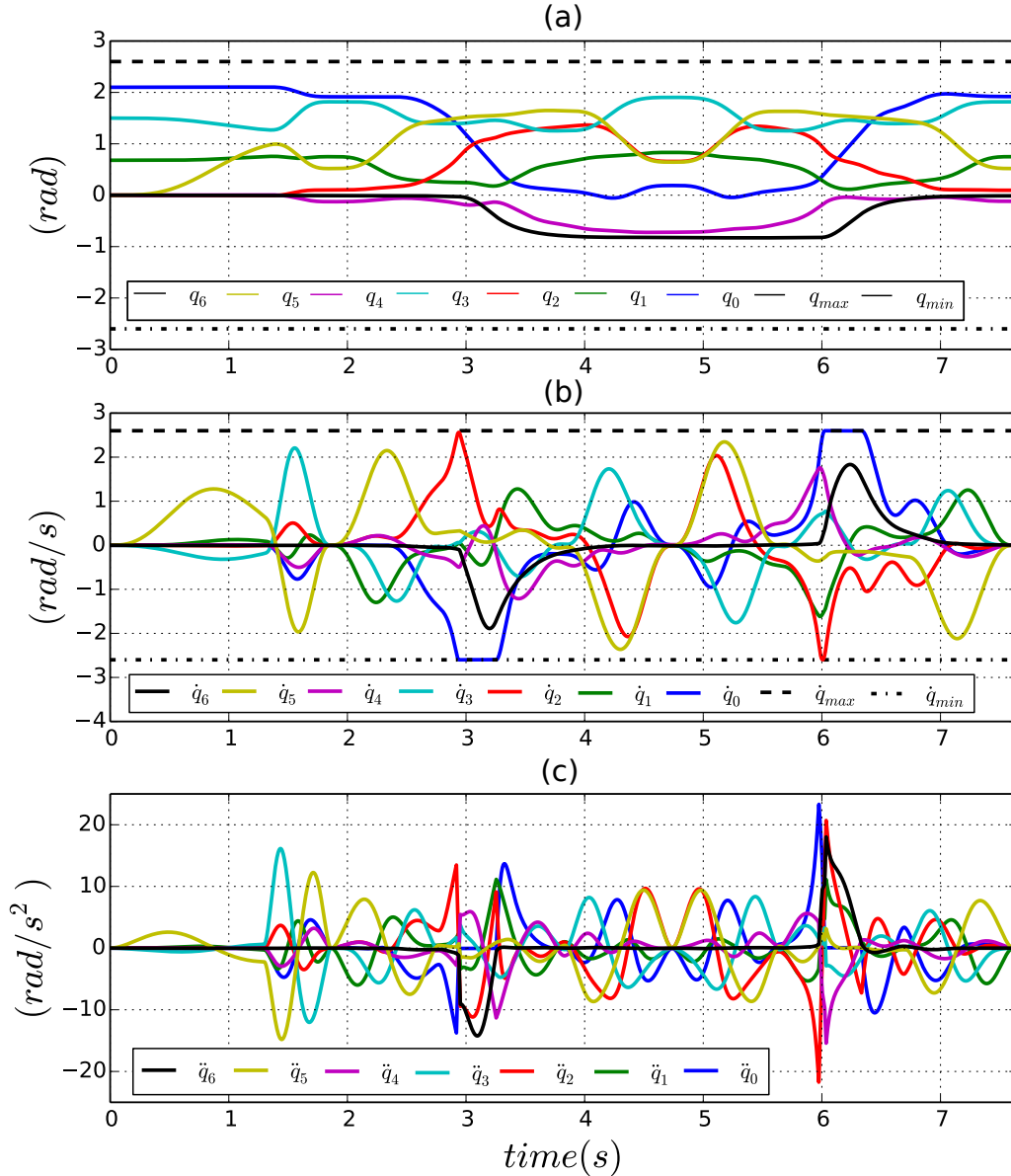


Figure 2.8: Articular position, velocity and acceleration corresponding to the pick and place movement as the energy of the robot is not constrained.

And:

$$S_c = E_{C|k}^{EE,O} = \sum_{n=1}^{k-1} S_{p_{free}|n} = \sum_{n=1}^{k-1} -m(\mathbf{q}_{|n})_{EE,O}^{eq} \dot{\mathbf{X}}_{C|n}^{EE,O} \left\| \mathbf{X}_{C|n+1} - \mathbf{X}_{C|n} \right\|_{EE,O} \quad (2.55)$$

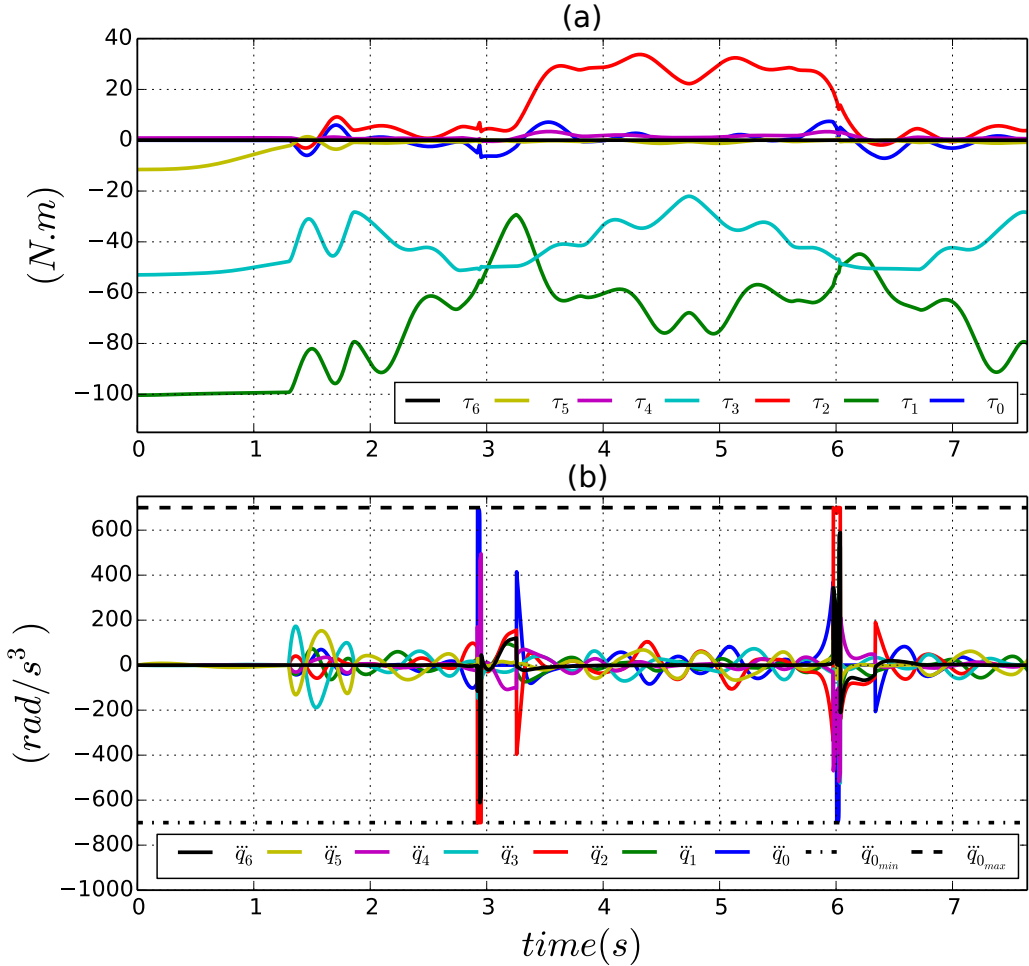


Figure 2.9: Articular torque and jerk corresponding to the pick and place movement as the energy of the robot is not constrained.

Fig. 2.10.a illustrates how the kinetic energy of the system at time-step k is indeed equal to the sum of all previously *injected* potential energies²⁶.

2.5.2 Obstacle intersecting with the robot trajectory and no constraints on energy

In this scenario, the obstacle intersects with the ②-③ segment of the pick and place movement trajectory (case O_1 in Fig. 2.5). When collision occurs between the robot

²⁶The small difference between the two curves is mainly caused by the variation of articular configuration between the successive time-steps $k - 1$ and k (Jacobian and equivalent mass are not considered at the same time-step).

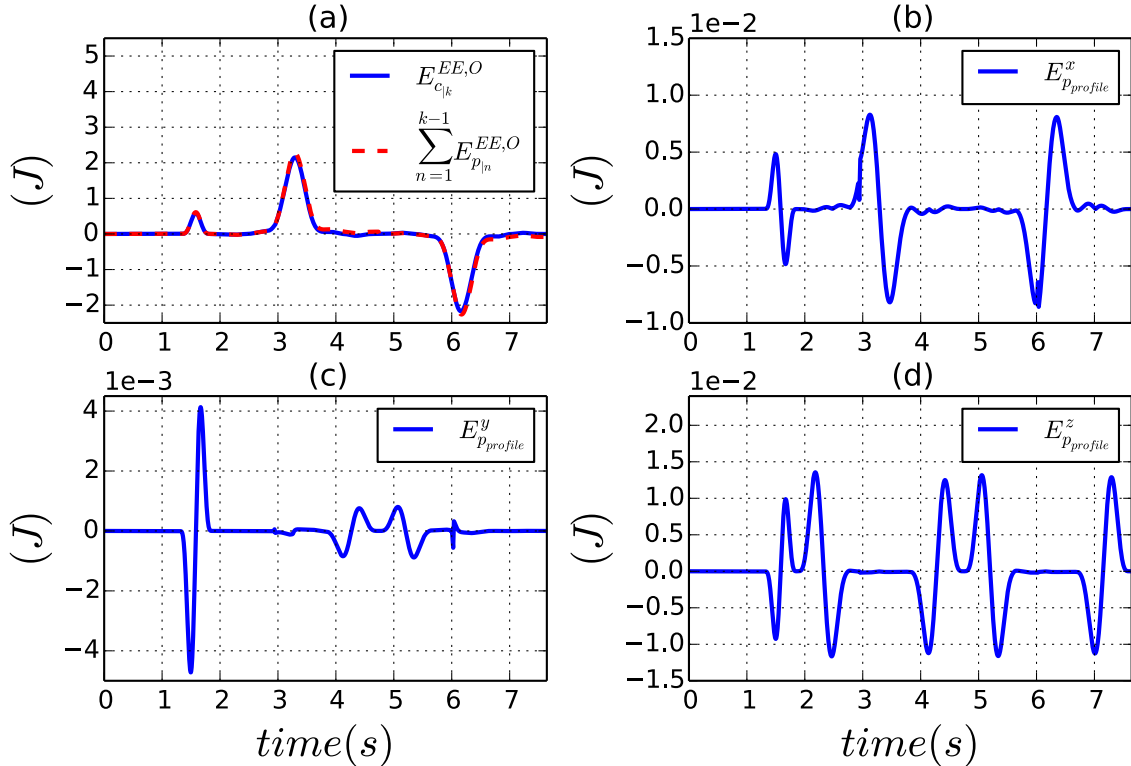


Figure 2.10: (a) Kinetic energy of the robot in the direction of the considered obstacle (case O_2 in Fig. 2.5), computed using (2.54) and (2.55) during the pick and place movement. (b), (c) and (d) are the energy profiles corresponding to the pick and place task along the x , y and z axis in cartesian space.

and the rigid object, most kinetic energy of the system is instantaneously dissipated. Fig. 2.11 shows how 1.66 J of this kinetic energy are instantaneously dissipated at impact. According to (2.1) and as can be seen in Fig. 2.12.b, this fast dissipation induces a large impact force of 551 N ²⁷; Which can damage to the collided obstacle.

After the peak of force corresponding to the first collision, physical contact between the robot and the wall is established. As the obstacle is blocking the movement of the KUKA LWR4, the divergence between the desired and real positions for the end-effector results into the augmentation of the amount of potential energy generated within the robot-obstacle system (see Fig. 2.12.a). Consequently, the resulting contact force along the x axis also intensifies. Torques generated by the actuators of the robot can be seen in Fig. 2.12.c. Contact force along the x axis is mainly caused by the torques generated by joint 0 and

²⁷A force sensor is linked to the base of the collided object (i.e. the wall). The main impact force is along the x axis, which is the main direction of movement of the end-effector before collision.

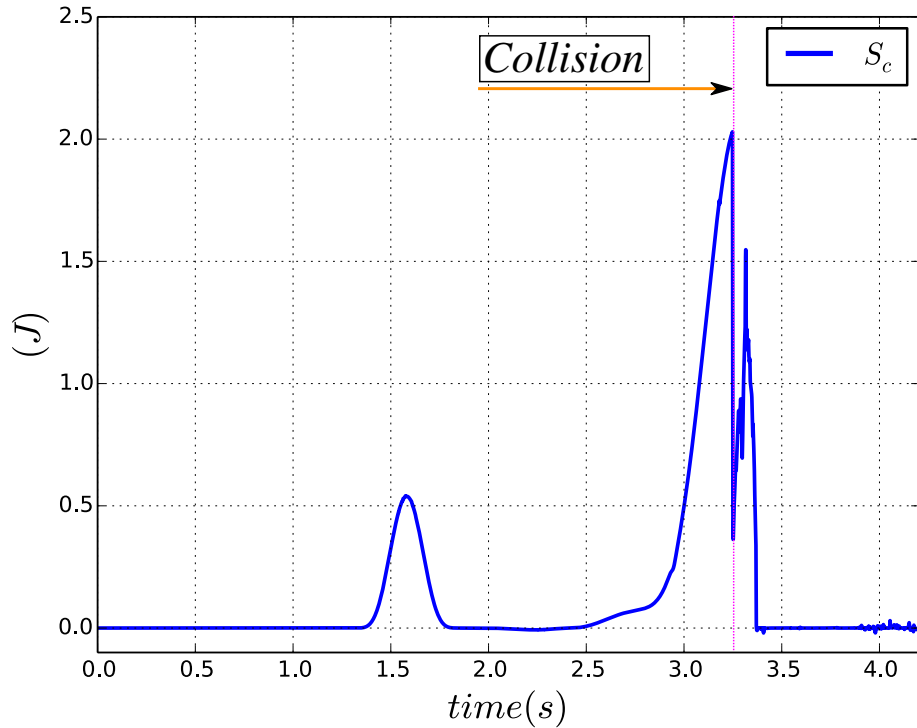


Figure 2.11: Dissipated kinetic energy of the KUKA LWR4 expressed at the end-effector in the direction of the considered obstacle during collision.

joint 2. Fig. 2.12.c shows how τ_0 and τ_2 increase to respectively reach $\approx -115 \text{ N.m}$ and $\approx -95 \text{ N.m}^{28}$. As depicted in Fig. 2.12.b, the corresponding contact force settles around 250 N .

Finally, considering the big amounts of generated impact and contact forces, the controller with its current configuration is not appropriate for enabling *safe* interactions between the robot and its environment. Therefore, the introduced energy related constraints will be included.

2.5.3 Nearby obstacle, not intersecting the robot trajectory and constraint on kinetic energy

In this case, the first formulation of the kinetic energy related constraint (2.43) is included in the controller to safely account for the presence of a nearby obstacle (i.e. the wall,

²⁸Negative torques on joint 0 and/or joint 2 cause the end-effector of the robot to move towards the wall. Positive torques make it move in the opposite direction.

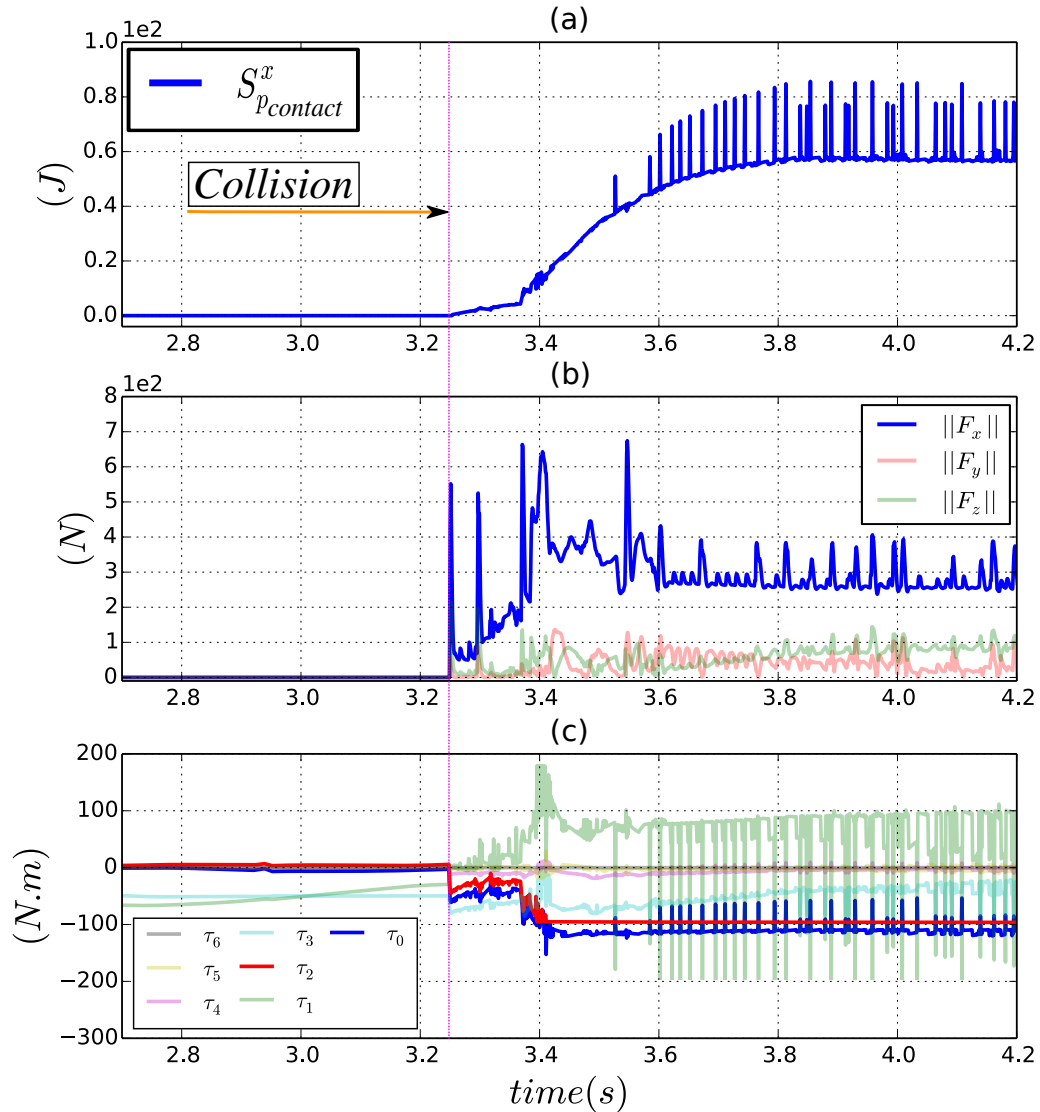


Figure 2.12: (a) Potential energy generated within the robot-obstacle system during physical contact along the x axis in cartesian space. (b) Contact forces between the robot and the wall after establishment of physical contact along the x , y and z axis in cartesian space. (c) Actuation torques during physical contact with the considered obstacle.

case O_2 in Fig. 2.5). This constraint limits the actuation torques and, according to (2.21), has a direct impact on the velocity of the end-effector. Depending on how the controller parameters d_{safe} , $E_{c_{safe}}$ and K are fixed, physical contact can be enabled or disabled²⁹. In this scenario, as shown in Fig. 2.13, the obstacle does not intersect with the trajectory

²⁹For example, fixing $d_{safe} = 2$ and $E_{c_{safe}} = 0$ forces the end-effector of the robot to stop at 2 m from the obstacle.

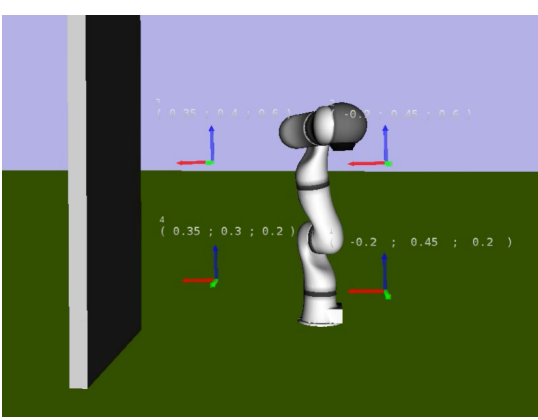


Figure 2.13: Screen-shot of the KUKA LWR4 robot within the XDE simulator with the wall not intersecting its trajectory.

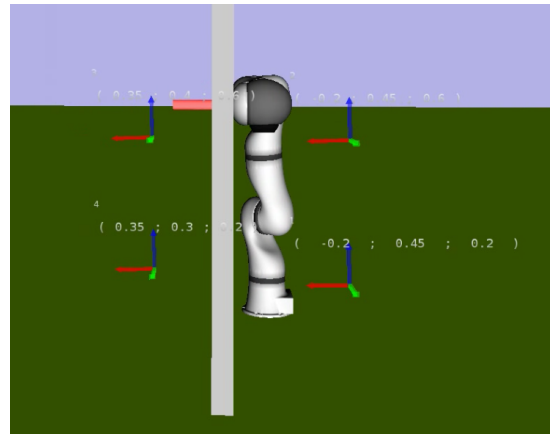


Figure 2.14: Screen-shot of the KUKA LWR4 robot within the XDE simulator during collision with the wall intersecting its trajectory.

of the pick and place movement. In addition to the constraint on the amount of kinetic energy generated in the direction of obstacle O_2 , the controller is implemented with inequality constraints corresponding to the articular limitations of the robot (2.33)³⁰ plus the dynamic equality constraints (2.34). The controller parameters are fixed as following: $E_{c_{safe}} = 0.1 \text{ J}$, $K = 5 \text{ N}$, $d_{safe} = 0.25 \text{ m}$ and $d_{max} = 0.8 \text{ m}$. In this particular case, the robot succeeds in achieving the pick and place movement but with diminished dynamic performances compared to the test case scenario in which the kinetic energy of the system is not constrained. Indeed, as shown in Fig. 2.16, constraining the kinetic energy of the robot has a direct influence on its velocity but also on its apparent inertia.

Fig. 2.15 shows how the kinetic energy related constraint is respected at every time-step; Accordingly, a drop in the velocity of the end-effector can be observed in Fig. 2.16.d along the x axis³¹ component in cartesian space. When the constraint on kinetic energy is active, we highlight the resulting de-synchronisation between the real and desired position/velocity for the end-effector. Caused by this same constraint, a discontinuity in the actuation torques (mainly τ_0 and τ_2) can be seen in Fig. 2.17.a. As the kinetic energy

³⁰Because of possible incompatibility problems, the constraint on articular jerk (2.33d) is removed when the constraint on the kinetic energy of the system (2.43) is to be activated.

³¹Direction of the closest distance vector between the end-effector and obstacle O_2 .

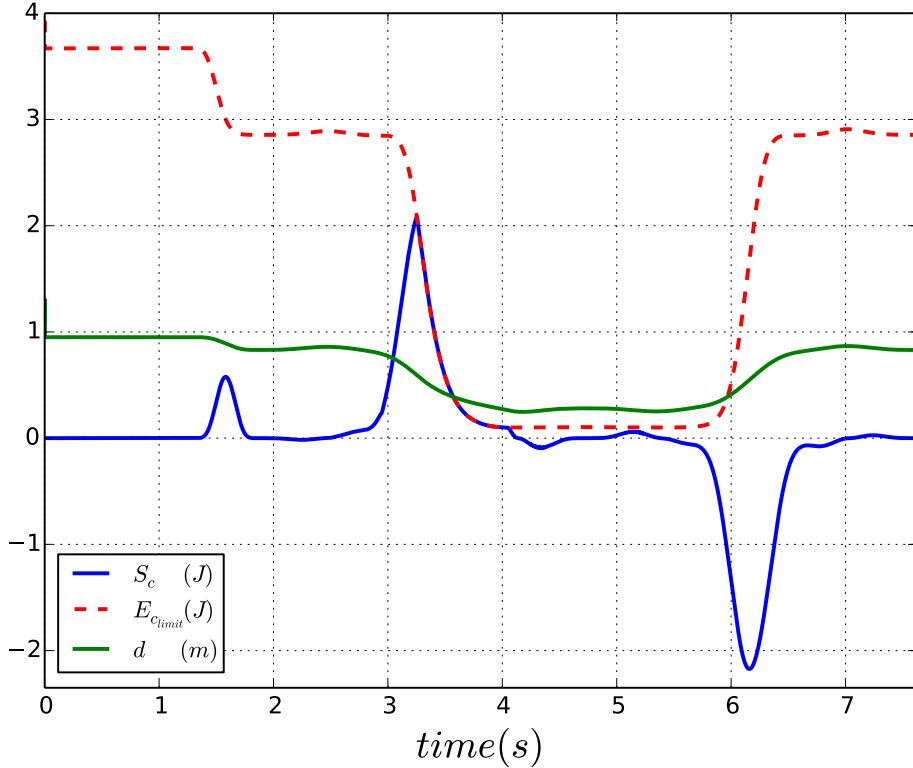


Figure 2.15: Constrained kinetic energy of the robot expressed at the end-effector in the direction of a nearby considered obstacle (case O_2 in Fig. 2.5).

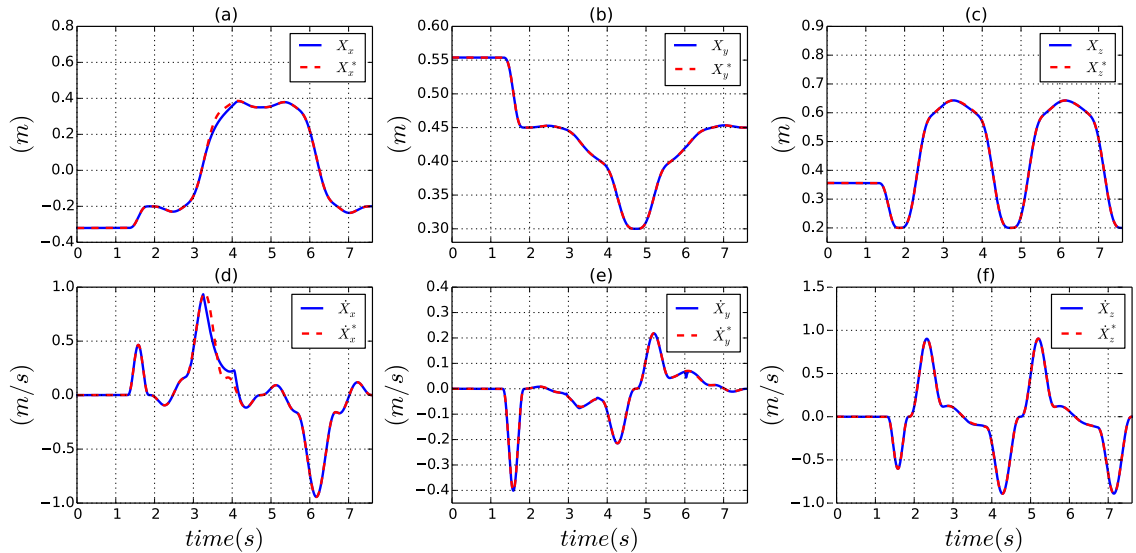


Figure 2.16: (a), (b) and (c) depict the real and desired position for the end-effector in cartesian space as the kinetic energy of the robot is constrained. (d), (e) and (f) are the real and desired velocity for the end-effector as the robot is submitted to the same constraint (case O_2 in Fig. 2.5).

related constraint is activated³² only one time-step before reaching the considered limit $E_{c_{limit}}$, high jerk performances are needed to comply with this bound in such a small window of time. As shown in Fig. 2.17.b, 10788 rad/s^3 of jerk is needed for joint 0 at the activation of the constraint on kinetic energy.

On the other hand, shattering phenomena in both articular torque and jerk (see Fig. 2.17) are caused by discontinuities in the real-time computed distance³³ between the robot and obstacle O_2 . These discontinuities are reflected on the maximum allowed kinetic energy $E_{c_{limit}}$ and thus on the control input $\tau_{|k}^c$.

Finally, as the kinetic energy of the robot is successfully constrained, the controller with its current configuration seems more appropriate for establishing safe physical interactions between the KUKA LWR4 and its environment. Which is presented in the following test.

2.5.4 Obstacle intersecting the robot trajectory and constraint on the kinetic energy

In this scenario, the obstacle intersects with the ②-③ segment of the pick and place movement trajectory. As the robot moves towards the wall, the first formulation of the kinetic energy related constraint (2.43) is included in the controller and used to reduce the kinetic energy of the KUKA LWR4 before collision (see Fig. 2.14). Articular constraints³⁴ and equality constraints described in (2.33) and (2.34) are also considered. The controller parameters are fixed as following: $E_{c_{safe}} = 0.05 \text{ J}$, $K = 50 \text{ N}$, $d_{safe} = 0.1 \text{ m}$ and $d_{max} = 0.3 \text{ m}$.

³²At the activation of the constraint on kinetic energy, a braking movement is induced by the actuators to decrease the kinetic energy of the robot. As the braking capabilities of the system are not considered in the mathematical formulation of this constraint (2.43); Coping with the maximum allowed amount of kinetic energy $E_{c_{limit}}$ may be impossible during only one control time-step. Because of incompatibility issues between the constraint on kinetic energy and the hard-coded constraint on articular jerk (2.33d), the LQP problem can become impossible to solve (Both constraints cannot be satisfied at the same time). For this reason, constraints on articular jerk are removed whenever an energy related constraint is activated.

³³The smallest distance between the end-effector and the obstacle is computed in real-time. It is directly fed to the controller without any filtering. This actually mimics the kind of data that can be acquired with a real-life system (e.g. a Microsoft Kinect).

³⁴The same as for the previous case, the constraint on articular jerk is removed from the controller whenever the constraint on kinetic energy (2.43) is activated.

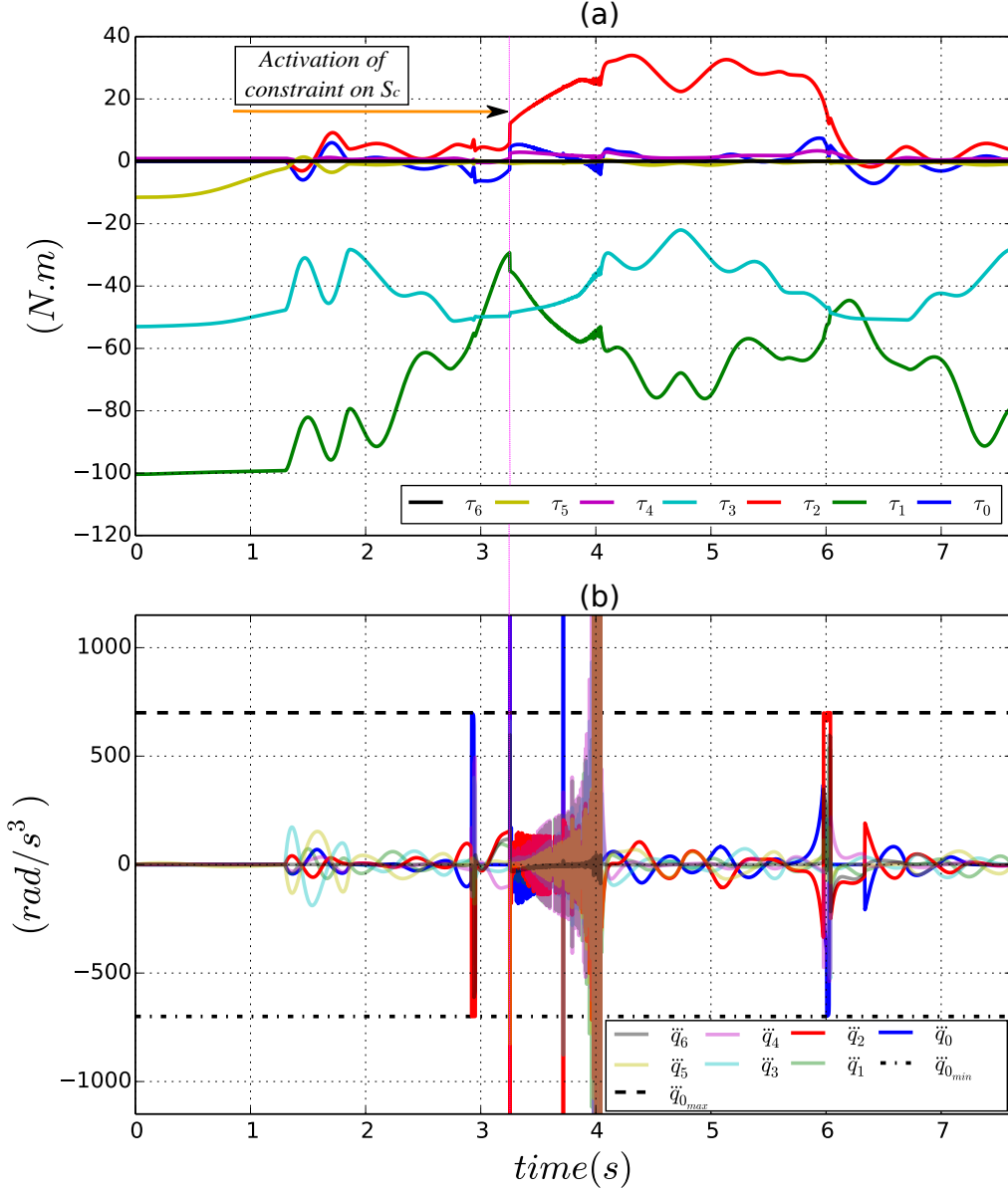


Figure 2.17: Generated articular torque and jerk as the constraint on the kinetic energy of the robot is activated (case O_2 in Fig. 2.5).

The dissipated kinetic energy at collision is shown in Fig. 2.18. Compared to the collision case where the kinetic energy of the robot is not constrained (as shown in Fig. 2.11), we underline the benefit of using the safety criterion introduced in (2.3). Indeed, at collision, the amount of dissipated kinetic energy ($0.035 J$) when this latter is initially constrained is far less than the dissipation without any constraint ($1.66 J$). Accordingly, the result-

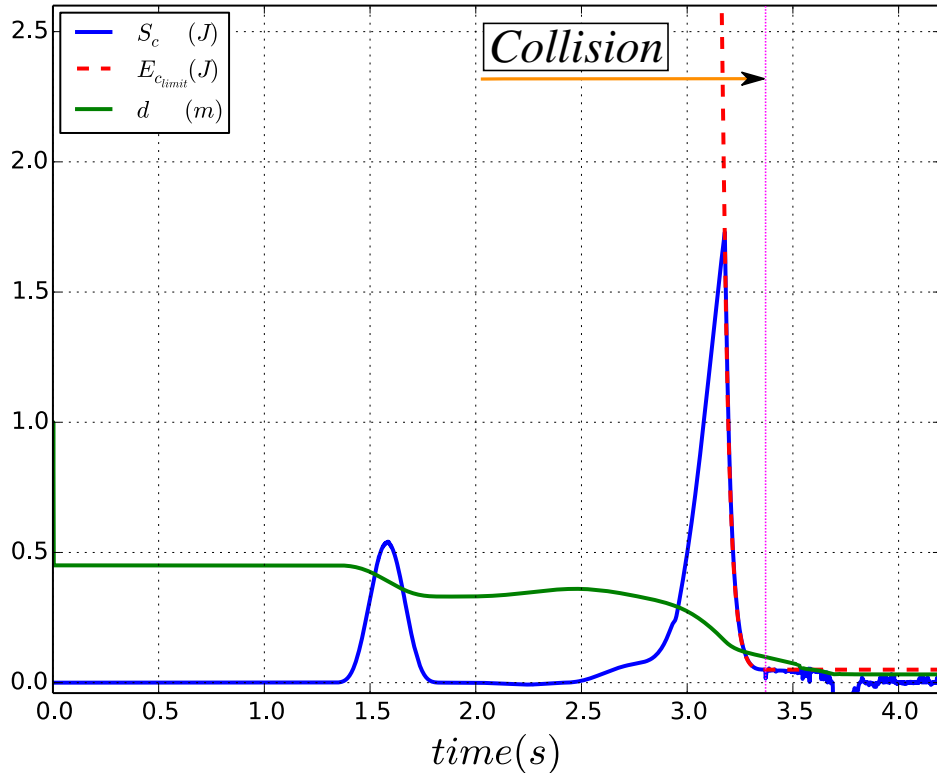


Figure 2.18: Constrained kinetic energy of the robot expressed at the end-effector in the direction of the collided obstacle (case O_1 in Fig. 2.5).

ing impact force shown in Fig. 2.19.a is much more reduced (86 N) when compared to the generated impact force in case the kinetic energy of the robot is not pre-constrained (551 N as shown in Fig. 2.12.b). This particular property³⁵ of the presented constraint (2.43) allows safer physical contact establishments/impacts between the robot and its environment.

On the other hand, as in scenario 2.5.2, after the establishment of physical-contact, potential energy starts building up within the robot-obstacle system (see Fig. 2.19.a). Consequently, as illustrated in Fig. 2.19.b, contact force also increases to reach an average value of 100 N. Which may be harmful for any human operator within the workspace of the robot. Actuation torques are shown in Fig. 2.19.

In this scenario, the constraint on kinetic energy is never removed from the controller³⁶.

³⁵The ability to impose the maximum amount of kinetic energy allowed to be dissipated at collision.

³⁶Even after the establishment of physical contact.

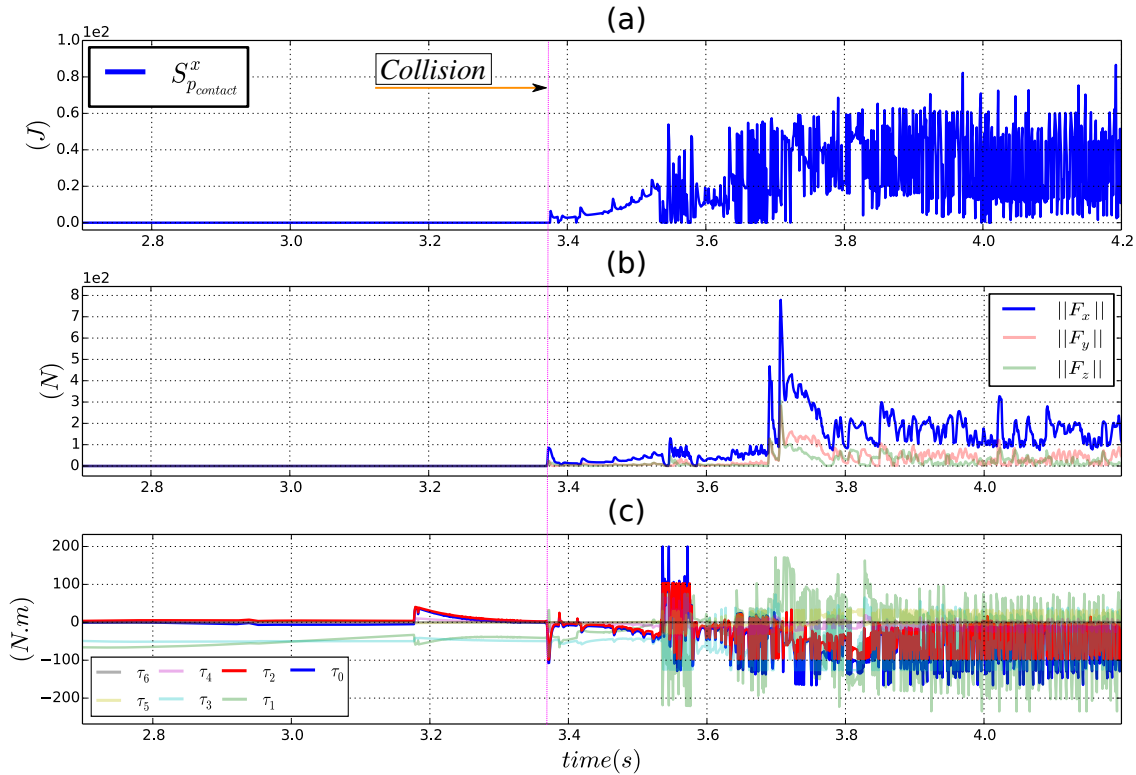


Figure 2.19: (a) Potential energy generated within the robot-obstacle system during physical contact along the x axis in cartesian space. (b) Corresponding contact forces along the x , y and z axis in cartesian space. (c) Actuation torques during physical contact with the considered obstacle (case O_1 in Fig. 2.5).

However, as it depends on the distance d between the robot end-effector and the considered obstacle, this constraint may be released if case d is equal to zero. To resume, the presented controller including the constraint on kinetic energy is safer during collisions compared to the case when the kinetic energy of the robot is not considered. To ensure safety even after the establishment of physical contact, the generated potential energy from which the hazardous contact forces are derived must also be constrained.

2.5.5 Obstacle intersecting the robot trajectory and constraint on the kinetic then potential energy

Same as before, in this scenario, the wall intersects with the ②-③ segment of the pick and place movement trajectory. As the robot moves, the second formulation of constraint (2.45) on the kinetic energy of the robot is included in the controller and used to limit

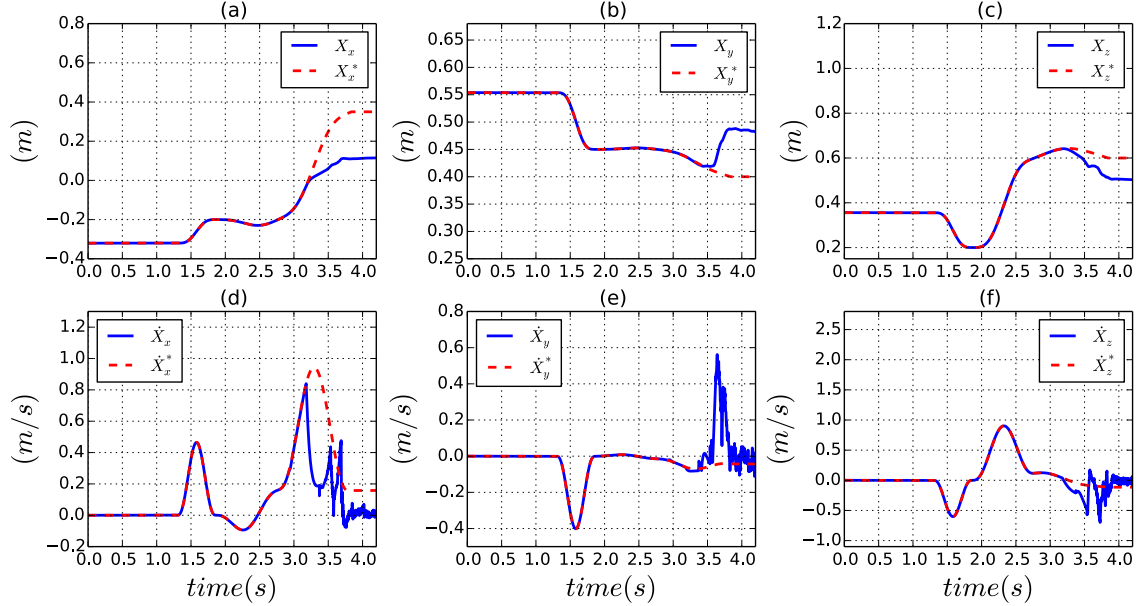


Figure 2.20: (a), (b) and (c) depict the real and desired position for the end-effector in cartesian space as the kinetic energy of the robot is constrained. (d), (e) and (f) are the real and desired velocity for the end-effector as the robot is submitted to the same constraint (case O_1 in Fig. 2.5).

the amount of kinetic energy, the KUKA LWR4 is allowed to deploy in the direction of obstacle O_1 . This constraint also depends on the real-time closest distance between the wall and the end-effector of the robot.

After the establishment of physical contact, the constraint (2.48a) is added³⁷ to the controller and used to saturate the amount of potential energy generated within the robot-obstacle system. Articular constraints and equality constraints described in (2.33) and (2.34) are also considered³⁸. The controller parameters are fixed as following: $E_{safe} = 0.05 \text{ J}$, $K = 50 \text{ N}$, $d_{safe} = 0.1 \text{ m}$, $d_{max} = 0.3 \text{ m}$ and $E_{psafe}^x = 0.1 \text{ J}$ ³⁹. Dissipated kinetic energy at collision is shown in Fig. 2.21. As this energy is pre-constrained, only 0.035 J of kinetic energy are dissipated at collision; Resulting into an impact force of 85 N (see Fig. 2.22.b).

As shown in Fig. 2.21, the second formulation of the constraint on kinetic energy (2.45)

³⁷Without removing the constraint (2.45) on kinetic energy.

³⁸Only when the energy related constraints are not activated.

³⁹During physical-contact, contact forces applied by the robot are *mainly* along the x axis. Consequently, only the potential energy along this axis is constrained.

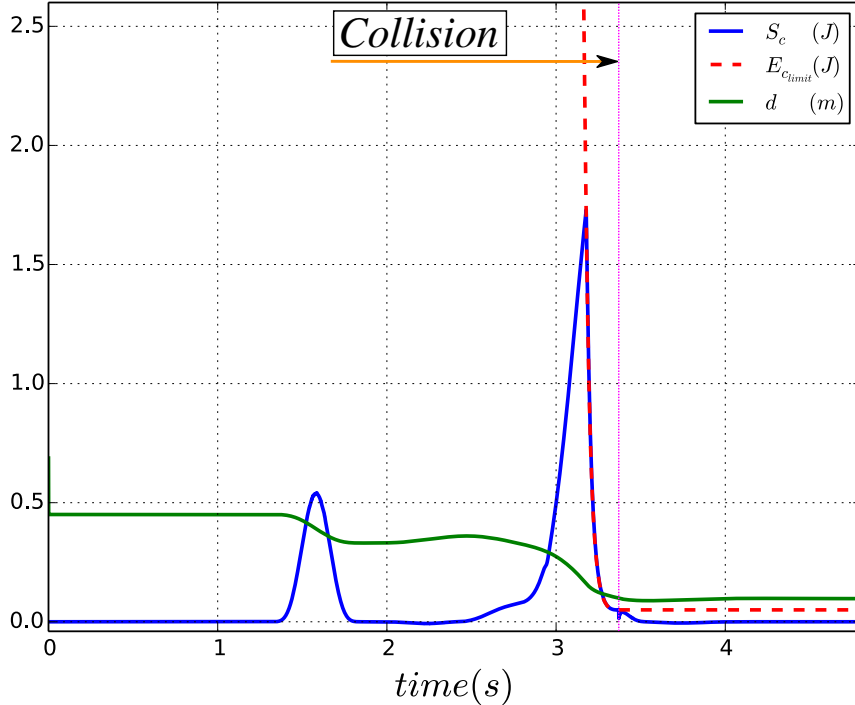


Figure 2.21: Constrained kinetic energy of the robot expressed at the end-effector in the direction of the collided obstacle (case O_1 in Fig. 2.5).

is respected at every time-step, exactly the same as when the first formulation (2.43) is used (see subsection 2.5.4). On the other hand, Fig. 2.22.a shows how the constraint on the potential energy generated within the robot-obstacle system is also respected at every time-step during physical contact. Because this potential energy is saturated at a constant value of 0.1 J , the contact force deriving from it decreases over time to reach 0 N ⁴⁰ (see Fig. 2.22.b) as the desired position for the end-effector diverges from its real position. In case the physical contact is established with a human operator, the robot can easily and safely be moved or pushed away. This behaviour⁴¹ is actually exactly the inverse of what happens when the potential energy related constraint is not included in the controller. Potential energy increases and accordingly hazardous contact forces (as shown in scenario 2.5.2). Fig. 2.22.c shows the actuation torques of joint 0 and joint 2 as the braking movement for the end-effector is induced to cope with the kinetic energy constraint

⁴⁰Physical contact is released.

⁴¹Decreasing of the contact force as the error between the desired and real position for the end-effector increases.

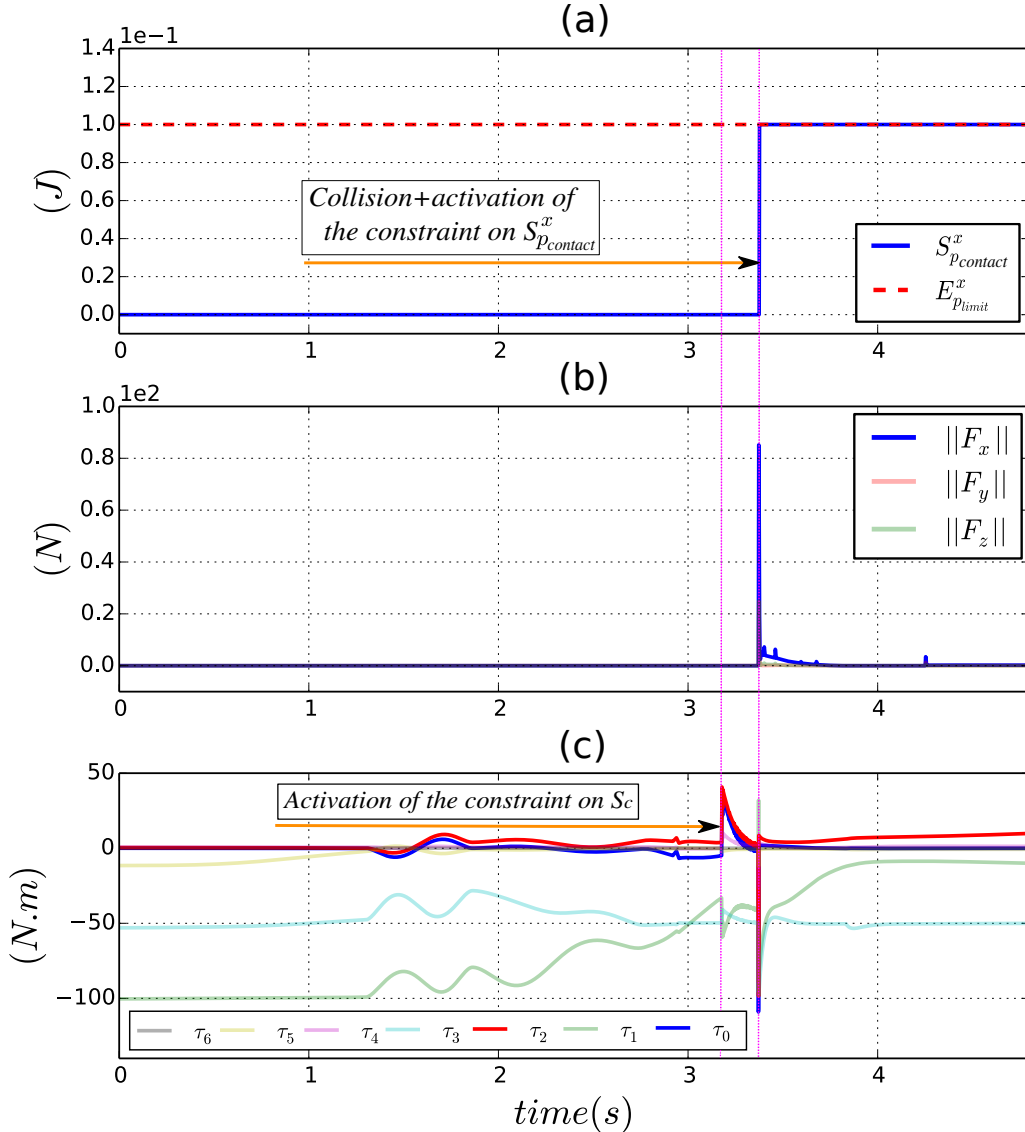


Figure 2.22: (a) Constrained potential energy within the robot-obstacle system during physical contact along the x axis in cartesian space. (b) Corresponding contact forces along the x , y and z axis in cartesian space. (c) Actuation torques during the physical contact with the considered obstacle (case O_1 in Fig. 2.5).

and also the resulting torques after collision when the constraint on potential energy is activated.

2.5.6 Obstacle intersecting the robot trajectory and constraint on the task energy profile

In this scenario, the obstacle intersects with the ②-③ segment of the pick and place movement trajectory. During the movement of the robot, its energy profile⁴² described in subsection 2.3.4 is constrained using (2.52). The kinetic energy of the KUKA LWR4 is not constrained and the articular and equality constraints respectively described in (2.33) and (2.34) are also included in the controller. Based on the measured energy profiles along the x , y and z axis as shown in Fig. 2.10, The controller parameters are fixed as following:

$$E_{p_{profile}}^x + \epsilon_{E_p}^x = 0.01 \text{ J}, E_{p_{profile}}^y + \epsilon_{E_p}^y = 0.0045 \text{ J} \text{ and } E_{p_{profile}}^z + \epsilon_{E_p}^z = 0.015 \text{ J}.$$

As can be seen in Fig. 2.23, performances related to the trajectory tracking task are not altered by the energy profile constraint during the pre-collision phase. Desired position and velocity are tracked exactly the same way as if this constraint is not included. At collision, the impact is not detected and the desired position (also the velocity) for the end-effector starts diverging from its real value. Potential energy between the robot and the wall starts to increase and triggers the activation of the energy profile constraint. During physical contact, this constraint behaves exactly the same as (2.50). As shown in Fig. 2.24, Potential energy within the robot-obstacle system is successfully limited along the x , y and z axis. The peak of potential energy along the x axis is caused by the impact force.

Fig. 2.25.a shows how 1.66 J of kinetic energy are dissipated at collision. Fig. 2.25.b depicts the resulting collision and contact force: 551 N are induced at the first impact⁴³ and due to the task energy profile constraint, contact forces are reduced and also decrease over time as the desired position for the end-effector is diverges. The robot in this case is compliant and can easily and safely be moved by a human operator. Related torques generated by the actuators of the robot during this scenario are shown in Fig. 2.25.

⁴²This energy profile is related to the accomplished task.

⁴³The other collision peaks are caused by collisions between other parts of the robot and the wall. The constraint on potential energy during physical contact does not prevent the accumulation of kinetic energy on the other free parts of the robot. For this reason, the kinetic energy related constraint should also be implemented in the controller.

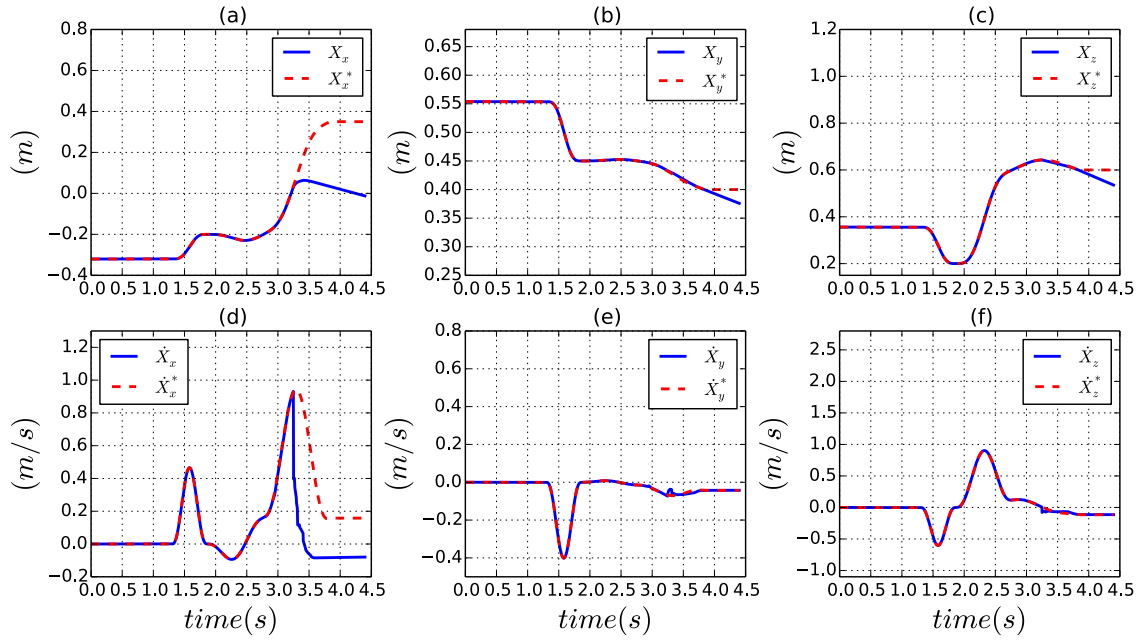


Figure 2.23: (a), (b) and (c) depict the real and desired position for the end-effector in cartesian space as the task energy profile of the robot is constrained. (d), (e) and (f) are the real and desired velocity for the end-effector as the robot is submitted to the same constraint (case O_1 in Fig. 2.5).

2.6 Conclusion

The energy based safety indicators proposed and validated in this chapter hold a great potential for human-robot collaboration tasks. Indeed, energy is a universal component that can describe all physical phenomena occurring during the interaction between the robot and its environment. Velocity, inertia, impact and also contact forces can all be expressed and modulated with this same entity. Using the presented control framework and the introduced energy based criteria, it has been proven possible to control the energy of the robot. During its movement, at every time-step, its kinetic energy can be tracked and saturated to meet the imposed safety criteria for the establishment of physical contact. Dissipated kinetic energy at impact is limited and the resulting collision force is safe.

After the establishment of physical contact, contact forces can also be saturated by constraining the potential energy generated between the robot and the considered obstacle. In case of a human-robot interaction, the robot can easily and safely be pushed and

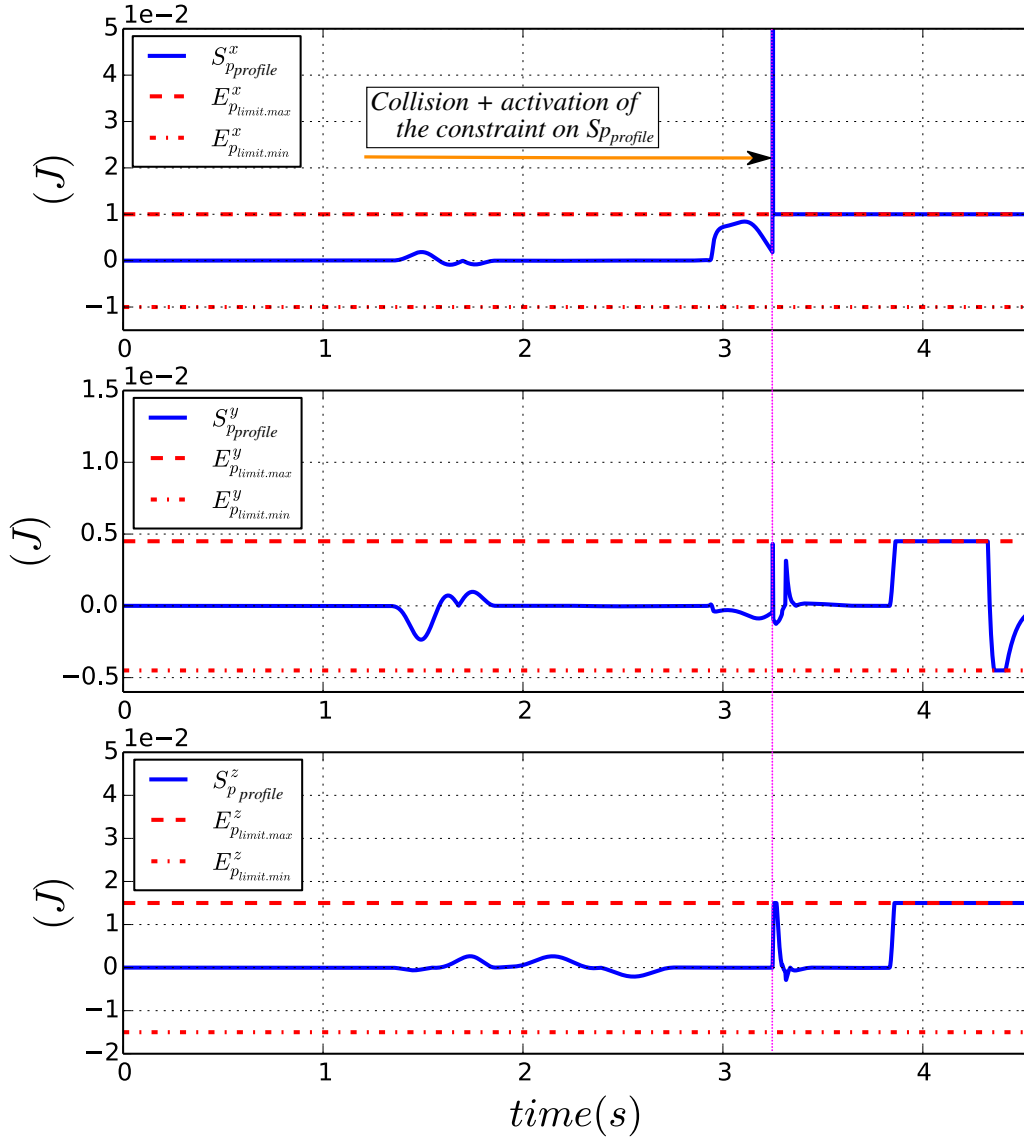


Figure 2.24: Constrained energy profile for the pick and place task along the x , y and z axis in cartesian space.

moved. As the energy of the robot can be controlled, physical contact releasing has also been made safer as the hazardous transformation of the controller related potential energy into kinetic one is prevented. In addition to the energy related constraints, the constraint on kinetic energy is reformulated as a constraint on the potential energy instantaneously held in the controller of the robot. Consequently, the amount of potential energy *injected* in the controller of the robot at every time-step can be used as a safety indicator for both pre and post collision phases.

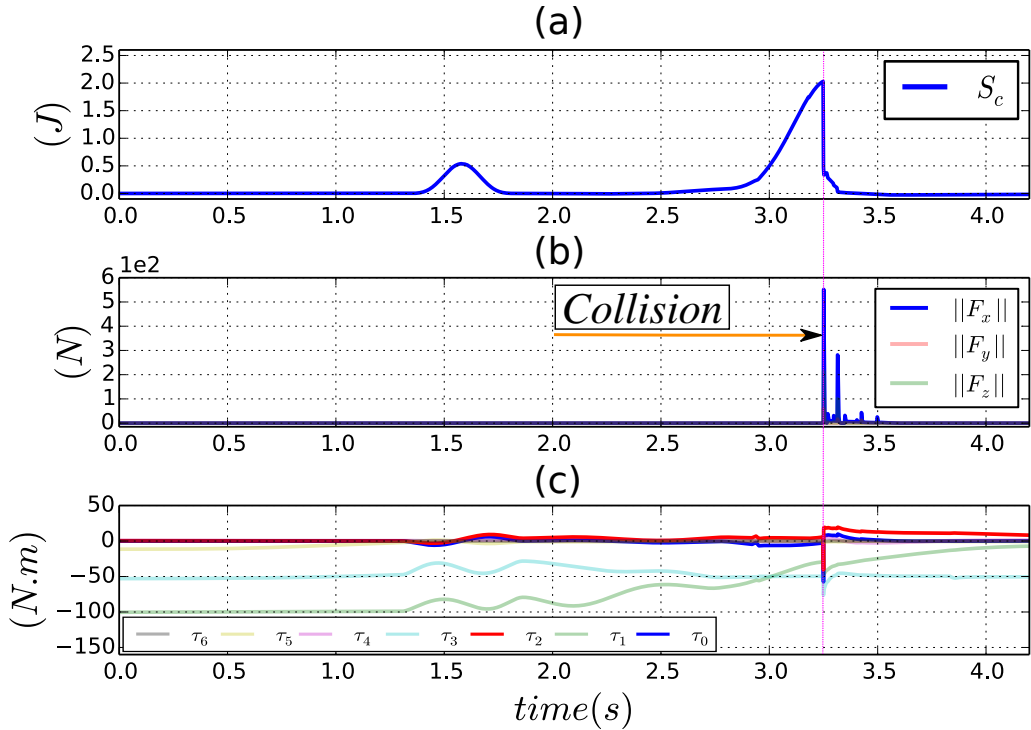


Figure 2.25: (a) The kinetic energy of the robot expressed at the end-effector as it physically interacts with the nearby obstacle (case O_1 in Fig. 2.5). (b) Corresponding contact forces along the x , y and z axis in cartesian space. (c) Actuation torques during the physical contact.

Moreover, the concept or *task energy profile* has been introduced and used to synthesise a low-level security layer to deal with non-deliberate or undetected collisions between the robot and its environment. This constraint on the task energy profile allows the robot to produce only the needed amount of energy to perform its main task; Which prevents any harmful contact forces as the controller of the robot is restrained from loading any additional amount of potential energy in case of collision.

Constraints on kinetic and potential energies are expressed in cartesian space and related to the instantaneous state $S_{|k} = \{\mathbf{q}_{|k}, \dot{\mathbf{q}}_{|k}, \ddot{\mathbf{q}}_{|k}, \dddot{\mathbf{q}}_{|k}\}$ of the robot. These constraints are of type 6 (see table 1.1) and are activated only one time-step before their respective limits. For example, the robot may not have sufficient braking capabilities to cope with the kinetic energy limit $E_{c_{limit}}$. Its braking capabilities, namely: producible articular deceleration $[\ddot{\mathbf{q}}_m, \ddot{\mathbf{q}}_M]$ and jerk $[\dddot{\mathbf{q}}_m, \dddot{\mathbf{q}}_M]$ should imperatively be part of the formulation of these constraints; Otherwise, constraints incompatibility issues (see chapter 1) may appear and

it may be impossible to implement these constraints on a real robot.

Chapter 3

Safe human-robot interaction: experimental results

Abstract

In this chapter, the control strategy and energy related constraints introduced in previous chapter are tested on a real KUKA LWR4 robot for interaction with a human operator. As the person approaches the robot, the distance between the two is computed in real-time using a point-cloud based algorithm acquired with a set of depth sensors (Kinects). This distance is used to generate a constraint on the kinetic energy of the robot. At collision, dissipated energy and the resulting impact force are reduced. After the establishment of physical contact, the second constraint is used to limit the amount of potential energy allowed to be generated within the human-robot system. Contact forces are saturated and the robot can safely be pushed or moved if needed. The overall framework allows a human operator to safely enter the workspace of the KUKA LWR4 and physically interact with it.

3.1 Introduction

In the following sections, the experimental setup for the KUKA LWR4 serial robot and the vision system used to detect the human operator are described. A test case scenario is presented and behaviours that can be induced using the presented controller and the energy related constraints are discussed.

3.2 Experimental setup

The distance between the robot and the human operator is computed using data from a set of 3 Kinects strategically placed around the workspace of the robot to avoid occlusions (see Fig. 3.1). RGB and depth images from each sensor are calibrated and the pose of each device in the robot’s base frame is computed. The robot and background are removed [KaewTraKulPong 02] from the depth images then the related pointclouds are down sampled and combined together. Finally the cluster of the human operator is extracted from the resulting pointcloud [Rusu 11] and the minimum distance between the end-effector of the robot and the human-operator is computed and published via a ROS topic. The controller described in section 3 is implemented as a C++ OROCOS [Soetens] component inside a generic software architecture developed at ISIR for robot manipulators[Hoarau]. The remote control PC runs a Xenomai [Chanteperrdrix] kernel with RTnet [Marx] to ensure minimum jitter in the real-time Ethernet communication. Finally, the communication with the KUKA LWR4 Robot Controller (KRC) is performed via the Fast Research Interface (FRI) [Schreiber 10].

3.3 Test case scenario

As a main activity, the robot performs a repetitive movement where it tracks a desired position on a straight line between two points (A) and (B)¹ in Cartesian space (see Fig. 3.1). The controller described in (2.53) is implemented with the articular constraints corresponding to the physical limitations of the KUKA LWR4 (2.33)² and with the equality constraints described in (2.34) corresponding to the dynamic model of the system. The LQP problem is solved at every time-step $\delta t = 15\text{ ms}$ to compute the needed control torque $\tau_{|k}^c$. Same as before, the LQP is solved in real-time using Gurobi, a commercial optimization software. The maximum tracking error for position in cartesian space (see Fig. 3.2.c) is around 0.051 m ; This is due to the activation of the articular velocity constraint (2.33b) as the velocity of joint 0 reaches its max/min limits. As shown

¹It’s only when the end-effector of the robot reaches one point (e.g. (A)) that the trajectory to the other point is generated (e.g. (B)).

²In this case, jerk related constraints are not considered.

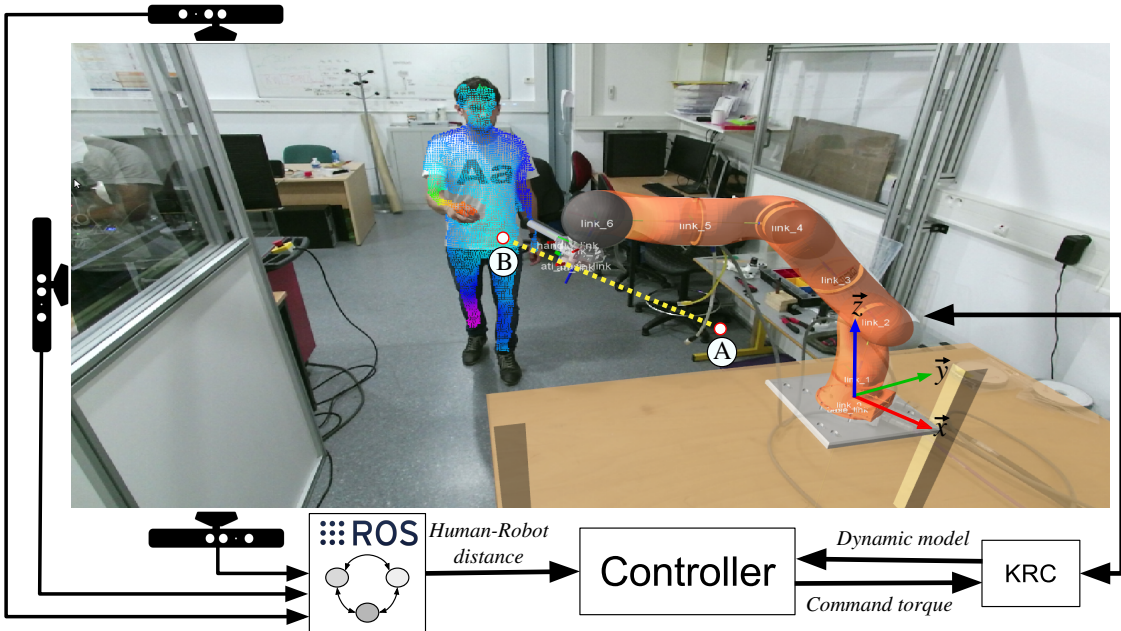


Figure 3.1: View of a user sharing its workspace with a KUKA LWR4 manipulator; with the experimental setup used to detect the human operator and control the robotic system.

in Fig. 3.2, during the pre-collision phase, the maximum reached velocity by the end-effector in cartesian space is about 2 m/s . Maximum kinetic energy in the direction of the human-operator³ is 2.8 J . K_p is fixed at 200 and $K_d = 28$

3.3.1 Human-operator intersecting with the robot trajectory and no constraints on energy

In this case, the human-operator enters the workspace of the robot and intersects with its trajectory, a physical contact is engaged and the movement of the robot is blocked as it tries to catch the desired position towards point B⁴. the controller is implemented as described in the test case scenario. No energy related constraints are considered. At collision⁵, 2 J of kinetic energy are instantaneously dissipated to create the resulting impact force (see Fig. 3.2.a).

³The direction of the human-operator is mainly along the x axis.

⁴The trajectory generator is blind to any collision with the environment. It continues generating desired position, velocity and feed forward acceleration for the end-effector.

⁵see video in [Meguenani b]

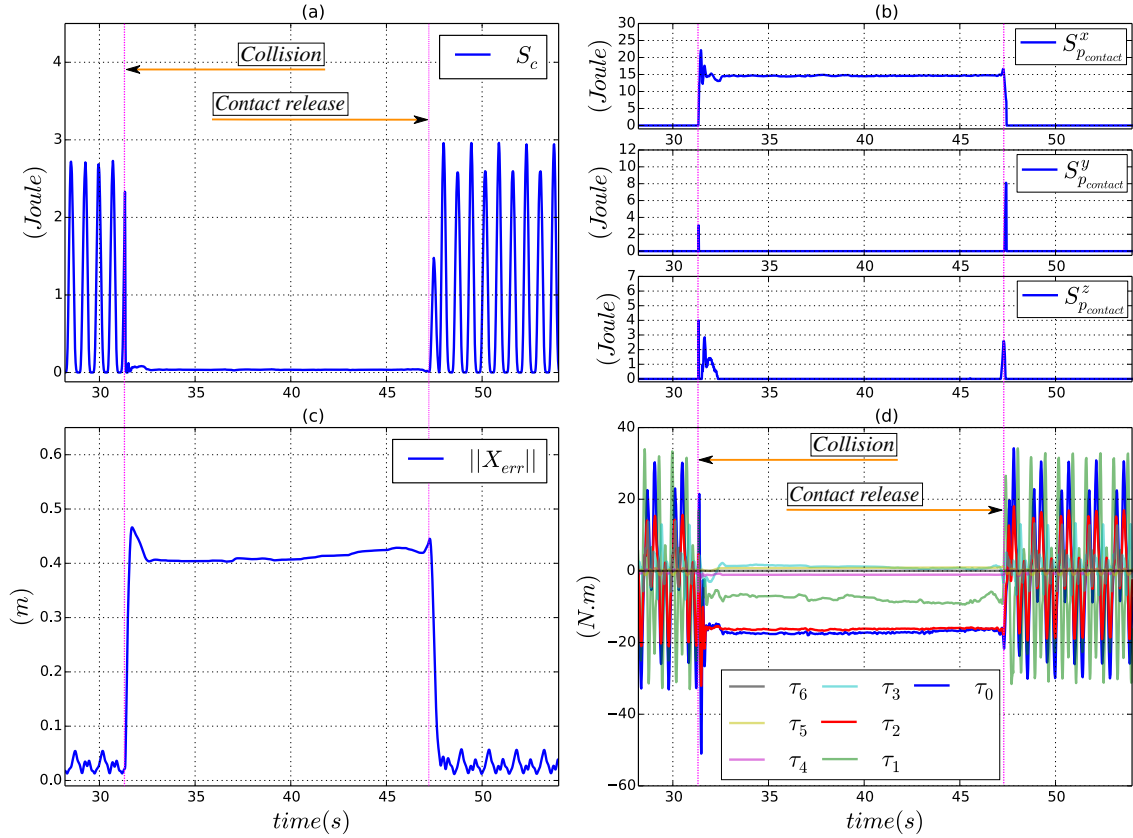


Figure 3.2: (a) Kinetic energy of the robot in the direction of the human operator; (b) Potential energy within the human-robot system during physical contact. (c) Top: position tracking error; Middle: constraint of the articular acceleration of the first joint; Bottom: articular velocity of the first joint. d) Articular torques.

As shown in Fig. 3.2.b, after the establishment of physical contact, potential energy within the human-robot system increases to reach a maximum value of 14 J. Consequently, a contact force in the direction of the desired position is created. Generated articular torques can be seen in Fig. 3.2.d. We highlight the amount of torques in joint 0 and joint 2: $\tau_0 \simeq -18$ N.m and $\tau_2 \simeq -16$ N.m⁶. Once physical contact is released, potential energy loaded in the system is transformed into kinetic one as fast as possible; Which can be dangerous in case of a second collision with the nearby operator. Finally, the robot goes back to its normal behaviour.

⁶The contact force between the robot and the operator is mainly caused by the generated torques in joint 0 and joint 2.

3.3.2 Human-operator intersecting with the robot trajectory and constraint on kinetic energy

In this scenario, the human-operator gets within the workspace of the robot and intersects with its movement. As the person moves towards the robot, the first formulation of the kinetic energy related constraint (2.43) is included⁷ in the controller and used to reduce the kinetic energy of the KUKA LWR4 before collision. Inequality and equality constraints used in the test case scenario are also considered. The controller parameters are fixed as following: $E_{c_{safe}} = 0.02 \text{ J}$, $K = 0.4 \text{ N}$, $d_{safe} = 0.3 \text{ m}$ and $d_{max} = 7 \text{ m}$. As seen in chapter 2 (subsection 2.5.3), choosing a big value for K (e.g. 50) will result in high articular jerks when the constraint on kinetic energy is activated (see Fig. 2.17.b). For this reason, a smaller value of K is used when implementing the kinetic energy related constraint on the real robot. Also, a bigger distance⁸ ($d_{max} - d_{safe}$) = 6.7 m is used to reduce this kinetic energy.

Dissipated kinetic energy at collision is shown in Fig. 3.3. Only 0.02 J of energy are dissipated compared to the previous scenario in which the kinetic energy of the robot is not pre-constrained (2 J). The constraint is respected at every time-step and the impact between the robot and the operator is considered safer.

After the establishment of physical contact, the non-constrained potential energy starts building up within the human-robot system to reach $\approx 14 \text{ J}$ (see Fig. 3.4.a). Actuation torques of joint 0 and joint 2 that are directly proportional to the generated contact force are shown in Fig. 3.4.b: $\tau_0 \simeq -20 \text{ N.m}$ and $\tau_2 \simeq -17 \text{ N.m}$. We highlight the shattering phenomenon on the actuation torques during physical contact. Indeed, during this phase, the distance between the robot and the human operator is more difficult to compute⁹ and may become null. In this case, the constraint on kinetic energy can be released and consequently the robot forces its way towards point \textcircled{B} as it is blocked by the human operator.

After releasing physical contact, the constraint on kinetic energy prevents the loaded potential energy from rapidly¹⁰ transforming into kinetic one. The distance related con-

⁷The constraint is not removed from the controller even after the establishment of physical contact.

⁸Compared with the braking distance used in simulation $d_{max} - d_{safe} = 0.2 \text{ m}$

⁹Because of the inevitable occlusions.

¹⁰Which can be dangerous regarding the nearby human operator.

straint on the kinetic energy of the robot makes both physical-contact enabling and disabling processes safer for human-robot interactions.

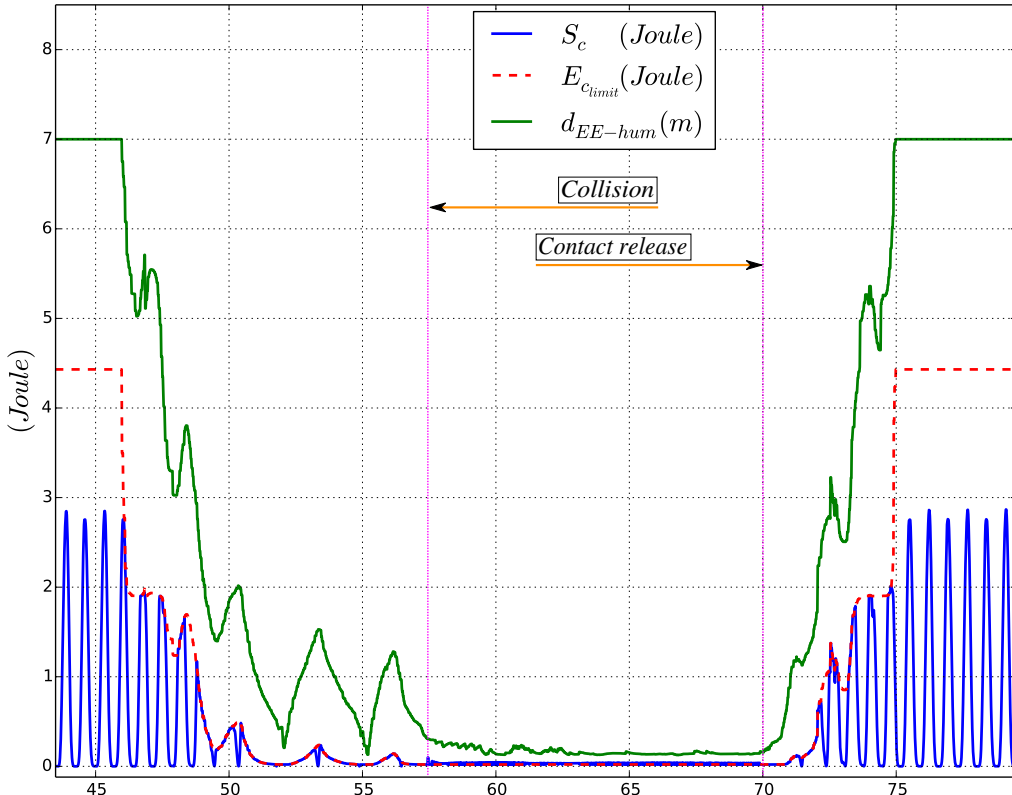


Figure 3.3: Constrained kinetic energy of the robot expressed at the end-effector in the direction of the approaching operator.

3.3.3 Human-operator intersecting with the robot trajectory and constraint on potential energy

In this scenario, the person also intersects with the trajectory of the robot between points **(A)** and **(B)**. The kinetic energy of the KUKA LWR4 is not constrained during the approach of the operator. After the establishment of physical contact, collision is detected¹¹ then, the constraint (2.50) is added to the controller and used to limit the amount of potential energy generated within the human-robot system. Inequality and equality articular constraints described in (2.33)¹² and (2.34) are also considered. The controller parameters are

¹¹Collision between the robot and the human operator is detected using the proprioceptive torque sensors.

¹²Except for the constraint on articular jerk.

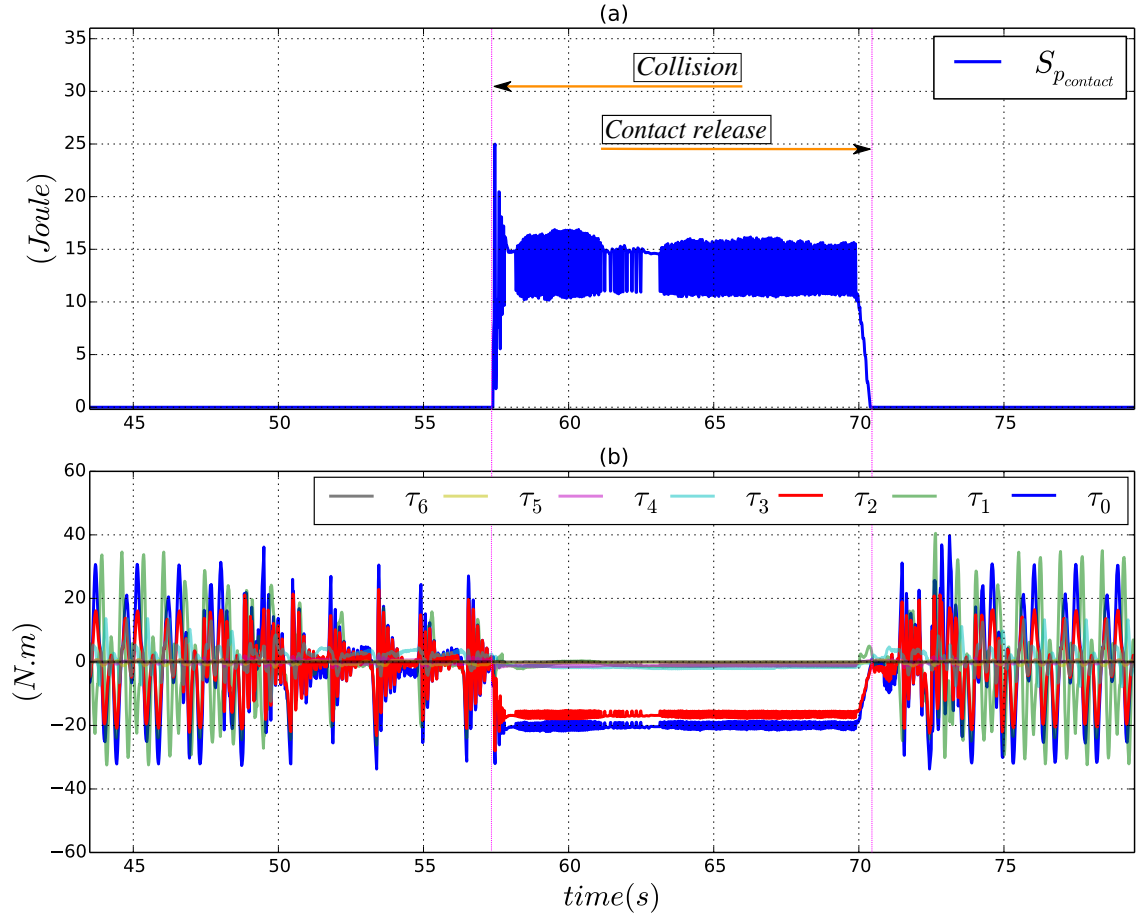


Figure 3.4: (a) Potential energy within the human-robot system during physical contact. (b) Articular torques.

fixed as following: $E_{p_{safe}}^x = 0.001 \text{ J}$, $E_{p_{safe}}^y = 0 \text{ J}$, $E_{p_{safe}}^z = 0 \text{ J}$.

At impact, as depicted in Fig. 3.5, 1.83 J of kinetic energy are instantaneously dissipated inducing a more dangerous collision force; Compared to the kinetic energy (0.02 J) dissipated in the previous scenario. Fig. 3.6.a shows how the potential energy related constraint is respected at every time-step during physical contact. Consequently, contact forces applied to the operator are harmless. Corresponding actuation torques and particularly of joints¹³ 0 and 2 are shown in Fig. 3.6.b: $\tau_0 \simeq -4 \text{ N.m}$ and $\tau_2 \simeq -3 \text{ N.m}$; Compared to the two previous scenarios in which the constraint on potential energy is not considered: $\tau_0 \simeq -20 \text{ N.m}$ and $\tau_2 \simeq -17 \text{ N.m}$ during physical contact. When using

¹³The generated contact force during physical contact is mainly caused by the articular torques on these two joints

the introduced constraint on potential energy, the robot is more passive and if needed, it can safely and easily be moved or pushed away by the operator. Also, thanks to this constraint, no vibrations are induced by the actuators of the robot during physical contact.

Once contact is released, the constraint on potential energy is de-activated and removed

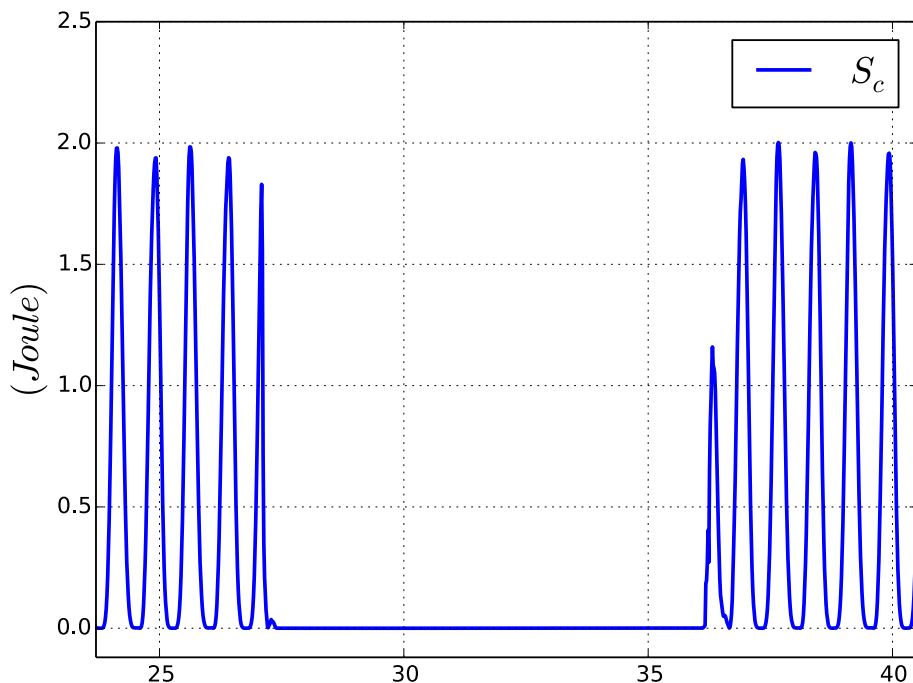


Figure 3.5: Kinetic energy of the robot in the direction of the human operator.

from the controller. Because of the accumulated position error¹⁴, the controller of the robot holds a bigger amount of potential energy $S_{p_{profile}}$ ¹⁵. This energy is transformed into kinetic one as fast as possible as the robot reaches point ②. This makes the contact breaking phase more dangerous¹⁶ for any nearby operator compared to the previous scenario in which the kinetic energy of the robot is constrained. Finally, the KUKA LWR4 goes back to its normal behaviour.

¹⁴As the robot is blocked during physical contact, the error between the real and desired position for the end-effector accumulates and increases.

¹⁵ $S_{p_{profile}}$ is the potential energy injected in the robot at time-step k (see 2.3.4).

¹⁶As the kinetic energy of the robot is not constrained, a harmful second collision is still possible with the nearby human operator.

3.3.4 Human-operator intersecting with the robot trajectory and constraints on kinetic then potential energies

In this last scenario¹⁷, the human-operator gets within the workspace of the robot and also intersects with its trajectory as the end-effector moves from point \textcircled{A} to point \textcircled{B} . Using (2.43), the kinetic energy of the KUKA LWR4 is constrained during the approach of the operator. At impact, collision is detected, physical contact is established and the potential energy related constraint (2.50) is added¹⁸ to the controller. This constraint is used to limit the amount of potential energy generated within the human-robot system along the x , y and z vectors in cartesian space. Inequality and equality articular constraints described in (2.33)¹⁹ and (2.34) are also considered. The controller parameters are fixed as following: $E_{c_{safe}} = 0.06 \text{ J}$, $K = 0.4 \text{ N}$, $d_{safe} = 0.3 \text{ m}$, $d_{max} = 7 \text{ m}$, $E_{p_{safe}}^x = 0.001 \text{ J}$, $E_{p_{safe}}^y = 0 \text{ J}$ and $E_{p_{safe}}^z = 0 \text{ J}$.

As shown in Fig. 3.7, the kinetic energy related constraint in the direction of the human-operator is respected at every time-step. At collision, only 0.02 J of energy are dissipated; Which results into a safe physical contact establishment. During the post-collision phase, the constraint on potential energy generated within the human-robot system is also respected at every time step (see Fig. 3.8.a). This constraint is decoupled along the x , y and z axis in cartesian space and results into a reduced and safer contact force between the human operator and the robot. The KUKA LWR4 in this case is compliant and can safely be moved by the operator if needed.

Actuation torques of joint 0 and joint 2 directly proportional to the contact force are shown in Fig. 3.8.b): $\tau_0 \simeq -4 \text{ N.m}$ and $\tau_2 \simeq -3 \text{ N.m}$. compared to the case when the constraint on potential energy is not considered: $\tau_0 \simeq -20 \text{ N.m}$ and $\tau_2 \simeq -17 \text{ N.m}$ during physical contact.

Once contact is released, the constraint on potential energy²⁰ is removed from the controller; At this moment, the robot contains sufficient potential energy

$E_p = -m(\mathbf{q})_{EE,*}^{eq} \ddot{\mathbf{X}}_{EE|k}^{EE,*} \left\| \mathbf{X}_{EE|k}^* - \mathbf{X}_{EE|k} \right\|_{EE,*}$ to move towards point \textcircled{B} . Considering the nearby operator, without the kinetic energy related constraint, E_p can transform

¹⁷see video in [Meguenani a]

¹⁸Without removing the constraint on kinetic energy. Both constraints are compatible.

¹⁹Except for the constraint on articular jerk.

²⁰Defined only during physical contact as $S_{p_{contact}}$.

rapidly into a hazardous amount of kinetic energy; however, thanks to this constraint (2.43), physical contact is safely released and the potential energy loaded in the controller of the robot progressively and harmlessly transforms into kinetic one as the end-effector reaches its goal (see Fig. 3.7).

3.4 Conclusion

In this chapter, the controller and energy related constraints presented in chapter 2 are implemented on a real KUKA LWR4 robot during its physical interaction with a human operator. As the person approaches the robot and enters its workspace, the constraint on its kinetic energy forces the robot to reduce the amount of kinetic energy it generates in the direction of the operator; Physical contact is safely established.

During the post collision phase, potential energy within the human-robot system is also successfully constrained. Depending on the allowed amount of potential energy, the resulting contact force is reduced and the robot can easily and safely be moved by the operator.

After releasing the physical contact, the constraint on kinetic energy ensures a smooth and safe transformation of the potential energy held in the controller of the robot into kinetic one as the human operator progressively moves away from the workspace of the robot. Task related dynamic performances of the robot are then fully recovered.

As explained in chapters 1 and 2, a solution for the optimization control problem cannot be guaranteed every time-step if the formulation of the energy related constraints does not include the reaction capabilities²¹ of the robot actuators. This is actually the reason why the controller sample time for the implementation on the real robot is increased to 15 ms, compared to 1 ms in simulation. The KUKA LWR4 was not able to brake and cope with E_{climit} in just 1 ms. 15 ms is the smallest window of time needed for the robot to cope with the kinetic energy related constraint (as seen in ()). Moreover, increasing the control time-step deteriorates the tracking performances of the robot regarding the trajectory tracking task.

²¹i.e. producible articular torque/deceleration and jerk

The only way to ensure a solution to the optimization control problem for every time-step is to reformulate the energy related constraints and take into account the Max/min producible articular torque/deceleration and jerk. However, the dynamic and non-predictable²² nature of E_{climit} makes guaranteeing viability for the robot during human robot interaction even more difficult.

²²The kinetic energy related constraint depends on the non-predictable movements of the human operator and the distance between him and the robot. This constraint is of type 6 (see table 1.1).

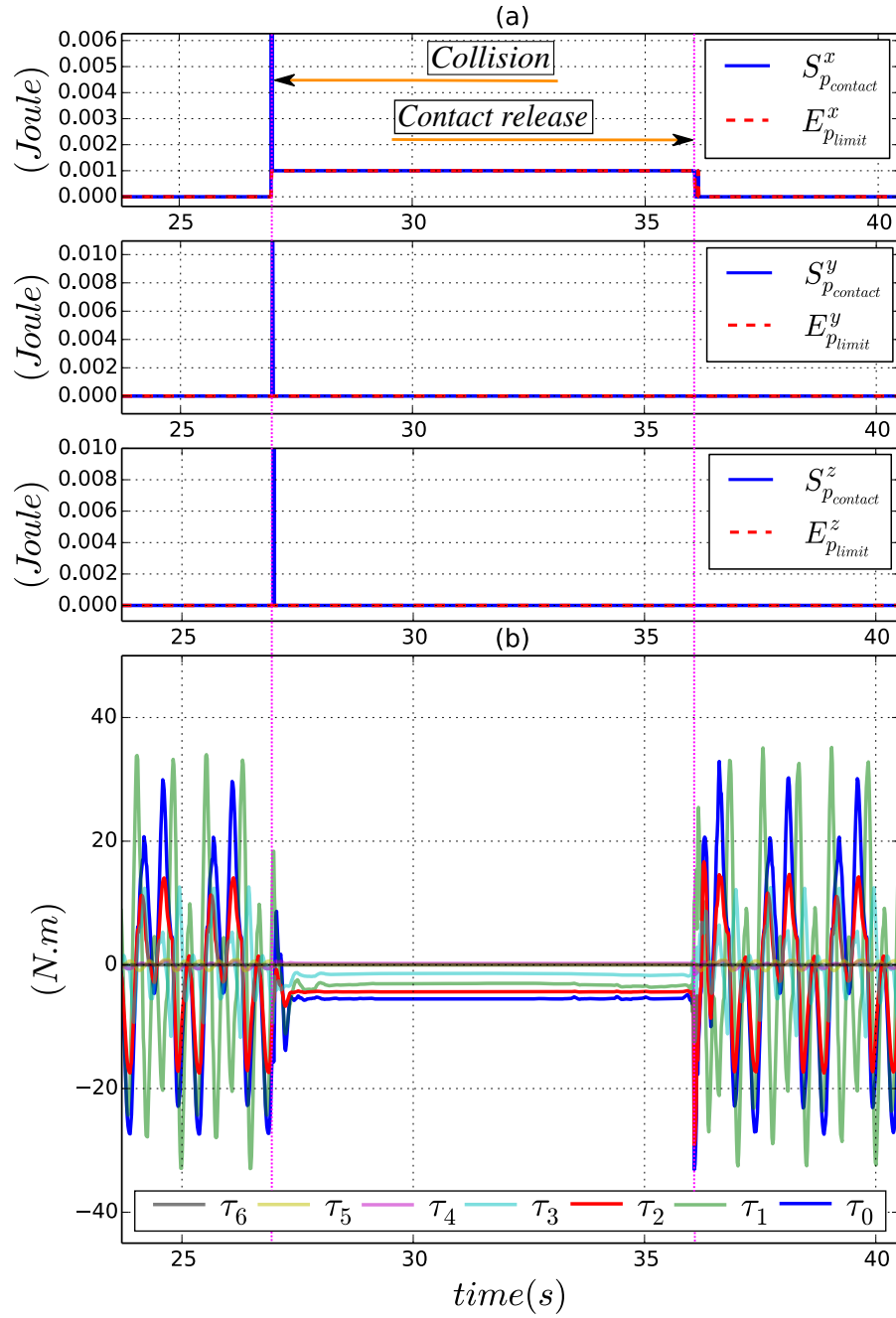


Figure 3.6: (a) Potential energy within the human-robot system during physical contact along the x , y and z axis in cartesian space. (b) Articular torques.

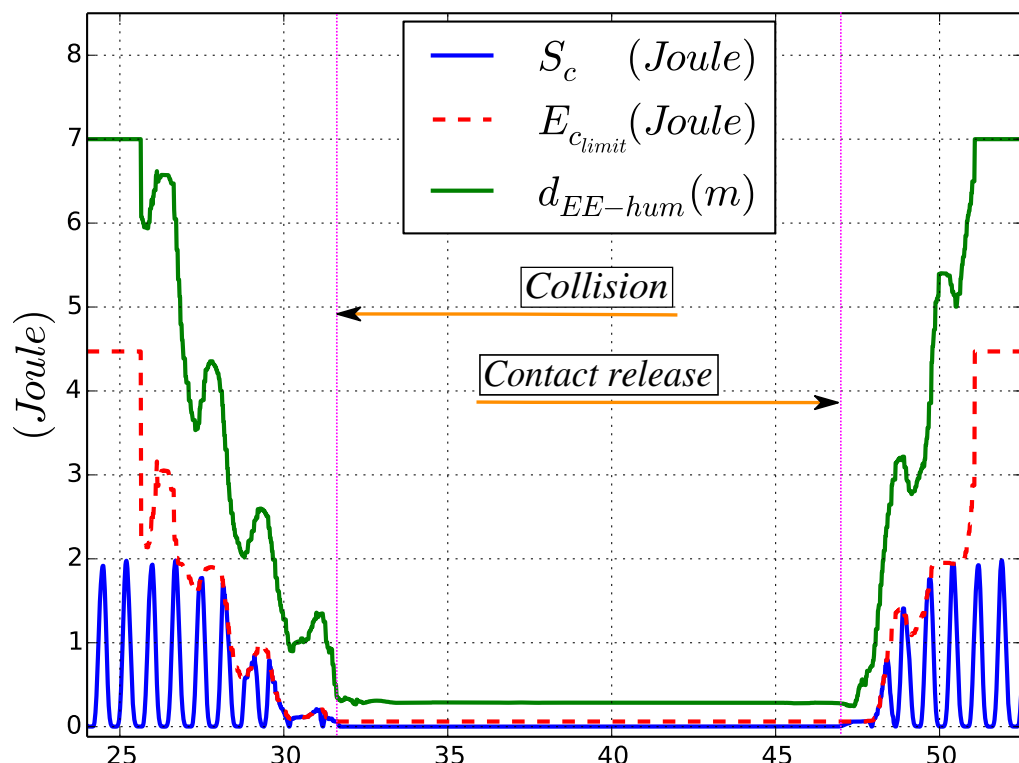


Figure 3.7: Constrained kinetic energy of the robot expressed at its end-effector in the direction of the approaching operator.

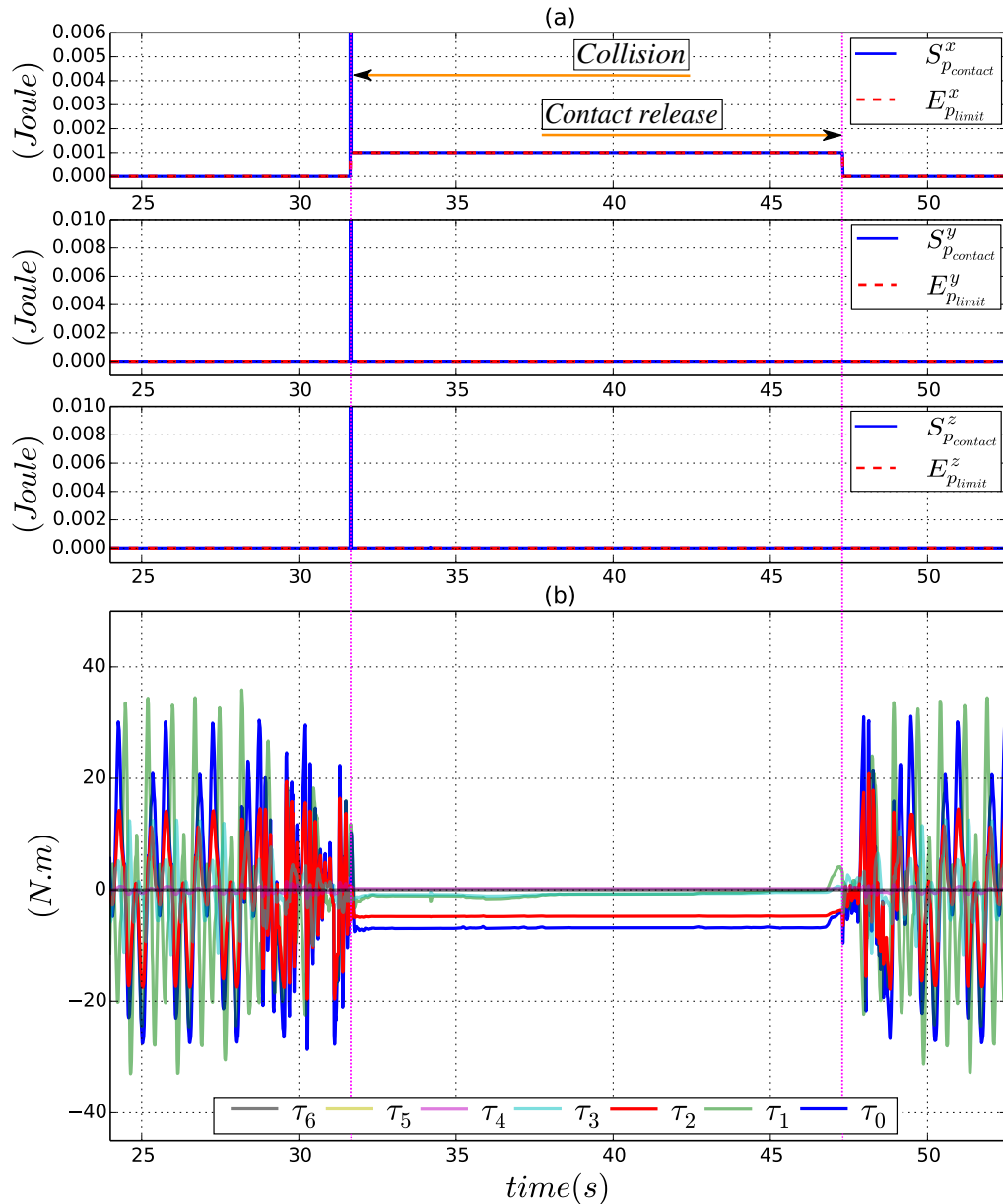


Figure 3.8: (a) Potential energy within the human-robot system during physical contact along the x , y and z axis in cartesian space. (b) Articular torques.

Appendix A

Computation of deceleration capabilities for a robotic system

For a robotic system, the relation between joint torques τ and the generated accelerations \ddot{q} is expressed by the dynamic equation:

$$M(\mathbf{q})\ddot{\mathbf{q}} + \mathbf{b}(\mathbf{q}, \dot{\mathbf{q}}) = \boldsymbol{\tau} \quad (\text{A.1})$$

Therefore, acceleration/deceleration capabilities (\ddot{q}_M , \ddot{q}_m) are related to the maximum and minimum producible torques (τ_M , τ_m) in addition to the current state of the system (\mathbf{q} , $\dot{\mathbf{q}}$). Instantaneous maximum and minimum producible decelerations (\ddot{q}_M^{inst} , \ddot{q}_m^{inst}) can be computed as following :

$$\arg \min_{\boldsymbol{\tau}} M(\mathbf{q})^{-1}(\boldsymbol{\tau} - \mathbf{b}(\mathbf{q}, \dot{\mathbf{q}})), \quad (\text{A.2})$$

$$\arg \max_{\boldsymbol{\tau}} M(\mathbf{q})^{-1}(\boldsymbol{\tau} - \mathbf{b}(\mathbf{q}, \dot{\mathbf{q}})), \quad (\text{A.3})$$

$$\text{s.t: } \tau_m \leq \boldsymbol{\tau} \leq \tau_M$$

Then:

$$\ddot{q}_M^{inst} = M(\mathbf{q})^{-1}(\tau_{max} - \mathbf{b}(\mathbf{q}, \dot{\mathbf{q}})), \quad (\text{A.4})$$

$$\ddot{q}_m^{inst} = M(\mathbf{q})^{-1}(\tau_{min} - \mathbf{b}(\mathbf{q}, \dot{\mathbf{q}})), \quad (\text{A.5})$$

τ_{min} and τ_{max} are respectively the solutions for (A.2) and (A.3).

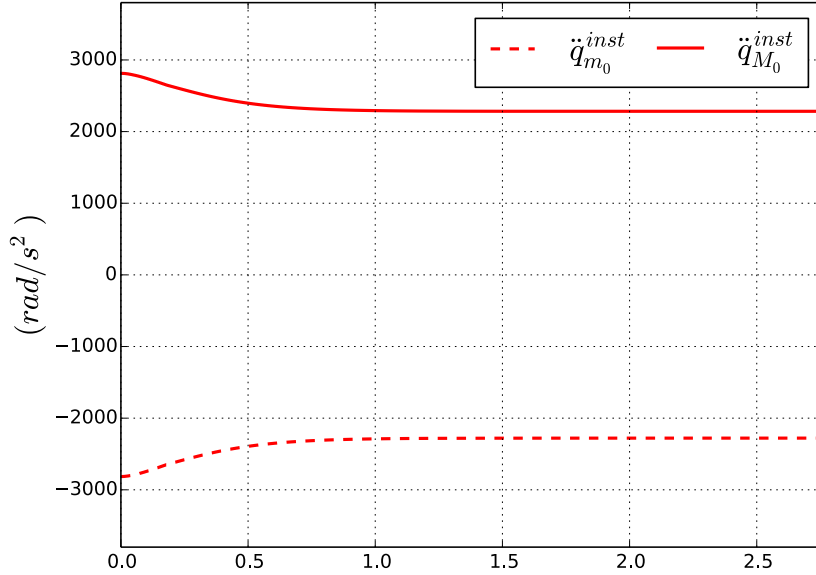


Figure A.1: Instantaneous producible maximum and minimum articular accelerations for joint 0 during the movement of the KUKA LWR4 as shown in Fig. 1.6.

For a KUKA LWR4 serial robot with $\tau_M^T = -\tau_m^T = [200, 200, 100, 100, 100, 30, 30]$, instantaneous maximum and minimum accelerations for joint 0 during the movement shown in Fig. 1.6 are as in Fig. A.1.

However, as \ddot{q}_M and \ddot{q}_m are used as constants in the formulation of the static articular constraints, the final upper and lower bounds will be computed using algorithm 6 :

Algorithm 6 Compute \ddot{q}_M and \ddot{q}_m

Require: $q_M, q_m, \dot{q}_M, \dot{q}_m, \tau_m, \tau_M, N$

```

1:  $\ddot{q}_m \leftarrow -[\infty, \dots, \infty]$ 
2:  $\ddot{q}_M \leftarrow [\infty, \dots, \infty]$ 
3: for ( $i = 1 \rightarrow N$ ) do
4:    $q \leftarrow \text{random}(q_m, q_M)$ 
5:    $\dot{q} \leftarrow \text{random}(\dot{q}_m, \dot{q}_M)$ 
6:   compute  $\tau_{\max}$   $\tau_{\min}$  using (A.2) and (A.2)
7:    $\ddot{q}_M^{inst} \leftarrow M(q)^{-1}(\tau_{\max} - b(q, \dot{q}))$ 
8:    $\ddot{q}_m^{inst} \leftarrow M(q)^{-1}(\tau_{\min} - b(q, \dot{q}))$ 
9:   if ( $\ddot{q}_M^{inst} \leq \ddot{q}_M$ ) then
10:    |  $\ddot{q}_M \leftarrow \ddot{q}_M^{inst}$ 
11:   end if
12:   if ( $\ddot{q}_m^{inst} \geq \ddot{q}_m$ ) then
13:    |  $\ddot{q}_m \leftarrow \ddot{q}_m^{inst}$ 
14:   end if
15: end for
16: return  $\ddot{q}_M, \ddot{q}_m$ 

```

Bibliography

[Alami 06]

R. Alami, A. Albu-Schaeffer, A. Bicchi, R. Bischoff, R. Chatila, A. De Luca, A. De Santis, G. Giralt, J. Guiochet, G. Hirzinger et others. *Safe and dependable physical human-robot interaction in anthropic domains: State of the art and challenges.* In Intelligent Robots and Systems, 2006 IEEE/RSJ International Conference on, pages 1–16. IEEE, 2006.

[Aubin 91]

Jean-Pierre Aubin. *Viability theory. Systems & control: Foundations & applications.* Birkhäuser, Boston. doi, vol. 10, n° 1007, pages 978–0, 1991.

[Bischoff 10]

Rainer Bischoff, Johannes Kurth, Günter Schreiber, Ralf Koeppe, Alin Albu-Schäffer, Alexander Beyer, Oliver Eiberger, Sami Haddadin, Andreas Stemmer, Gerhard Grunwald et others. *The KUKA-DLR Lightweight Robot arm-a new reference platform for robotics research and manufacturing.* In 41st International Symposium on Robotics, pages 1–8, 2010.

[Boyd 04]

Stephen Boyd et Lieven Vandenberghe. Convex optimization. Cambridge university press, 2004.

[Chanteperdrix]

Gerum Chanteperdrix. *Xenomai.* <https://xenomai.org>.

- [Chen 94] **Tsing-Hua Chen, Fan-Tien Cheng, York-Yih Sun et Min-Hsiung Hung.** *Torque optimization schemes for kinematically redundant manipulators.* Journal of Robotic Systems, vol. 11, n° 4, pages 257–269, 1994.
- [De Luca 06] **Alessandro De Luca, Alin Albu-Schäffer, Sami Haddadin et Gerd Hirzinger.** *Collision detection and safe reaction with the DLR-III lightweight manipulator arm.* In IEEE/RSJ International Conference on Intelligent Robots and Systems, pages 1623–1630, 2006.
- [De Luca 08] **Alessandro De Luca et Lorenzo Ferrajoli.** *Exploiting robot redundancy in collision detection and reaction.* In IEEE/RSJ International Conference on Intelligent Robots and Systems, pages 3299–3305, 2008.
- [Decré 09] **Wilm Decré, Ruben Smits, Herman Bruyninckx et Joris De Schutter.** *Extending iTaSC to support inequality constraints and non-instantaneous task specification.* In Robotics and Automation, 2009. ICRA'09. IEEE International Conference on, pages 964–971. IEEE, 2009.
- [Ebert 02] **Dirk M Ebert et Dominik D Henrich.** *Safe human-robot-cooperation: Image-based collision detection for industrial robots.* In IEEE/RSJ International Conference On Intelligent Robots and Systems, pages 1826–1831, 2002.
- [Gurobi Optimization Inc. 15] **Gurobi Optimization Inc.** *Gurobi Optimizer Reference Manual*, 2015.
- [Haddadin 08] **Sami Haddadin, Alin Albu-Schäffer, Alessandro De Luca et Gerd Hirzinger.** *Collision detection and reaction: A contribution to safe physical human-robot interaction.*

- In IEEE/RSJ International Conference on Intelligent Robots and Systems, pages 3356–3363, 2008.
- [Haddadin 12a] **S. Haddadin, A. Khouri, T. Rokahr, S. Parusel, R. Burgkart, A. Bicchi et A. Albu-Schäffer.** *A truly safely moving robot has to know what injury it may cause.* In IEEE/RSJ International Conference on Intelligent Robots and Systems, pages 5406–5413, 2012.
- [Haddadin 12b] **Sami Haddadin, Nico Mansfeld et A Albu-Schäffer.** *Rigid vs. elastic actuation: Requirements & performance.* In Intelligent Robots and Systems (IROS), 2012 IEEE/RSJ International Conference on, pages 5097–5104. IEEE, 2012.
- [Heinzmann 03] **Jochen Heinzmann et Alexander Zelinsky.** *Quantitative safety guarantees for physical human-robot interaction.* The International Journal of Robotics Research, vol. 22, n° 7-8, pages 479–504, 2003.
- [Hirzinger 01] **Gerd Hirzinger, A Albu-Schäffer, M Hahnle, Ingo Schaefer et Norbert Sporer.** *On a new generation of torque controlled light-weight robots.* In IEEE International Conference on Robotics and Automation, volume 4, pages 3356–3363, 2001.
- [Hoarau] **Ibanez Hoarau DaSilva et Padois.** *rtt-kuka-lwr: Control software architecture for lightweight robots.* https://www.github.com/kuka-isir/rtt_lwr.
- [Ikuta 03] **Koji Ikuta, Hideki Ishii et Makoto Nokata.** *Safety evaluation method of design and control for human-care robots.* The International Journal of Robotics Research, vol. 22, n° 5, pages 281–297, 2003.

- [KaewTraKulPong 02] **Pakorn KaewTraKulPong et Richard Bowden.** *An improved adaptive background mixture model for real-time tracking with shadow detection.* In Video-based surveillance systems, pages 135–144. Springer, 2002.
- [Katzschmann 13] **Robert Katzschmann, Torsten Kröger, Tamim Asfour et Oussama Khatib.** *Towards online trajectory generation considering robot dynamics and torque limits.* In 2013 IEEE/RSJ International Conference on Intelligent Robots and Systems, pages 5644–5651. IEEE, 2013.
- [Khatib 95] **Oussama Khatib.** *Inertial properties in robotic manipulation: An object-level framework.* The International Journal of Robotics Research, vol. 14, n° 1, pages 19–36, 1995.
- [Lange 14] **Friedrich Lange et Michael Suppa.** *Predictive path-accurate scaling of a sensor-based defined trajectory.* In 2014 IEEE International Conference on Robotics and Automation (ICRA), pages 754–759. IEEE, 2014.
- [Lange 15] **Friedrich Lange et Michael Suppa.** *Trajectory generation for immediate path-accurate jerk-limited stopping of industrial robots.* In 2015 IEEE International Conference on Robotics and Automation (ICRA), pages 2021–2026. IEEE, 2015.
- [Loughlin 07] **Clive Loughlin, A Albu-Schäffer, S Haddadin, Ch Ott, A Stemmer, T Wimböck et G Hirzinger.** *The DLR lightweight robot: design and control concepts for robots in human environments.* Industrial Robot, vol. 34, n° 5, pages 376–385, 2007.
- [Lumelsky 93] **Vladimir J Lumelsky et Edward Cheung.** *Real-time collision avoidance in teleoperated whole-sensitive robot arm ma-*

- nipulators.* IEEE Transactions on Systems, Man and Cybernetics, vol. 23, n° 1, pages 194–203, 1993.
- [Ma 02] **Shugen Ma et Mitsuru Watanabe.** *Time-optimal control of kinematically redundant manipulators with limit heat characteristics of actuators.* Advanced Robotics, vol. 16, n° 8, pages 735–749, 2002.
- [Marx] **et al. Marx.** *RTnet: Hard Real-Time Networking for Real-Time Linux.* <http://rtnet.org>.
- [Meguenani a] **Da Silva Hoarau Bidaud Meguenani Padois.** *KUKA: HR interaction with constraints on Ec and Ep.* http://pages.isir.upmc.fr/~padois/website/fichiers/videos/Kuka_Human_interaction_constraints_on_Ec_and_Ep.mp4.
- [Meguenani b] **Da Silva Hoarau Bidaud Meguenani Padois.** *KUKA: HR interaction with no constraints.* http://pages.isir.upmc.fr/~padois/website/fichiers/videos/Kuka_Human_interaction_no_constraints.mp4.
- [Merlhiot 12] **X. Merlhiot, J.L. Garrec, G. Saupin et C. Andriot.** *The XDE mechanical kernel: efficient and robust simulation of multibody dynamics with intermittent nonsmooth contacts.* In International Conference on Multibody System Dynamics, Stuttgart, Germany, 2012.
- [Ngo 05] **Khoi B Ngo, Robert Mahony et others.** *Passivity-based control of robot manipulators subject to constraints.* In Proc. of the 2005 Australian Conf. on Robotics and Automation, 2005.
- [Ngo 06] **Khoi B Ngo et Robert Mahony.** *Bounded torque control for robot manipulators subject to joint velocity constraints.* In Pro-

- ceedings 2006 IEEE International Conference on Robotics and Automation, 2006. ICRA 2006., pages 7–12. IEEE, 2006.
- [Park 98] **Ki Cheol Park, Pyung Hun Chang et Seung Ho Kim.** *The enhanced compact QP method for redundant manipulators using practical inequality constraints.* In Robotics and Automation, 1998. Proceedings. 1998 IEEE International Conference on, volume 1, pages 107–114. IEEE, 1998.
- [Rubrecht 10] **Sébastien Rubrecht, Vincent Padois, Philippe Bidaud et Michel De Broissia.** *Constraints Compliant Control: constraints compatibility and the displaced configuration approach.* In Intelligent Robots and Systems (IROS), 2010 IEEE/RSJ International Conference on, pages 677–684. IEEE, 2010.
- [Rubrecht 11] **Sébastien Rubrecht.** *Contributions à la commande de robots sous contraintes.* Thèse de doctorat, Université Pierre et Marie Curie-Paris VI, 2011.
- [Rusu 11] **Radu Bogdan Rusu et Steve Cousins.** *3D is here: Point Cloud Library (PCL).* In IEEE International Conference on Robotics and Automation (ICRA), Shanghai, China, May 9-13 2011.
- [Salini 12] **J. Salini.** *Dynamic control for the task/posture coordination of humanoids: toward synthesis of complex activities.* Ph.d. thesis, Université Pierre et Marie Curie, Paris, France, June 2012.
- [Schreiber 10] **Günter Schreiber, Andreas Stemmer et Rainer Bischoff.** *The fast research interface for the kuka lightweight robot.* In IEEE International Conference on Robotics and Automation (ICRA). Citeseer, 2010.

- [Soetens] **P. Soetens.** *RTT: Real-Time Toolkit.* <http://www.orocos.org/rtt>.
- [Yoshikawa 85] **Tsuneo Yoshikawa.** *Manipulability of robotic mechanisms.* The international journal of Robotics Research, vol. 4, n° 2, pages 3–9, 1985.
- [Zinn 04] **Michael Zinn, Oussama Khatib, Bernard Roth et J Kenneth Salisbury.** *Playing it safe [human-friendly robots].* Robotics & Automation Magazine, IEEE, vol. 11, n° 2, pages 12–21, 2004.